5-2019

DESIGN, SYNTHESIS, AND STUDY OF ZINC-RESPONSIVE LIPID SWITCHES FOR TRIGGERED RELEASE OF LIPOSOMAL CONTENT

Alexa Joy Watson
University of Tennessee

To the Graduate Council:

I am submitting herewith a thesis written by Alexa Joy Watson entitled "DESIGN, SYNTHESIS, AND STUDY OF ZINC-RESPONSIVE LIPID SWITCHES FOR TRIGGERED RELEASE OF LIPOSOMAL CONTENT." I have examined the final electronic copy of this thesis for form and content and recommend that it be accepted in partial fulfillment of the requirements for the degree of Master of Science, with a major in Chemistry.

Michael D. Best, Major Professor

We have read this thesis and recommend its acceptance:

Shawn R. Campagna, Christopher A. Baker

Accepted for the Council:
Dixie L. Thompson

Vice Provost and Dean of the Graduate School

(Original signatures are on file with official student records.)

DESIGN, SYNTHESIS, AND STUDY OF ZINC-RESPONSIVE LIPID SWITCHES FOR TRIGGERED RELEASE OF LIPOSOMAL CONTENT

A Thesis Presented for the
Master of Science
Degree
The University of Tennessee, Knoxville

Alexa Joy Watson
May 2019

ACKNOWLEDGEMENTS

An incredible amount of work goes in to the attainment of a degree. The work put toward my education was not all my own; many people have been there to encourage me throughout the years. I would like to thank my parents and siblings for encouraging me throughout undergrad and graduate school. A very special thanks goes to my chemistry professors at Tennessee Wesleyan, Dr. John Berch and Dr. Daniel Blumling. Without their encouragement and support, from literally babysitting to advising and teaching, I would never have considered graduate school. A forever thank you to my husband Shane who put up with me, the crazy schedules, and the ups and downs from undergrad to grad school and beyond without missing a beat.

There are countless people at UT who have helped me along the way. Dr. Best provided my first real taste of research chemistry when I was still an undergrad when I participated in the summer undergraduate research program. That opportunity really sealed the deal for me as I truly enjoyed working in a research lab, so much so that I returned for grad school; I just couldn't get enough of the lipids. My group members, past and present, have been a priceless resource. Dr. Adam Carr, the synthetic genie, always had suggestions for what to try if a reaction just wasn't working out. Most importantly Jinchao Lou assisted in the design of some of my target compounds and was always the perfect sounding board for "does this make sense?" in feeling out new reaction schemes.

Thank you again to my P.I. Dr. Michael Best for constant encouragement over the years and for giving me the opportunity to pursue this research. Thank you to my committee members Dr. Shawn Campagna and Dr. Christopher Baker for assisting with my academic career over the course of my education here. Everyone in the main office, business office, general chemistry office, staff and facility services at UT were just as instrumental as the next in keeping things running smoothly and I thank them for their support as well.

ABSTRACT

Smart drug delivery platforms such as designer liposomes can be used to enhance medicinal properties by enabling control over the time and location of therapeutic cargo release. This can be achieved by designing liposomes that respond to different stimuli by releasing encapsulated contents. Specifically, this work focuses on the synthesis of ion recognition lipid switches. These lipids are designed such that their physical properties are altered upon chelation of a given metal ion, in this case Zn^{2+}, becoming membrane destabilizing upon molecular recognition. This contributes to the current state of passively controlled release, where pathophysiological conditions associated with a diseased site are used to control spatiotemporal release of therapeutic cargo. The use of molecular recognition events to effect conformational change and thus cargo release is a newly emerging field of research. Here, a panel of zinc recognition lipids based on known zinc chelating moieties including trispicoylamine (TPA) and N,N,N′,N′-Tetrakis(2-pyridylmethyl) ethylenediamine (TPEN) were synthesized and their release potential analyzed. With incorporation into a liposome platform, these lipids can be used to enhance the selectivity of release at diseased cells exhibiting elevated zinc concentrations including ischemic tissues, neurodegenerative diseases, and certain cancer types.[3-8]

TABLE OF CONTENTS

LIST OF ABBREVIATIONS

AMF	alternating magnetic field
AML	acute myeloid leukemia
Ar	argon
$CaCl_2$	calcium chloride
$CDCl_3$	deuterated chloroform
CPP	cell penetrating peptide
CuI	copper iodide
d	doublet
DAG	diacylglycerol
DCC	N,N'-Dicyclohexylcarbodiimide
DCM	dichloromethane
dd	doublet of doublets
DIBAL-H	diisobutylaluminium hydride
DMAP	4-dimethylaminopyridine
DMF	dimethylformamide
DOPE	1,2-dioleoyl-sn-glycero-3-phosphoethanolamine
EDCI	1-Ethyl-3-(3-dimethylaminopropyl)carbodiimide
EPR	enhanced permeability and retention effect
equiv	equivalent
EtOAc	ethyl acetate
EtOH	ethanol
Fab’	fragment of antigen binding
fM	femtomolar
FR	folate receptors
GUV	giant unilamellar vesicle
h	hours
H_2	hydrogen
HER2	human epidermal growth factor receptor-2

HNO_3	nitric acid
J	coupling constant
K_2CO_3	potassium carbonate
KOH	potassium hydroxide
KOtBu	potassium tert-butoxide
$LiCO_3$	lithium carbonate
LUV	large unilamellar vesicle
m	multiplet
M	molar
mAb	monoclonal antibody
MeCN	acetonitrile
MeOD	deuterated methanol
MeOH	methanol
mg	milligram
$MgSO_4$	magnesium sulfate
MHz	megahertz
mL	milliliter
MLV	multilamellar vesicle
mM	millimolar
mmol	millimoles
MMP	matrix metalloproteinases
MT	metallothionein
N_2	nitrogen
$NaBH(OAc)_3$	sodium triacetoxyborohydride
$NaBH_4$	sodium borohydride
NaCl	sodium chloride
$NaHCO_3$	sodium carbonate
NaN_3	sodium azide
NaOH	sodium hydroxide
NH_4OAc	ammonium acetate

nm	nanometer
NMR	nuclear magnetic resonance
ONB	o-nitrobenzyl
PA	phosphatidic acid
PBr_3	phosphorus tribromide
PC	phosphatidylcholine
$Pd(PPh_3)_4$	Tetrakis(triphenylphosphine)palladium(0)
Pd/C	palladium on carbon
$PdCl_2(PPh_3)_2$	Bis(triphenylphosphine)palladium(II) dichloride
PE	phosphatidylethanolamine
PEG	polyethylene glycol
PIPES	piperazine-N,N′-bis(2-ethanesulfonic acid)
PIP_nS	phosphatidylinositol polyphosphate family of isomers
PKCs	protein kinase Cs
pM	picomolar
PS	phosphatidylserine
*p*TsCl	*para*-Toluenesulfonyl chloride
quant	quantitative yield
quint	quintet
R8	octa-arginine
RES	reticulo-endothelial system
ROS	reactive oxygen species
rt	room temperature
s	singlet
S	shape parameter
siRNA	signaling ribonucleic acid
$SOCl_2$	thionylchloride
$sPLA_2$	secretory phospholipase A2
SUV	small unilamellar vesicle
t	triplet

TAT	transactivator of transcription
TBS	tris buffered saline
TEA	triethylamine
THF	tetrahydrofuran
TLC	thin layer chromatography
TPA	Tris(2-pyridylmethyl)amine
TPEN	N,N,N',N',-Tetrakis(2-pyridylmethyl)ethylenediamine
UV	ultraviolet
ZIP	zinc importer protein
$Zn(OAc)_2$	zinc acetate
ZnT	zinc transporter protein
μL	microliter

LIST OF FIGURES

CHAPTER ONE

LIPIDS AND LIPOSOMES: PROPERTIES, STRUCTURES, AND GENERAL INFORMATION

Lipids are unique biomolecular structures, each with a specific set of physical and chemical properties. Via their self-assembly into liposomes, lipids can be harnessed for desired applications in molecular recognition and drug delivery. Liposomes are advantageous on this front due to their controllable size, potential for surface modifications, non-immunogenicity, and ability to solubilize multiple drug types. First, we will discuss the general physical attributes of lipids and biologically relevant lipids and their functions. Then, we will discuss the power of the liposome as a drug delivery platform. Finally, we will dive into synthetic lipids and their numerous applications.

1.1. General Structure and Properties of Lipids

Lipids are defined by their amphiphilic structures. When dispersed in aqueous media, they spontaneously form aggregates driven by the disparity of polarities that exist within the structure. Each lipid is composed of a polar (hydrophilic) headgroup and a nonpolar (hydrophobic) tail region, as depicted in Figure 1. Lipids have an overall shape based on the size ratio between these two sections of the structure. Lipids with varying molecular shapes will form different self-assembled materials to maximize attractive properties when dispersed in aqueous media. The lipid shapes fall into one of three general categories: cylinder, cone, or wedge. These shapes are calculated via the shape parameter (S), as defined in equation 1.[9] The shape of the lipid will determine its membrane

$$S = \frac{cross\text{-}sectional\ area\ of\ polar\ headgroup\ x\ lipid\ length}{lipid\ volume} \qquad \text{(Equation 1)}$$

forming capabilities. The different lipid shapes and their resultant aggregate formations are shown in Figure 1. When lipids possess S=1, they exhibit cylindrical shapes and are membrane forming with polar headgroups of

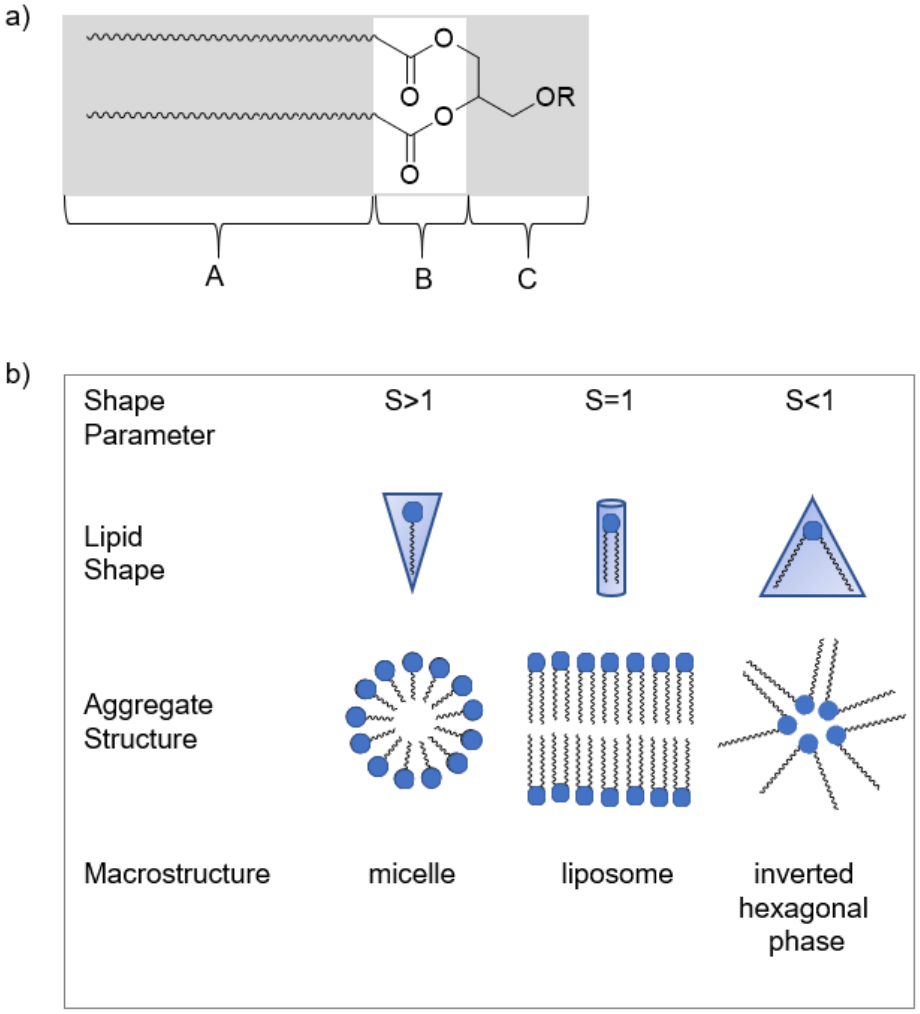

Figure 1. ***Lipid structure and shape properties.***
a) The general structure of a lipid. Lipids are composed of (A) a hydrophobic tail region consisting of alkyl tails with varying degrees of unsaturation (B) a linking group between tail and head and (C) a polar head group. b) Lipid shapes and their resultant aggregate and macrostructures when dispersed in aqueous media.

approximately the same diameter as the lipid tails. When dispersed in aqueous media, these lipids preferentially form bilayer materials including spherically shaped liposomes. These lipid bilayers close themselves into vesicles in order to maintain separation of their hydrophobic tails from the aqueous media which forms an aqueous pocket inside of the lipid bilayer. Lipid vesicles include unilamellar vesicles, also called liposomes, and multilamellar vesicles, which are large vesicles containing smaller vesicles within their aqueous core. The advantages and properties of these lipid vesicles will be discussed at length in a future section.

When S>1, lipids take on a cone shape. These lipids have a larger headgroup radius as compared to their tail area, and as a result favor assembly into micelles in aqueous solution. Micelles lack the aqueous inner pocket of liposomes with instead their inner layer being composed of the hydrophobic tails. However, they operate under the same properties to shield their hydrophobic tails from aqueous media. The final lipid shape is the inverted cone. These lipids possess a small, usually highly charged, headgroup with a comparably large hydrophobic region, giving them a shape parameter of S<1. The lipids in this category induce negative curvature in a membrane environment, and preferentially self-assemble into inverted micelles. Here, the hydrophilic headgroups form the inner core with the hydrophobic tails extending outward and composing the outer layer. In the same way that bilayers will self-assemble into liposomes to shield their hydrophobic tails from aqueous conditions, inverted micelles will aggregate into an inverted hexagonal phase structure, where multiple inverted micelles come together tail-to-tail. This shields the outer hydrophobic layer of the inverted micelle from aqueous conditions. Of these three macrostructures, liposome, micelle, hexagonal phase, the liposome presents the most interesting possibility as a drug delivery platform due to the ability to manipulate their membrane properties. By exploiting lipids of different shapes, membrane stability can be controlled and utilized as a method of achieving cargo release. This property is at the core of

liposomal controlled release platforms, where switching from membrane forming (S=1) to non-bilayer (S>1) lipids is the main method for the release of encapsulated cargo.

1.2. Lipids in the Biological Setting

Natural lipids, those produced through biological processes, are key cell to viability. They compose 50% of the mass of eukaryotic cellular membranes and are responsible for the membrane structural integrity.[10] It is the unique structure of lipids that makes them suitable for membrane formation, as previously discussed. Non-membrane supporting lipids, such as inverted cone shaped lipids, are also present in the biological milieu, but only at lower percentages that don't disturb bilayer stability. These serve important and tightly regulated functions within the cell as well. Natural lipids fall into two main categories, glycerophospholipids and sphingolipids. These groups are determined by which molecule the lipids are derived from, glycerol or sphingosine, respectively. Sterols, such as cholesterol, are also grouped under the definition of lipids because they are also amphiphilic membrane components, though they don't follow the same general structure of other lipids. Nevertheless, cholesterol is an abundant membrane component and

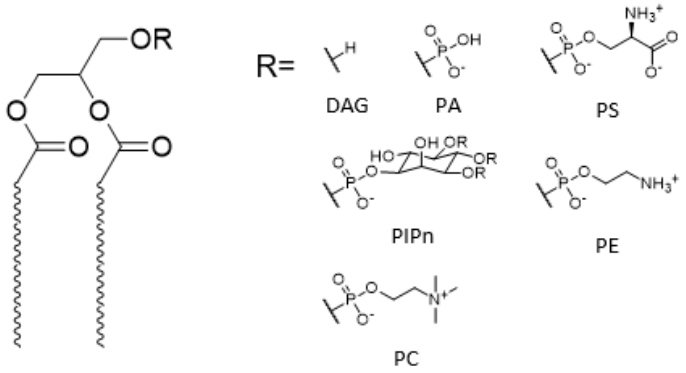

Figure 2. ***The structures of some biologically relevant lipids.***
Polar headgroups for DAG, PA, PS, PIP_ns, PE, and PC are as shown. Hydrophobic tail length and degree of saturation vary between each lipid. In the PIP_ns isomer family, R can equal any combination of H or PO_3^-.

important to membrane integrity. Lipids dictate numerous processes in the cell, performing structural and functional roles. The exact structures of natural lipids dictate their function within the cell. The structures of some biologically relevant lipids are shown in Figure 2. The variation in headgroup size and functionality determines the function of each lipid. One of the most notable structural lipids is phosphatidylcholine (PC). PC is the most abundant lipid in eukaryotic cell membranes and is the classical example of a cylindrical shaped lipid, favoring bilayer formation. The remainder of the cellular membrane is composed of less abundant lipids that exhibit functional roles within the cell, proteins, and other membrane stabilizing molecules like cholesterol. PC is key to liposomal drug delivery platforms as well, as it serves as a main bulk lipid for many of the lipid formulations used to produce therapeutic liposomes.

Functional lipids, generally termed signaling lipids, represent the other branch of lipids within the cell. Through recruitment of proteins to the membrane surface, through either intra- or extra-cellular binding events, these lipids can regulate cell activities controlling such processes as cell proliferation, apoptosis, metabolism, gene expression, and membrane trafficking.[11-13] The specific interactions between lipids and proteins that mediate these processes can be as simple as a monovalent binding event between a lipid and its target protein, or as complex as a microdomain of lipids acting together to bind protein in a multivalent fashion.[14] These complex interactions recruit proteins to the cell surface and trigger a cascade of important processes within the cell. Thus, aberrations in the interaction of these vital signaling lipids with their corresponding peripheral proteins can lead to the onset of diseases such as cancer, inflammation, autoimmunity, and degenerative diseases.[11, 15] These intricate interactions have led to a burgeoning field involving the study of the activities of signaling lipids.

Many of the notable signaling lipids are glycerophospholipids including diacylglycerol (DAG), phosphatidic acid (PA), phosphatidylserine (PS),

phosphatidylethanolamine (PE), and phosphatidylinositol polyphosphates (PIP_ns).[11, 15-16] DAG, the simplest of the signaling lipids, controls vital processes within the cell. DAG activates protein kinase Cs (PKCs), enzymes that control the cell cycle and exhibit tumor suppressing activity.[17-19] PKC is one of the most highly misregulated proteins in cancer. Thus, tightly regulated DAG activity is necessary for the maintenance of human health. PA interacts with Raf-1, a kinase involved in cancer.[20] In healthy cells, PS is found mainly in the inner leaflet of the cellular bilayer and is only translocated to the outer membrane leaflet, where it recruits proteins, to signal apoptosis.[21] PIP_ns regulate vesicular trafficking and modulate lipid distribution within the cell by their interaction with lipid transfer proteins.[22] Each of these regulatory functions of lipids help maintain a healthy cellular environment. Again, the abilities of these lipids to stabilize, destabilize, and perform signaling roles within the cell are due to their specific shape and chemical structure. This highlights the importance of lipid characteristics not only in the biological setting, but when considering synthetically designed lipids.

1.3. The Liposome as a Drug Delivery Platform

Liposomes represent a key platform for delivery of drugs within a biological system. They exhibit tunable properties in size, surface functionalization, cargo type, surface charge, and release mechanism that allow for a customizable platform. The properties of liposomes will be discussed below as they relate to their use as a nanoscale drug delivery platform.

1.3.1. Liposome Formation

Lipids will self-assemble into vesicles when dispersed in aqueous media due to their amphiphilic nature. While these arbitrarily formed vesicles are not formed with homogeneous and predictable size or lamellarity, they can subsequently be manipulated to be of uniform characteristics. A popular method for obtaining liposomes of reliable size is through thin film formation, hydration, and extrusion.[23] In this method, lipids in organic solvent are mixed in a defined ratio based on the

desired liposomal content. This lipid mixture is dried into a film, removing all organic solvent from the sample. The film is then hydrated with water or an aqueous buffer and subjected to freeze/thaw cycles to form large mulitilamellar vesicles (MLVs) of various sizes. The solution of MLVs is subjected to extrusion through polycarbonate filters with pores of the desired liposome diameter. Multiple passes through the extrusion filter give liposomes of reliable size. Generally, liposomes are composed of PC, the main bulk lipid of cell membranes. Other lipids including synthetic analogs bearing desired properties or functionalities for the specific liposomal platform can also be added to the film composition yielding vesicles of desired lipid content.

Liposomes are formed in a variety of sizes depending on the desired application. Utilizing different pore sizes in the extrusion step, or other less conventional vesicle formation techniques[24], liposomes of 20-1000 nm in diameter can be formed. Small unilamellar vesicles (SUVs) are from 20-100 nm, large unilamellar vesicles (LUVs) are greater than 100 nm in diameter, and giant unilamellar vesicles (GUVs) are larger than 1000 nm in diameter. Generally, liposomes of 100-200 nm are utilized for drug delivery applications. Vesicles of this size have a higher propensity to fuse with cell membranes due to the strain exerted on the lipids in the highly curved liposome surface. They also benefit from an increased circulation time by avoiding the reticulo-endothelial system (RES) longer than their larger counterparts.[24-25] Structures of this size are also able to make use of the enhanced permeability and retention (EPR) effect. This effect arises since the vasculature surrounding rapidly expanding cells, such as tumors, as well as other diseased tissues like those in inflammatory diseases and ischemia, have loose junctions between the endothelial cells of the blood vessel walls. [26-28] These gaps in the vessel lining are 0.1-3 μM in size allowing nanosized structures to leak from the blood vessel to the diseased area. A lack of drainage of lymphatic fluids, another hallmark of the EPR effect, allows the leaked nanomaterials to remain at the diseased site. However, the EPR effect only increases delivery 2-fold to tumor

sites versus other common accumulation organs.[28] This makes the EPR effect, on its own, not a powerful enough phenomenon to effect efficient drug delivery, though it can be coupled with other modifications to increase liposomal delivery and efficiency.

The ability of liposomes to encapsulate multiple drug types is also an attractive factor in their use as a drug delivery platform. Liposomes can house hydrophobic and hydrophilic cargo within the membrane bilayer or the aqueous core, respectively. Prodrugs can also be incorporated via attachment to a synthetic lipid at either the head group or as a hydrophobic tail, depending on the nature of the drug. Further examples of this will be provided in the next section.

1.3.2. Liposomal Surface Modifications

Modifications to the surfaces of classical liposomes can drastically enhance their power as a drug delivery vehicle. Surface modifications can act as shielding groups to protect liposomes from clearance from the body. Other surface modifications can increase the rate of fusion with target cells, while a very important group of surface ligands is comprised of active targeting moieties to enhance the selectivity for delivery to diseased cells within a complex biological mixture. The main surface modifications are depicted in Figure 3. Multiple surface modifications can be combined in one liposomal platform to enhance the overall efficiency of the drug delivery system.

1.3.2.1. Surface Modifications for Creation of Stealth Liposomes

Synthetic modifications to bare liposomes can drastically enhance their power as a drug delivery vehicle. Bare liposomes have a short half-life and are quickly cleared from the bloodstream by the RES system.[29] Though smaller liposomes inherently have longer circulation times than larger vesicles, they still have relatively short half-lives from an efficiency of drug delivery standpoint. Surface

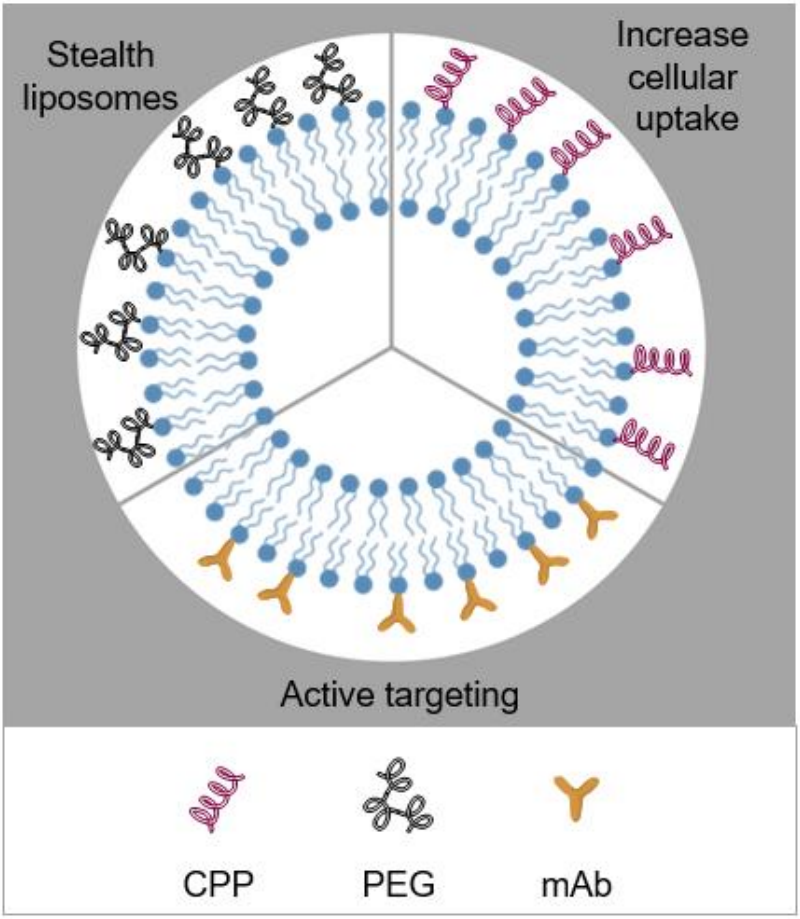

Figure 3. ***Surface modifications for increased efficiency of liposomal drug delivery systems.***
Representative modifications for the creation of stealth liposomes, the increase of liposome fusogenicity and cellular uptake, and actively targeted liposomes are shown, though multiple modifications to effect each desired outcome are available. Cellular penetrating peptides (CPPs), polyethyleneglycol (PEG), monoclonal antibody (mAb) are shown as examples.

modifications can shield the liposome from clearance, thus increasing their half-life. These surface modifications act as a physical barrier to keep opsin proteins from binding to the surface of the liposome, thus marking them for clearance by the immune system.[30] Initially, groups such as gangliosides and sialic acid derivatives were used to decorate liposomes.[25] These are common surface markers found on red blood cells, so by mimicking the native cell population of the administration route, the liposomes were able to evade the immune response. Now, the most common stealth coating is polyethylene glycol (PEG). Incorporation of PEG-PE conjugates into PC based liposomes showed an increase of circulation half-life from 30 minutes for bare liposomes to 5 hours in the earliest studies in PEGylation.[31] PEGylation also decreases the leakiness of liposomes, better harboring cargo for less off-site drug interactions.[29-30] PEG incorporation is relatively simple and there are now commercially available versions of lipids with PEG of a range of molecular weights appended to the headgroup.[32] Advances in PEGylation methods can now give circulation half-lives of 5-16 hours dependent on PEG polymer length.[29] PEG coatings can be purely polymer based or can be terminated with a functional group for further synthetic modification to the cloaked liposome surface. The impetus for this will be covered in the next section. Overall, the size control and potential for surface modification of liposomes help to increase circulation time and accumulation at diseased sites by evasion of the RES system and taking advantage of the EPR effect.

1.3.2.2. Surface Modifications for Active Targeting with Liposomes

Liposomes can be decorated with a variety of small molecules to increase their efficacy of delivery through active targeting. When based solely on the EPR effect, liposomes only make it to the general vicinity of the target site. Surface modification with targeting groups will pull these liposomes to the surface of target cells, increasing the therapeutic index of the delivery platform. Binding partners with high affinity for ligands found overexpressed or solely expressed on the target cell surface are ideal for targeting moieties. These groups can be appended

directly to the liposomal surface through functionalized lipids or attached to the reactive end of a PEG-lipid conjugate present in the liposome formulation. Presentation outside of the PEG shell effects greater targeting ability, while shielding of the targeting moiety within the PEG shell protects the ligand from off target binding outside of the desired location. Still dependent on the EPR effect, once the small liposomes have leaked into the interstitial space of the diseased tissue, recognition of the targeting group by the cell surface will trigger uptake or fusion of the liposome. Induced removal of the PEG shell after arrival at the target site can also aid in delivery, methods of which will be explained shortly. Ideally, the liposome will fuse with the cell surface, dumping its molecular cargo into the target cell or be taken in by endocytosis and then effect escape from the endosome and cargo release. Specially formulated fusogenic liposomes increase the propensity of membrane-to-membrane fusion to effect cargo delivery while avoiding the lytic activity of lysosomes.[33]

Another class of surface modification that instigates higher cellular uptake in a non-cell-type specific manner are cell penetrating peptides (CPPs). CPPs are most commonly highly cationic short peptides with transactivator of transcription (TAT) and octa-arginine (R8) peptides as representative examples.[34] These cationic peptides function to enhance permeation of liposomal content into target cells. Also, due to their ability to attenuate the surface charge of the liposome, drug loading efficiencies for hydrophobic or negatively charged cargo such as siRNA are increased with CPP decorated liposomes due to the increased electrostatic interactions of these cargo with the surface CPP.[34] CPPs can be rendered inactive by enzyme removable or light cleavable groups.[35-38] This allows the CPP to affect its function only at the desired spatiotemporal location with application of the correct stimulus. Spatiotemporal control of liposomal content delivery is a research field of its own, and the work in this project contributes to that field.

Of heightened interest are the utilization of cell specific ligands for targeted delivery. Folate receptors (FR) are over expressed in their functional form on countless types of cancer cells, including ovary, breast, colon, lung, prostate, nose, throat, and brain cancers.[39] Also, metastatic cancers tend to express FRs at a higher rate than non-metastatic cells.[40] Likewise, FRs are also highly expressed on macrophages involved in inflammatory and autoimmune diseases providing multiple potential targets for folate mediated liposome therapies.[39] Folic acid functionalized liposomes have been successfully applied for the co-administration of multiple chemotherapeutics to FR expressing breast cancer cells.[41] Many folate mediated targeting methods have been successful for the preferred delivery of drugs and imaging agents to cancerous, inflammatory and autoimmune diseased cells.[42-44] One interesting study demonstrated delivery of microbial epitopes to cancer cells through folate receptor mediated delivery. Fusion of the tumor cell with the therapeutic liposome led to expression of the epitopes on the cell surface, activating the immune system causing cytotoxicity via complement mediated cell lysis.[45] Other surface markers that have been targeted by liposomal recognition include CD123. This surface marker is overexpressed on acute myeloid leukemia (AML) cells and increases cell resistance to apoptosis. Anti-CD123 monoclonal antibodies (mAb) were appended to drug loaded PEGylated liposomes for targeting. Specifically, liposomes that are targeted via mAb or antigen binding fragments (Fab') are termed immunoliposomes.[46] Anti-CD123 immunoliposomes were able to effect higher rates of cellular uptake and cytotoxicity versus nontargeted liposomes.[47] CD44 is a classic surface marker of cancer stem cells, a subset of cancer cells that promote malignancy and therapeutic resistance.[48] mAbs against CD44 have been integrated into immunoliposome platforms to increase targeting and cytotoxicity against this potent cell type.[49] Human epidermal growth factor receptor-2 (HER2) is another surface ligand of certain cancer types that has been harnessed for targeted delivery via antibody mediated processes.[50] Essentially, any overexpressed ligand on a deleterious cell surface

has the potential to be targeted for more efficient therapeutic delivery of cargo via active targeting liposomes.

1.3.3. Active vs. Passive Release Mechanisms

While liposomes are effective vehicles for transporting cargo due to their inherent amphiphilic nature, the specific release of cargo at the desired location within the body is key to an effective drug delivery vehicle. PEGylation, targeting ligands, and modification with CPPs help to increase local concentration and fusogenicity of liposomes, but do not directly effect a quick triggered release of drug. There are, however, various methods to trigger cargo release from therapeutic liposomes. These fall into two categories: active and passive release. Active release relies on some form of external stimulus to effect release of molecular cargo while passive release mechanisms utilize internal physiological stimuli, ie conditions within the diseased tissue itself, to effect release. A schematic representation of triggered release mechanisms is shown in Figure 4. Whether active or passive, these release mechanisms rely on one of a handful of methods for release. These are membrane restructuring, deshielding of the liposome, prodrug activation, lipid reconstruction, and conformational switching.

1.3.3.1. Active Release Mechanisms

Active release mechanisms require an input of some external stimulus. This is advantageous in the fact that it limits off target release of cargo. However, external stimuli can be limited by their ability to penetrate through healthy tissue to the diseased area. External stimuli are mainly reliant on photothermal effects, including the application of light, heat, ultrasound, or a magnetic field to induce release.

Light triggered release can be effected by a number of liposomal features. Liposomes loaded with or appended with photosensitizers, such as porphyrin, can increase the production of reactive oxygen species (ROS) upon application of light.

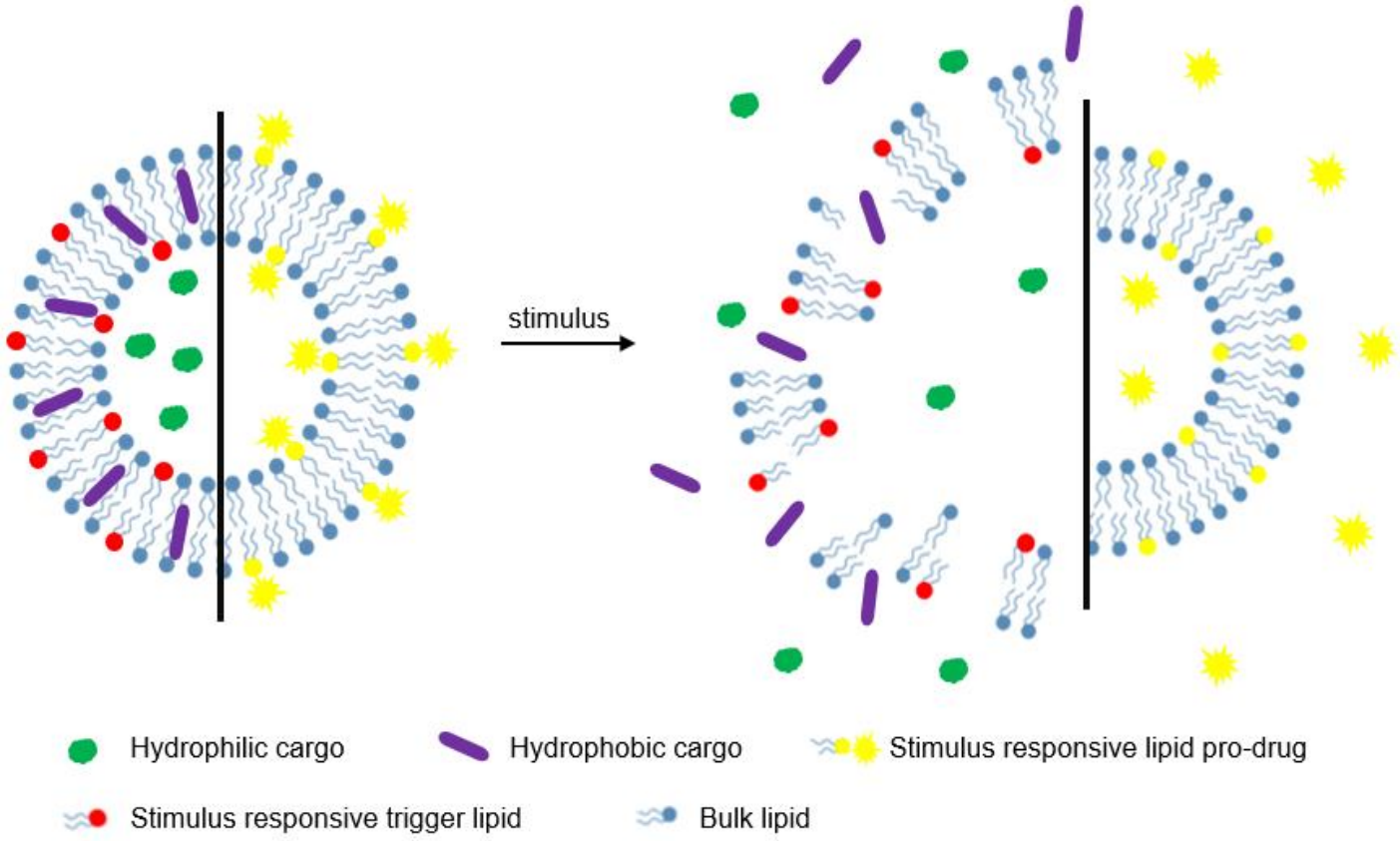

Figure 4. ***A schematic representation of stimuli responsive release of drug cargo from liposomes.*** Liposomes can be loaded with hydrophilic (green) or hydrophobic (purple) cargo in the aqueous core or lipid bilayer, respectively. Prodrugs can also be bound to synthetic lipids at the headgroup as shown in yellow, or integrated as a tail unit (not depicted here). Stimuli responsive lipids (red) can be incorporated for spatiotemporal control of drug delivery. Upon application of stimuli (light, heat, ultrasound, pH change, enzyme, molecular recognition) the drugs are release via membrane destabilization and/or prodrug activation.

These ROS will oxidize any unsaturated points in the lipid tails. This makes the lipid tails less hydrophobic, disrupting the membrane bilayer and effecting release.[51-53] Other methods of light triggered release rely on the light mediated degradation of a lipid's integrity, thereby disrupting the liposome. Photocleavable groups can be incorporated into a synthetic lipid to induce degradation. In one example,an o-nitrobenzyl (ONB) group was incorporated into a synthetic lipid tail.[54] With application of 350 nm light, the ONB group was cleaved, yielding single tailed lipids in the membrane, which are destabilizing to the liposomal integrity. Up to 80% cargo release of hydrophobic cargo was achieved via this method. These both represent lipid reconstruction methods of drug release. Photocleavable groups can also be used to tether a prodrug to the liposomal surface. Again, upon delivery of the liposome to the desired location a specific wavelength of light can be applied locally to stimulate the release and activation of the drug from the liposome surface.[55] In this way, photochemistry can be utilized to deliver molecular cargo from a number of loading sites of the liposome.

Similar to light reactivity, the application of heat itself can cause liposomal release. Lipids have a specific phase transition temperature above which they become more fluid. Phase transition temperatures are intrinsic to specific lipids, so required temperatures to increase membrane fluidity of a given liposomal formulation can be calculated. Localized heating of the diseased tissue will cause increased membrane fluidity, enhancing membrane permeability and effecting release in that area.[56] Unfortunately, these phase transition temperatures are only a few degrees above body temperature. While higher phase transition temperatures can be achieved, the negative side effects associated with the therapeutic application of higher temperatures are prohibitive.[56] Other examples of thermal effects include release through the destabilization of heat sensitive membrane incorporated peptides or polymers and the degradation of encapsulated cargo into gaseous components forming microbubbles.[24, 57] One method to achieve increased localized heating via external stimuli is through the addition of magnetic

nanoparticles in the liposomal formulation. Under application of an alternating magnetic field (AMF) the magnetic nanoparticles, generally iron based, will heat up, giving upconverted localized heating of the liposomes.[24] Ultrasound application can destabilize air pockets in the liposome, leading to their escape and thus destabilization of the liposomal membrane, ie cargo release.[24] All of these effects function under general membrane destabilization as their method of release. These represent spatiotemporal controlled external stimuli for drug release via exogenous methods.

These mechanisms are hindered by the power of their stimulus. The depth of penetration into living tissue for light, laser, heat or ultrasound require that the area for treatment be close to the surface. This limits therapeutic applicability of these systems to certain disease states. Deep tissue tumors, for example, would not be treated efficiently through these methods. These stimuli can also have negative effects on healthy cells. For example, UV light as a stimulus has the potential to harm healthy cells peripheral to the target diseased tissue. For these reasons, passive release mechanisms driven by the physiological differences between diseased and healthy tissue provide a less invasive method for effecting release at a desired point in the system.

1.3.3.2. Passive Release Mechanisms

In passive release, the stimulus for cargo release comes from the diseased tissue itself. These stimuli are mainly changes from normal physiological conditions associated with the target disease. Internal stimuli include lowered pH, increased reducing environment, altered enzyme expression, and increased surface or soluble molecule concentrations. By designing a liposome platform that is sensitive to these conditions, it will release therapeutic cargo only where these altered physiological stimuli are present. These internal stimuli don't suffer from the tissue penetration and localization issues of active release mechanisms, as the stimuli are inherently present at the diseased site. By spatiotemporal control of

cargo release, the dose requirement can be lowered providing a more desirable therapeutic index.

Passive release techniques are a powerful method for harnessing the unique microenvironment of the targeted diseased tissue. Specialized synthetic lipids have been designed to take advantage of these conditions. Lowered pH is one hallmark of cancer cells. As tumor cells rapidly grow, blood vessel formation throughout the new tissue is poorly controlled. This causes a hypoxic, or low oxygen, environment in the tumor and surrounding tissues. To maintain their growth in absence of sufficient oxygenation, tumor cells will switch to anaerobic metabolic pathways causing an increase in the production of acidic metabolites like lactic acid.[58] This build up of acidic products causes a lower pH in cancerous tissues as compared to healthy tissues. This difference in conditions can be utilized as a trigger for selective release of drug cargo at the desired location. Liposome formulations can effect cargo release under acidic conditions by a few different mechanisms. The protonation of susceptible groups such as carboxylates can change the electrostatic interactions of the polar headgroups of lipids in a bilayer. By decreasing the charge balance in the polar section of the bilayer, there is increased repulsion between headgroups and thus destabilization of the membrane.[59] This allows for the use of more classical lipids to effect release under acidic conditions. Another avenue to acid triggered release is the implementation of synthetic lipids that undergo a conformational change upon acidification. Various trans-2-aminocyclohexanol based lipids have been prepared so that protonation of the amino group causes a chair flip due to increased stabilization via hydrogen bonding of the newly protonated amine (Figure 5).[1, 60] In the unprotonated chair structure, the alkyl tails were ideally arranged to insert into a membrane, and after protonation the tails were maximally separated due to the change in conformation from diequatorial to diaxial in respect to the tail substitutions (Figure 5). A di(methoxyphenyl)pyridine based lipid operated similarly where protonation of the pyridine nitrogen led to hydrogen bonding of the

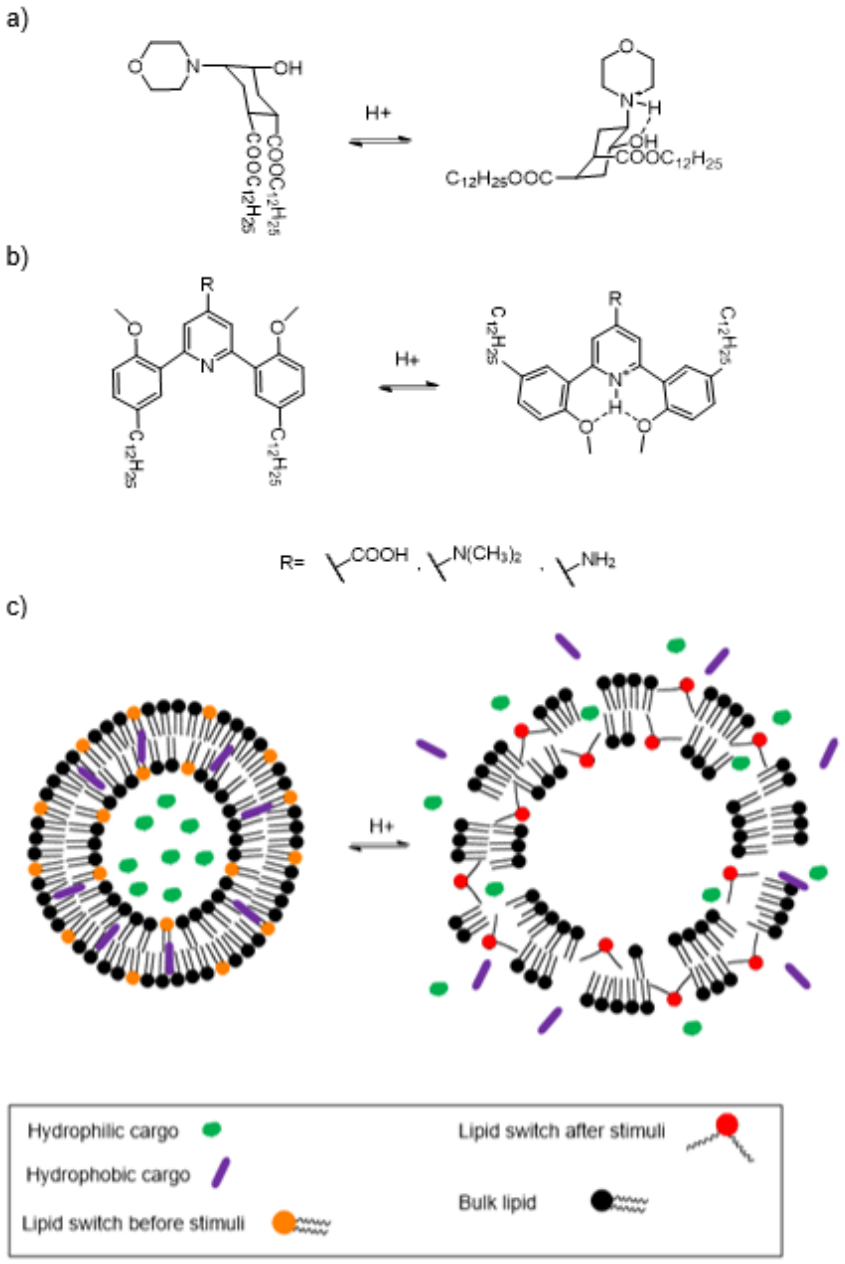

Figure 5. ***Examples of pH responsive conformational lipid switches.*** a) A trans-2-aminocyclohexanol based lipid switch that undergoes a chair flip upon protonation.[1] b) A di(methoxyphenyl)pyridine based lipid switch that undergoes extreme rotation at the headgroup upon protonation.[2] c) A schematic depicting cargo release based upon conformational change lipid switches.

adjacent methoxy groups, which effected maximal separation of the alkyl tails.[2] This changed the orientation of the alkyl tails to one another, increasing the cone angle and disrupting the membrane. Acidic conditions can also be utilized to deshield stealth liposomes. PEGylated liposomes with acid sensitive linkers between the PEG polymer chain and the liposomal surface have been developed. These lipids were formed into vesicles with DOPE, which forms hexagonal phase structures on its own favoring membrane fusion and cargo release. However, in mixtures with PEG-lipid conjugates DOPE can form lamellar structures.[61] Deshielding via the acidic environment revealed the fusogenic, destabilized DOPE liposomal surface leading to a phase change from lamellar to hexagonal phase and a release of contents. The induction of non-bilayer lipids, such as with this method, is a common route for destabilization of liposomes for cargo release. Here, this was achieved through the acid-catalyzed cleavage of vinyl ether, diorthoester, and hydrazone linked PEG-PE conjugates.[61-63] All of these release examples were based on the destabilization of PE based liposomes after the removal of the protective and stabilizing factor of the PEG coating.

Reducing conditions can also lead to drug release from liposomes based on synthetic modifications to the liposome components such as the incorporation of disulfide bonds. As with the acid sensitive method, disulfide linkages can be added between cloaking PEG groups and the liposomal surface. Upon reduction of the disulfide bond, the PEG layer is removed, destabilizing the liposomes and leading to liposome aggregation and cargo release.[64-66] Various other targeting moieties have been coupled with this method, including CPPs such as TAT, whereby the removal of the PEG polymer coating in the reductive environment of the diseased tissue revealed TAT for increased uptake of the liposomes into cells, rather than just destabilization based on the formation of hexagonal phase structures after PEG removal.[65]

The overexpression of certain enzymes in diseased cell lines has also been harnessed for targeted drug delivery. These enzymes include both intra- and

extracellularly expressed enzymes. Lipids for this drug delivery platform have been modified in similar ways to the other passive release techniques. That is, enzymatic activity can effect drug release by a number of methods: destabilization of the membrane through lipid restructuring, enzymatic removal of a polymer (PEG) shielding layer, or activation of a prodrug via enzymatic cleavage.[67] Phospholipase $sPLA_2$ can effect cargo delivery through the restructuring of PE. Enzymatic cleavage of PE into lysoPE and stearic acid prompted membrane destabilization and cargo release from liposomes composed of PE, PC, and PEGylated PE. These were 2.5 times more potent than non-targeted liposomes.[68] sPLA2 is upregulated in prostate, breast, and pancreatic cancers as well as infections where the enzyme is excreted by several bacteria types.[67] Lipid based prodrugs where the enzymatically cleavable tail is replaced with a prodrug have also been designed and applied. Various hydrophobic drugs were successfully released via phospholipase cleavage of the prodrug. This method increases encapsulation efficiency of lipophilic drugs as well as local concentration of drug upon triggered release.[67]

The matrix metalloproteinases (MMPs) compose another family of enzymes upregulated in cancer, where they are associated with angiogenesis. MMPs cleave specific peptide sequences, which can be incorporated into PEGylated liposomes as a deshielding technique. MMP sensitive linkers were inserted as a linker between PE and PEG as an effective means of dePEGylation at target tissue sites. These specific liposomes also had mAb and CPP functionalities that were revealed upon deshielding, providing a multitargeted platform for drug delivery.[69] The ability to combine multiple shielding, deshielding, targeting, and release triggers into a single liposomal platform is one of the desirable advantages to liposomes as a drug delivery system.

1.4. Summary and Implications

Designer liposomes are utilized to control the spatiotemporal release of therapeutic cargo by the incorporation of surface modifications and/or synthetic lipid analogs

into the liposomal composition. These modifications serve to increase circulation time, provide a targeted accumulation of therapeutic liposomes at diseased cells, and trigger release of drug cargo at the desired time and location. Currently, release from liposomes can be controlled via active (external) or passive (internal) stimulus as summarized above. Many of these methods rely on the production of non-bilayer lipids as the means of membrane destabilization to effect release. Passive release techniques present a unique situation where the characteristics of diseased cells can be harnessed to trigger the release of drugs or therapeutic cargo. Current work in this area relies mainly on pH differences between healthy and cancerous cells to trigger a membrane change and effect release. Molecular recognition events would hypothetically create a more specific release potential based on the concentrations of metabolites, enzymes, ions, or other biomolecules that are unique to the target site. This work seeks to utilize molecular recognition of increased ion concentrations to differentiate between healthy and diseased cells. These molecular recognition events will cause the bound lipid analog to undergo a conformational change leading to destabilization of the liposome membrane and thus leakage of encapsulated cargo. Currently, no controlled release strategies have been approved for clinical use, thus advances in controlled release platforms would contribute to the current toolbox of available liposomal release tactics expanding the applicability of liposomes to treat various diseases.

CHAPTER TWO
DESIGN AND SYNTHESIS OF ION RESPONSIVE LIPIDS FOR CONTROLLED RELEASE APPLICATIONS

2.1. Project Summary

The goal of this project is to synthesize a panel of lipid switches for zinc recognition. These lipids, upon binding of Zn^{2+}, will undergo a conformational change proposed to shift the lipid shape from a membrane supportive structure to a non-bilayer lipid leading to the destabilization of the surrounding membrane environment. By including these lipid switches in liposomal formulations, we can control membrane stability, and by extension content release, based on the ion concentration of the surrounding media. This platform is of specific interest for delivery of therapeutic cargo to diseased tissues in which local zinc concentrations are elevated including ischemic tissues, neurodegenerative diseases, and certain cancer types.[3-8] Through this platform, we propose to harness a physiological difference between healthy and diseased tissues, creating a new passive release technology.

2.2. The Biological Role of Zinc

Zinc is an essential element present at trace amounts in the human body. The bulk of zinc is bound to proteins, with approximately 10% of all human proteins containing zinc in its bound state.[70] In these proteins it plays structural and catalytic roles, being involved in the function of approximately 300 different enzymes.[71] The remaining minor fraction of zinc exists as its labile ion form. Free zinc is present at very low concentrations within the cytosol of cells, at estimated subnanomolar concentrations. The bulk of free zinc is tightly regulated in storage. Zinc importer proteins (ZIP) and zinc transporter proteins (ZnT) act to shuttle zinc in and out of the cytosol, respectively. These proteins are present in the cellular membrane as well as vesicular membranes including those of storage vesicles, endoplastic recticulum, mitochondira, and the golgi where they shuttle excess zinc for storage.[3] Zinc that is not stored in these subcellular compartments is buffered

by reversible binding to metallothionein (MT), a metal binding protein that will release free zinc upon receiving the appropriate signal.[72-73] Free zinc concentrations are increased in neuronal cells undergoing apoptosis as a consequence of ischemia or trauma in the brain.[3] Zinc dysregulation is also involved in certain cancers.[4-6] Chelation therapies have been applied for the treatment of Alzheimer's disease, further providing that zinc is a worthy target for a therapeutic platform.[7-8] In this work, a lipid switch will be designed so that upon recognition of Zn^{2+} conformational changes will drive cargo release.

2.3. Molecular Recognition Events as Stimuli for Cargo Release via Lipid Switches

This work specifically focuses on the utilization of lipid switches as a cargo release tactic, a newly developing approach based on the molecular recognition of upregulated ions or metabolites to effect cargo release from a liposome. This research will serve to expand the current available toolbox of controlled release tactics which is currently limited. Various physiological stimuli for cargo release have been discussed thus far, and while ion recognition falls into that category, it will be covered in detail now. Lipid switches, similar to the conformational release lipids discussed in the pH responsive section, rely on membrane destabilization to effect release. Recognition of the target molecule by a synthetic lipid switch leads to a conformational change of the lipid and thus a change in its membrane support characteristics. This method has been applied for the recognition of overexpressed surface markers of cancer cells, altered membrane compositions, and upregulated ion concentrations in diseased cells.[74-76] A boronic acid lipid was synthesized for molecular recognition of carbohydrates, which are overexpressed on cancer cell surfaces. Liposomes containing this molecular recognition lipid were shown to bind and enhance cellular delivery.[76] Liposomal membrane restructuring via multivalent recognition of carbohydrate moieties was the primary method of cargo delivery, where increased movement of the recognition lipid within the membrane caused increased membrane permeability.

Ion recognition events are another interesting method for membrane destabilization. For example, a calcium-responsive lipid switch was designed such that upon calcium chelation the lipid underwent a conformational change from membrane supportive to membrane destabilizing. Here, a previously described calcium sensor[77] was modified to suit the lipid requirement for membrane insertion. Alkyl tails were appended to the calcium sensor rather than a fluorescent indicator as in the original sensor. Through chelation with the carboxylate moteifs present at the lipid head, binding dependent cargo release was achieved (Figure 6) .[74] The lipid switches including the pH responsive examples discussed in section 1.3.4.2. undergo similar conformational changes where protonation and hydrogen bonding can be considered a type of molecular recognition.[1-2, 60] Specific to the interest of this work, other ion responsive lipids have been seen in literature as well. These include copper and zinc responsive lipid switches. A bispidinone based lipid was utilized to recognize copper via electrostatic interactions between nitrogens and Cu^{2+}, effecting a boat-to-chair conformational change at the headgroup causing convergence of the alkyl tails. Even though the tails became less distanced from one another via this chelation event, release was still seen with the application of Cu^{2+}. This shows that perturbation of the membrane in general by conformational changes may be enough of a driving force for efficient cargo release. A final example on ion chelation operates slightly differently than the previous examples. Dimeric zinc chelates of a sugar based lipid preferentially formed liposomes, where treatment of liposomes containing the zinc chelate with acid caused removal of the zinc from complexation via protonation, which effected cargo release.[78] These pre-complexed lipids were found to increase delivery of internalized cargo to gastric cancer cells, based on the inherent acidity of cancerous tissues.

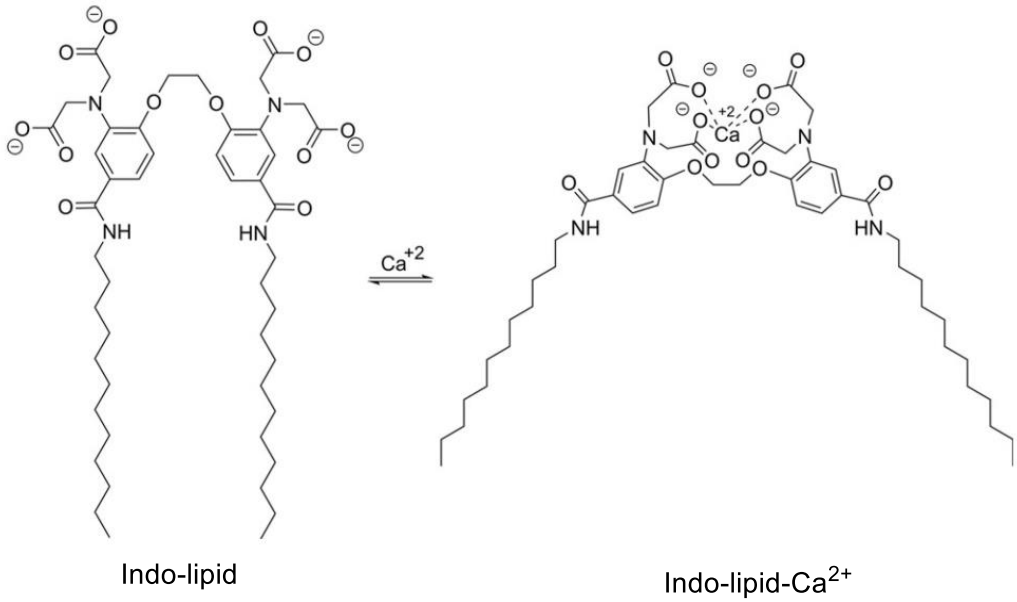

Figure 6. ***Calcium triggered lipid switch***
Lipid switch based on a fluorescent calcium sensor, indo-1. Titration with Ca^{2+} effected 65% release of hydrophobic dye nile red from liposomes containing 10% of Indo-lipid with PC comprising the remainder of the membrane.

2.4. Design Inspiration and Considerations for Zinc Switchable Lipids

In regards to the design of a zinc responsive lipid switch, we drew inspiration from previous work with the study of zinc chelating molecules. Trispicoylamine (TPA) and N,N,N′,N′-Tetrakis(2-pyridylmethyl) ethylenediamine (TPEN) are two well-known zinc chelators (Figure 7). They bind zinc with high affinity with dissociation constants of 10 pM and 0.3 fM, respectively.[79] Also, these chelating groups bind preferentially to zinc over other biologically available divalent transition metal cations such as iron or manganese, as predicted by the Irving-Williams series.[79-80] These nitrogen based chelators vary in the pK_a of their central tertiary nitrogens, wherein TPA exhibits a pK_a of 6.17 and TPEN has a pK_a 7.19. This makes TPA less likely to be protonated at physiological pH, resulting in more operational chelator available in the biological setting.[79] These pyridal core structures have been utilized to visualize zinc concentrations in live cells and tissues.[81-84] By appending a fluorescent molecule to the general TPA structure, a fluorescence turn on effect was seen following the chelation of zinc (using Zinpyr-1, Figure 7).

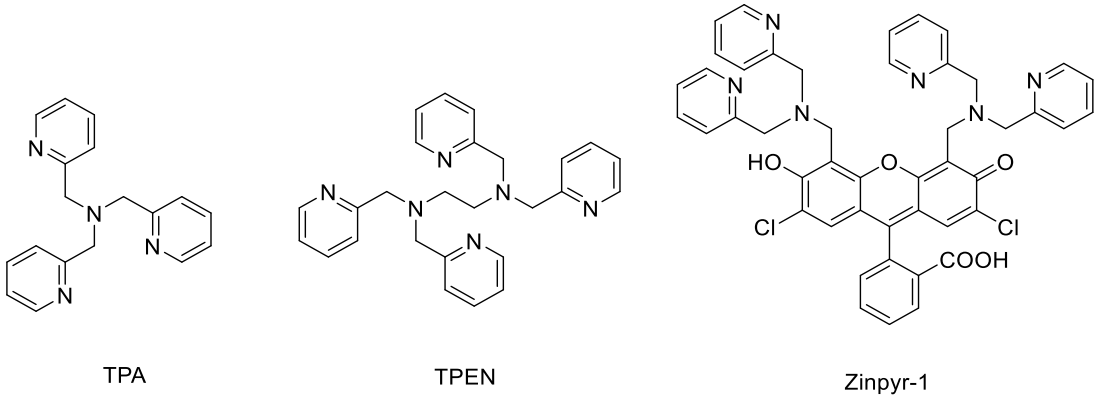

Figure 7: ***Zinc cheating molecules.***
Structures of pyridal zinc chelating molecules TPA and TEPN. Zinpyr-1 is a flurosecence turn-on probe for the detection of zinc in solution or the biological setting.

For our purposes, we do not require a fluorescent indicator. We instead envision using the chelator core structure as the polar headgroup of a lipid. Rigidly attached tails will build in the conformational change aspect that is required of the lipid and thus effect release of cargo upon binding of zinc to the chelating lipid core (Figure 8). In this manner we will be able to control membrane stability and by extension cargo delivery based on membrane composition of the given liposome. In the next sections, synthesis of lipids based on these design principles will be discussed.

2.5. Design and Synthesis of Zinc-Responsive Lipid ZnR1

2.5.1. ZnR1 Synthesis

Zinc responsive lipid ZnR1, Figure 9, was the original design for a zinc triggered lipid. In this structure, a TPA core is appended with three alkyl tails attached via amide linkages. These tails are attached at the 4-position of the pyridine subunit, allowing the alkyl tails to rest comfortably within a membrane bilayer when in the unbound state.

Synthesis of ZnR1 (Figure 9) began with the diesterification of commercially available 2,4-pyridinedicarboxylic acid. This acid catalyzed ester formation quantitatively gave intermediate Z1.1.[85] This diester intermediate then underwent a selective reduction with sodium borohydride to give aldehyde Z1.2.[86] The aldehyde functionality was utilized to perform successive reductive aminations in a one pot approach, yielding the TPA core bearing three pyridine esters in a 49% yield as intermediate Z1.3.[87] This gave the TPA core in good yield over few steps, as compared to previous attempts to form the TPA core via successive S_N2 substitution reactions (see further discussion below).

The addition of the amide tails was approached from a number of synthetic angles. The necessity of repeated additions to the trifunctionalized core was a stumbling

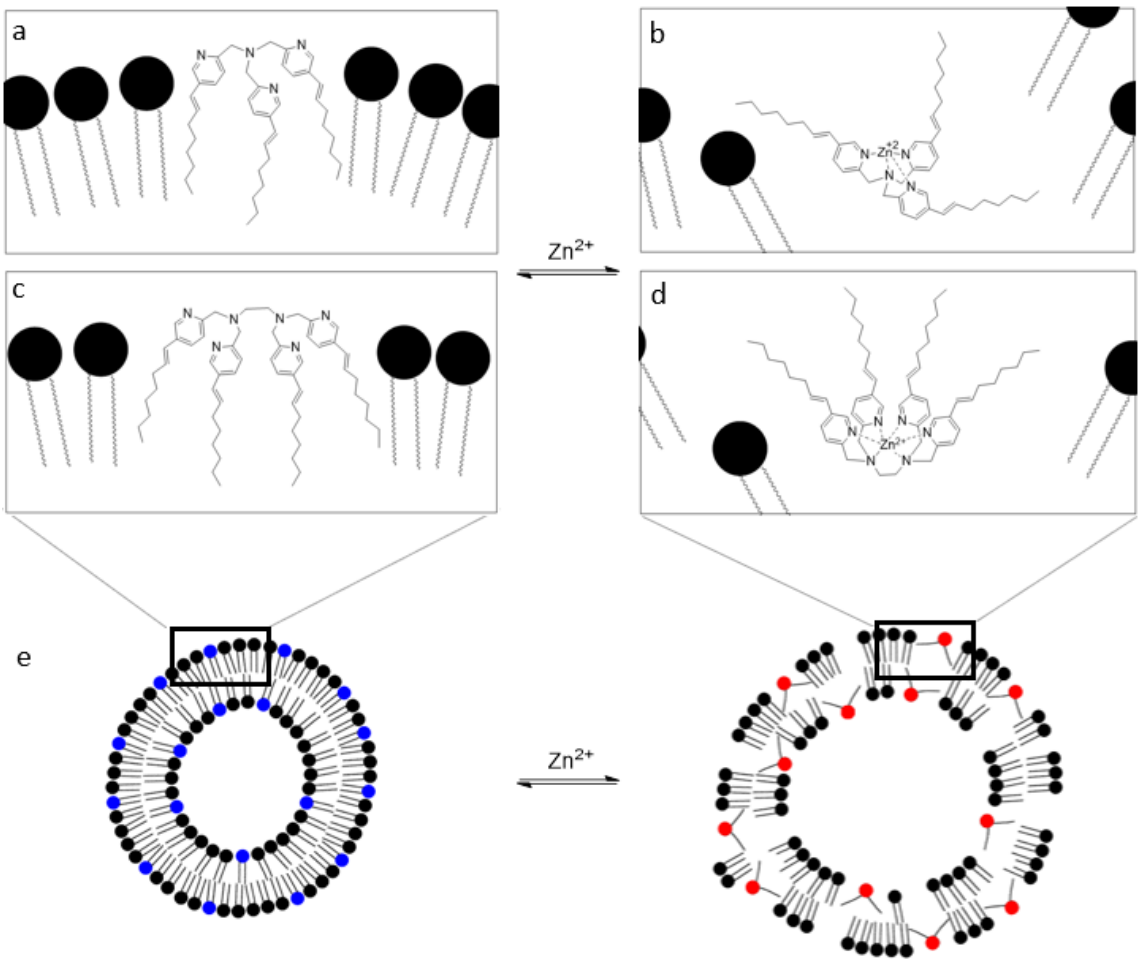

Figure 8. ***Proposed membrane disruption by zinc responsive lipid switches***

Lipid targets ZnR2.2 (panel a, TPA based) and ZnR3.1 (panel c, TPEN based) are depicted in their unbound state, inserted comfortably into the membrane bilayer. Upon treatment with Zn^{2+}, the lipid switches are proposed to bind zinc in a 1:1 ratio to give ZnR2.1-Zn^{2+} (panel b) and ZnR3.1-Zn^{2+} (panel d). The lipid switches are designed such that they take on non-bilayer lipid shapes upon binding with zinc. e) A schematic representation of the unbound lipid switches (blue) in a stable liposome and membrane destabilization caused by titration with zinc forming zinc-bound lipids (red) that have undergone the proposed conformational change.

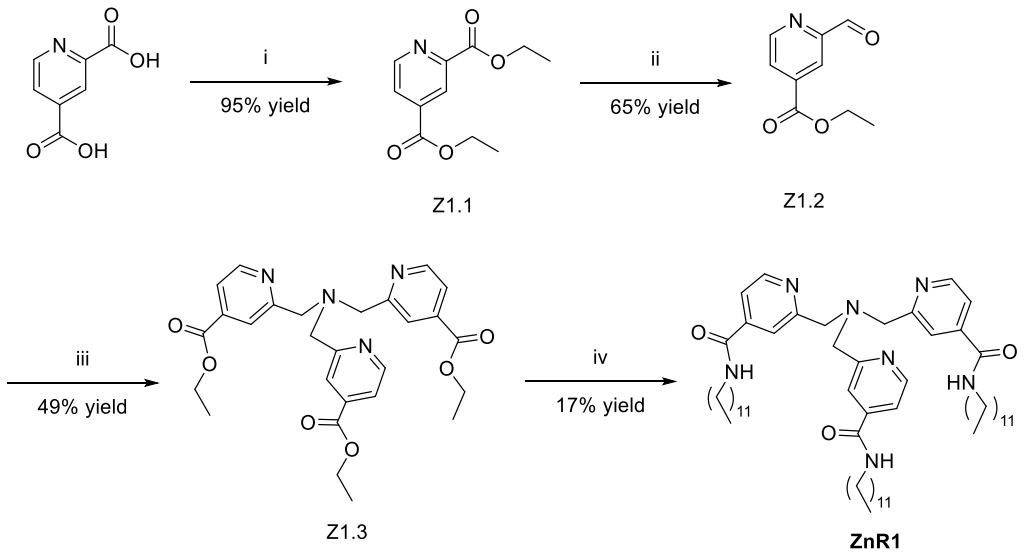

Figure 9. ***Synthesis of zinc lipid switch ZnR1***
Conditions: i) TsOH, EtOH, reflux ii) DIBAL-H, -78°C, dry THF iii) NH_4OAc, $NaBH(OAc)_3$, dry DCM iv) dodecylamine, DIBAL-H, dry THF, 0°C→ R.T. then Z1.3

block. While more traditional methods were originally pursued, ultimately an aminolysis of the ester groups was utilized. This was accomplished by activation of the tail precursor dodecylamine with DIBAL-H. Usually, DIBAL-H is used as a reducing agent. Here, as exemplified in the work by Huang et al where they prepared a number of ethylbenzoate derivatives via organometallic complexes of various amines with DIBAL-H, it is used to activate an amine for aminolysis of an ester.[88] This was key to overcoming previous complications with the addition of the tails. Other synthetic approaches involved proceeding through a hydrolyzed intermediate of the triester Z1.3. This intermediate, bearing three carboxylic acid functionalities, was very polar causing solubility issues as well as problems in the purification of said intermediate (see further discussion below). By utilizing these aminolysis conditions, we were able to bypass that troubled intermediate and proceed directly to the desired amide. This reaction also utilized an excess of a very reactive species, the organometallic complex, leading to full conversion of the triester to triamide, which was key to completion of this synthesis, as other synthetic methods, described below, failed to effect conversion of all three tail precursor units to the desired amide bonds. All of these considerations together led to the aminolysis method being an overall better route to pursue for completion of the target lipid.

2.5.2. Alternate Pathways to ZnR1

In the pursuit of lipid ZnR1, many synthetic routes were taken. Alternate pathways yielding interesting intermediates are given below. These attempts were focused on either first constructing the TPA core and then adding the alkyl tail units, or vice versa.

An alternate attempt to synthesize triester compound Z1.3 (Figure 10) was aimed at forming the TPA core via successive S_N2 substitutions to synthesize the central tertiary amine. This approach was hindered by the instability of intermediates containing a leaving group at the pseudo-benzylic position of the pyridine subunits

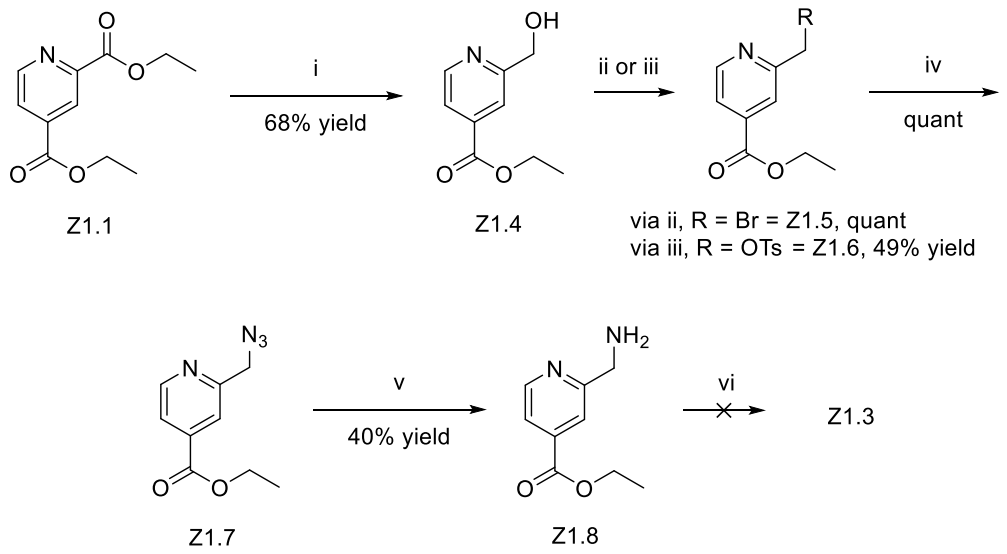

Figure 10. ***Alternate synthetic pathway to lipid intermediate Z1.3.*** Conditions: i) $NaBH_4$, $CaCl_2$, 0°C, degassed EtOH ii) PBr_3, dry DCM iii) p-TsCl, TEA, DMAP, dry DCM iv) NaN_3, dry DMF, 85°C v) 10% Pd/C, H_2, EtOAc vi) Z1.5 (or Z1.6), $LiCO_3$, dry DCM

which led to no quantifiable conversion of these intermediates to the desired tertiary amine core. These synthetic approaches will be discussed next.

The alternative synthesis of intermediate Z1.3 began with a selective reduction of intermediate Z1.1. The diester was selectively reduced at the 2-position adjacent to the pyridine nitrogen through the use of $CaCl_2$ to chelate that specific ester. This allowed for the selective reduction to an alcohol at the 2-position over the other available ester at the 4-position.[85] This reduction proceeded well to give intermediate Z1.4. The alcohol functionality was then transformed to a leaving group as bromine or tosylate in intermediates Z1.5 and Z1.6, respectively. To install the necessary nitrogen into the organic skeleton, a substitution reaction with sodium azide quantitatively gave intermediate Z1.7, which was reduced to primary amine Z1.8 through palladium catalyzed hydrogenation. Then, the primary amine of compound Z1.8 was reacted with two equivalents of either compound Z1.5 or Z1.6 to target triester Z1.3. This final successive S_N2 reaction was not successful due to the instability of intermediates with a leaving group at the pseudo benzylic position of the pyridine ring. This led to poor to no conversion to target compound Z1.3. It was then that the reductive amination pathway as described in the previous section was designed and pursued successfully, effectively bypassing the unstable intermediates and shortening the overall synthesis of Z1.3 from 6 to 3 steps.

With intermediate Z1.3 in hand, a number of methods for incorporating the alkyl tails were considered (Figure 11). The most classical way to construct an amide bond is through the activation of a carboxylic acid precursor with carbodiimide chemistry and subsequent attack by an amine yielding the desired amide bond. The required carboxylic acid precursor, Z1.9, proved difficult to purify and collect due to the polarity of the three carboxylic acid moieties within the molecule. This led to a thorough search of the literature to devise a new tactic for the incorporation of the three alkyl tail units. Kim et al published the direct amidation of various esters including ethyl isonicotinate with aromatic and aliphatic amines in the

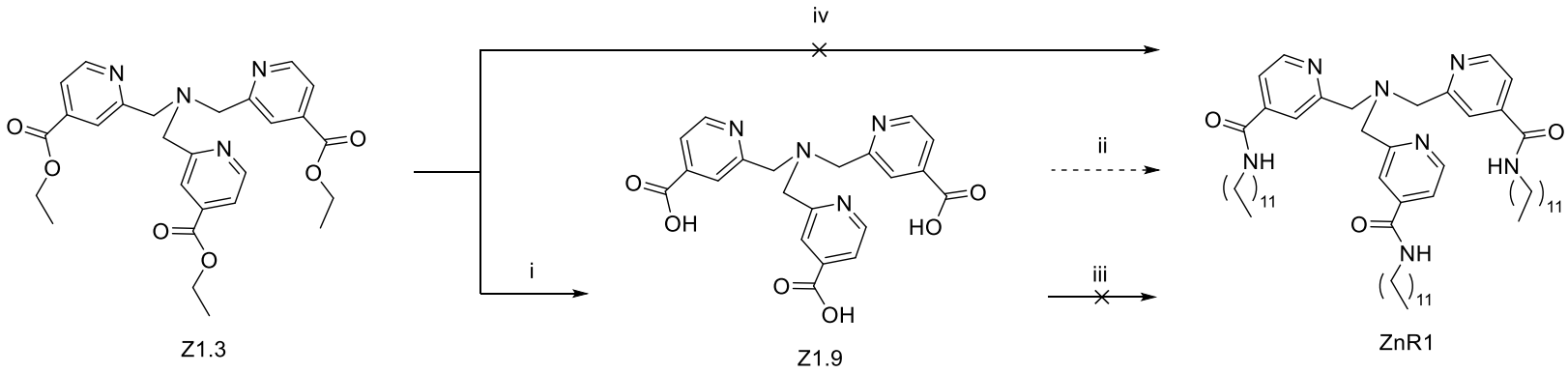

Figure 11. ***Alternate pathways for the synthesis of lipid ZnR1 from common intermediate Z1.3.***
Conditions: i) 2 M KOH, THF, 100°C ii) DCC, dodecylamine, DMAP iii) 1) $SOCl_2$, DCM 2) Dodecylamine, TEA, dry THF iv) KOtBu, dodecylamine, THF

presence of KOtBu under a proposed peroxide mediated mechanism.[89] These were achieved in good yields over short time periods, 5-60 minutes in most cases. However, the application of these conditions to triester Z1.3 did not yield the desired amide bonds. Next, an acid chloride version of Z1.3 was targeted to increase the reactivity of the carbonyl groups. To this end, intermediate Z1.3 was converted to carboxylic acid Z1.9 by refluxing with KOH and used without purification beyond an extractive workup. The triacid chloride was prepared and used directly for the next reaction without characterization. Full conversion of Z1.9 to acid chloride was monitored by the disappearance of the starting material spot (Z1.9) via TLC. Subsequent reaction with dodecyl amine did not provide the target compound ZnR1. Possible pitfalls of this avenue include the presence of three reactive or highly polar carbonyl groups attempting to couple with a long chain saturated amine causing solubility issues along with the inability to purify these highly polar intermediates. Ultimately, due to the combination of these issues, a new approach was devised to incorporate the three alkyl tail units. It was here that the aminolysis conditions utilizing DIBAL-H described in section 2.5.1 were applied successfully.

Concurrent with the previously described syntheses, attempts to construct individual pyridine tail units and then trimerize them were also considered (Figure 12). Again, the classical approach of carbodiimide coupling was pursued first. First, the ester of intermediate Z1.4 was hydrolyzed to give carboxylic acid intermediate Z1.10. This was coupled via carbodiimide chemistry with dodecyl amine. However, this was unsuccessful and did not yield intermediate Z1.11. The direct amidation with KOtBu conditions as given in the last section were applied to both intermediates Z1.4 and Z1.2. The reaction with Z1.4 yielded only starting materials without conversion to product. This was most likely due to the potassium tertbutoxide deprotonating the alcohol rather than interacting with the ester functional group was required for the desired transformation. Application of the same conditions to Z1.2 also did not yield the desired product, however the

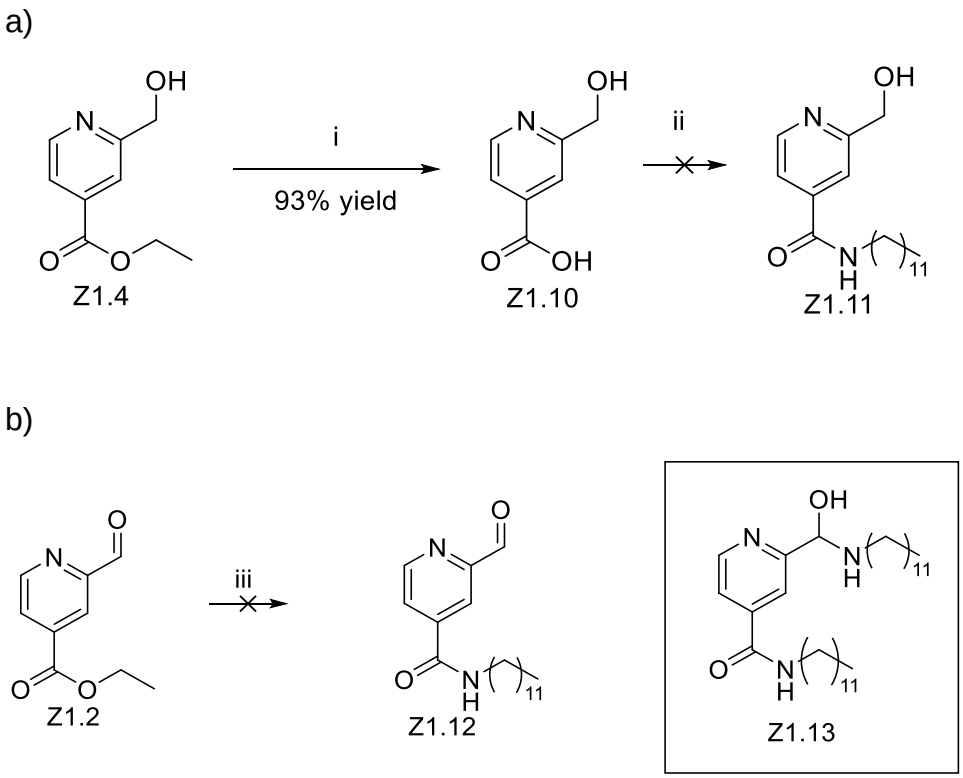

Figure 12. ***Alternative pathways to single pyridal tail units toward ZnR1.*** a) Formation via classical carbodiimide chemistry. Conditions: i) 2 M KOH, THF, 100°C ii) EDCI, dodecylamine, DMAP, dry DMF b) Formation of amide bond via direct amidation led to the hemiaminol Z1.14 rather than desired intermediate Z1.13. Conditions: iii) 1) $SOCl_2$, DCM 2) dodecylamine, TEA, dry THF

attempted conversion of Z1.2 to an acid chloride and subsequent substitution with dodecyl amine gave interesting results (Figure 12). The desired single tailed aldehyde Z1.12 was not formed, instead the hemiaminol Z1.13 was recovered. This was due to the conversion of the aldehyde unit to a geminal halohydrin and subsequent substitution of the chloride with dodecyl amine. Attempts to reverse the hemiaminol and eliminate the long chain amine were not successful and although this was not the desired outcome it did reveal the possibility for reactivity through this particular mechanism at the pyridal ethyl ester position, which could be useful information for future synthetic endeavors. It also supports the notion that previous TPA intermediate Z1.9 was probably the issue with the syntheses laid out in Figure 11, as the desired ester hydrolysis reaction was able proceed through a single version of the ester intermediate (Z1.4, Figure 12). Through the investigation of parallel synthetic routes, the formation of triester intermediate Z1.3 and direct conversion to ZnR1 via the aminolysis reaction described above provided the shortest and most straightforward route for the synthesis of the desired lipid.

2.5.3. Liposomal Release Studies with ZnR1

With lipid target ZnR1 successfully synthesized, next began liposomal release experiments. Liposomes containing 0, 10, and 20% of ZnR1 were investigated for their triggered release potential.

For all experiments, liposomes were formed via the thin film hydration method.[23] Stock solutions of lipids ZnR1 (5mM), PC (32mM), and hydrophobic dye nile red (5mM) were prepared in chloroform, with ZnR1 in a 1:1 mixture of chloroform and methanol. Lipids were aliquoted to clean, dry vials to prepare the desired lipid ratios at 2mM total lipid content. For example, to create liposomes containing 10% ZnR1 lipid, 13.3 μL of PC stock, 10 μL of ZnR1 stock, and 5 μL of nile red stock were combined in a clean, dry vial. The resulting solution was dried under a stream of nitrogen until all solvent was removed. The vial containing the lipid film was

then dried further under high vacuum to assure complete removal of residual solvent. Then, 250 μL of MilliQ purified water was added to the vial and the film was hydrated at 60°C for 45 minutes with vortexing every 15 minutes. The resulting liposome solution was put through ten freeze-thaw cycles with a dry ice/acetone bath and 60°C water bath. This gave a solution of non-uniform size or lamellarity vesicles which were then extruded 15 times through a 200 nm polycarbonate membrane to yield a solution of 200 nm diameter liposomes encapsulating nile red. These same methods of thin film hydration and extrusion were used to prepare all liposomes for this work.

To determine the release profile of ZnR1, prepared liposomes were titrated with Zn^{2+} wherein release would be indicated by a decrease in fluorescence upon precipitation of the hydrophobic dye with its release into the aqueous media. The choice of the zinc salt for the titration solution preparation became quite important in this case. In aqueous solutions of $ZnCl_2$, insoluble precipitates of zinc compounds are formed, lowering the Zn^{2+} concentration. Also, aqueous $ZnCl_2$ solutions are more acidic (pH ~2) than those formed from other zinc salts. 0.5 and 0.1 M solutions of zinc acetate in MilliQ water were found to have a pH of ~7, which was more desirable for our uses.

Initial fluorescence studies were completed with liposome solutions of 0, 10, and 20% ZnR1 with PC, hydrated in milliQ water. In each case, 100μL of liposome solution was added to a 50μL well microcuvette. An initial fluorescence reading was taken from 560 – 700 nm with excitation wavelength of 552 nm and the liposome solution was then titrated with a 0.1 M aqueous solution of $Zn(OAc)_2$ to a total zinc concentration of 10 mM. No significant release over the control liposomes (0% ZnR1) was seen for either the 10 or 20% ZnR1 liposomes. Dilution studies were also conducted where 50 μL of the given liposome solution was diluted to a final volume of 3 mL with MilliQ water giving a lipid concentration of 0.033 mM. Again, titration from 0 to 10 mM $Zn(OAc)_2$ resulted in no significant

release of dye in any case. Problems with release were attributed to the electronegativity of the neighboring carbonyl groups, drawing electron density from the TPA nitrogens. A more electron poor TPA molecule would result in a dampened chelation ability and thus hamper release. To combat this, other lipid skeletons were designed, as will be described in the next sections.

2.6. Design and Synthesis of Zinc-Responsive Lipids of ZnR2 Type

Lipids of type ZnR2 were designed with differing tail connections. In contrast to the electron withdrawing amide tails of ZnR1, these lipids exhibit a variety of bond types (Figure 13). The zinc chelating core is the same, with these lipids being based on TPA as well. The synthesis of these lipids proceeds through a common intermediate, lending the quick accumulation of target compounds via these methods.

2.6.1. Synthesis of ZnR2 Type Lipids

Synthesis of lipid ZnR2.1 (Figure 14) began with the formation of common intermediate Z2.1. This is a core-first approach similar to that utilized to synthesize lipid analog ZnR1. Beginning with commercially available 5-bromo-2-pyridinecarboxaldehyde, the TPA core was constructed by sequential reductive aminations forming primary and secondary amine intermediates in situ, giving intermediate Z2.1 at a 96% yield.[87] Toward ZnR2.1, the bromine functionality was utilized to perform a Sonogoshira coupling with 1-dodecyne. Despite varying conditions, full conversion of all three bromide substitutions to alkyne tails was not achieved in any appreciable yield, though product was detected by mass spectroscopy. Other avenues were explored to increase conversion. Rather than beginning with the fully constructed TPA core, individual pyridine-alkyne tail units were synthesized (Figure 14). This synthesis began with the same 5-bromo-2-pyridinecarboxaldehyde starting material that was utilized to form intermediate

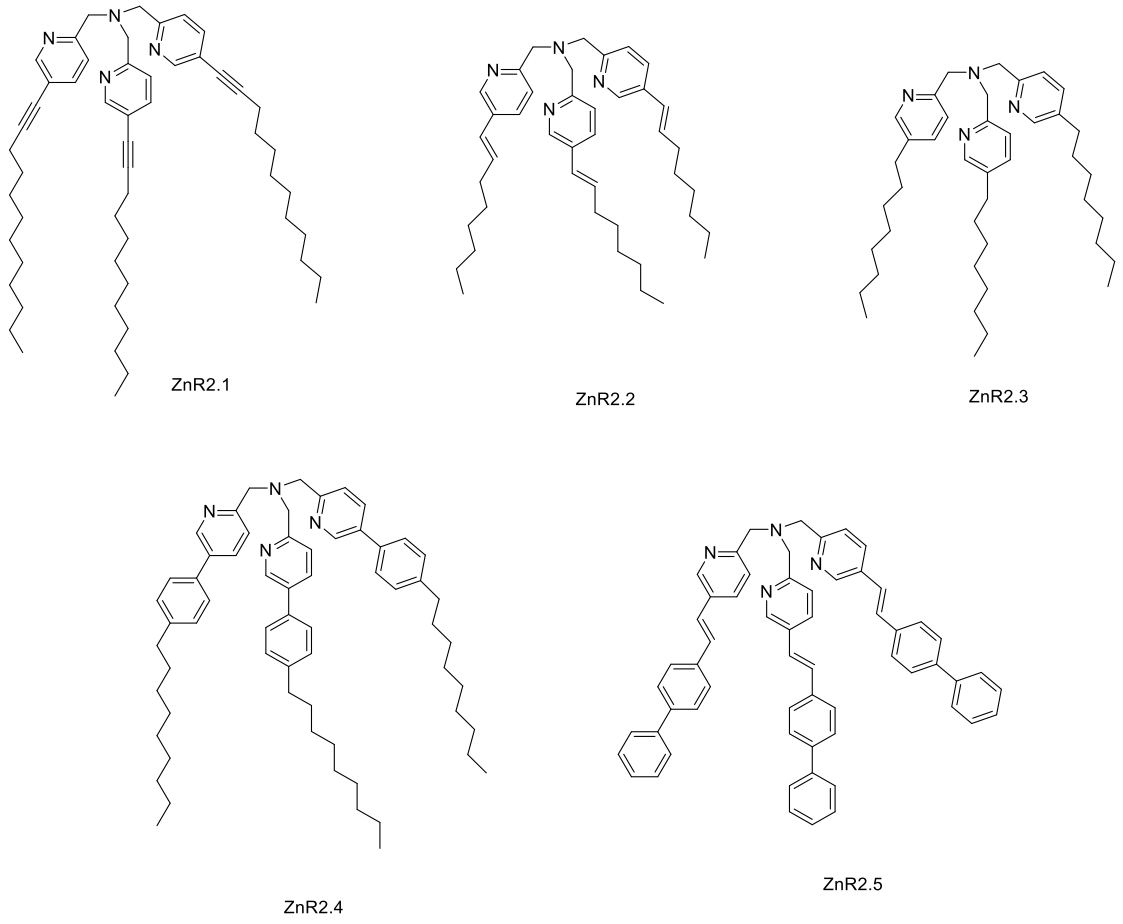

Figure 13. ***Structures of lipid targets ZnR2.1 – ZnR2.5.***
These lipids stem from a common TPA core intermediate. Tails of varying saturation and rigidity are designed to test the dependency of release on the structure of the lipid tails.

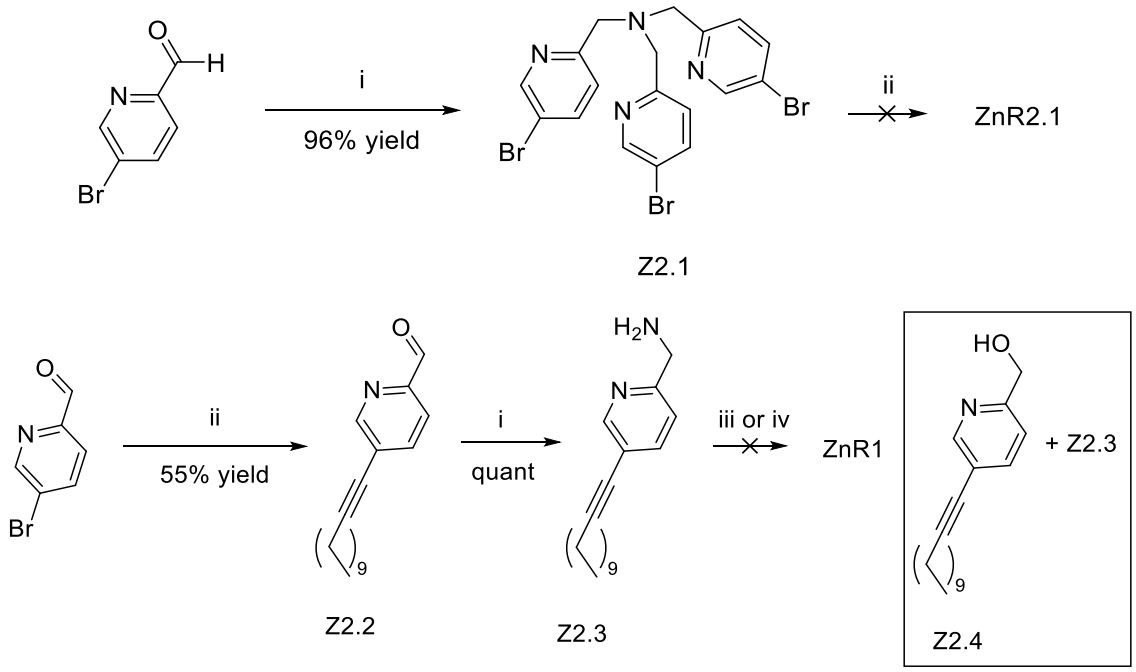

Figure 14. ***Synthetic steps toward ZnR2.1***
i) NH_4OAc, $NaBH(OAc)_3$, dry DCM ii) 1-dodecyne, $PdCl_2(PPh_3)_2$, CuI, 5:1 DMF:TEA iii) Z2.2, $NaBH(OAc)_3$, dry DCM iv) 1) Z2.2, TEA, toluene, Dean Stark trap, 100°C 2) $NaBH_4$

Z2.1. It was coupled successfully with 1-dodecyne in a palladium catalyzed cross coupling reaction to yield intermediate Z2.2. One pot reductive amination conditions toward formation of the TPA core gave primary amine Z2.3 as the sole product. Attempts to perform stepwise reductive aminations were also unable to proceed past the primary amine intermediate. Tested conditions depicted in Figure 14 include the reaction of aldehyde Z2.2 with primary amine Z2.3 with sodium trisacetoxyborohydride as the reducing agent, which gave only recovery of starting materials and none of the desired product, ZnR2.1. Stepwise reductive aminations with sodium borohydride as the reducing agent were also attempted, but only the starting primary amine Z2.3 and the reduced version of aldehyde Z2.4, where the aldehyde was reduced to a primary alcohol, were recovered in any case. The amphiphilic nature of the starting materials may cause solubility issues hampering the desired reactions. It was due to the hinderance of these steps that other lipid targets were also pursued.

Lipid ZnR2.2 was targeted next. Common intermediate Z2.1 was coupled with boronic acid precursor trans-octenylboronic acid via a palladium catalyzed Suzuki-Miyaura coupling reaction, modified from the similar reaction scheme of Bravin et al to suit these specific synthetic needs.[87] The successful coupling gave lipid ZnR2.2 at 34% yield (Figure 15). Based upon this success, other boronic acid derivatives can be utilized for the Suzuki-Miyaura coupling step to target TPA core lipids ZnR22.3-ZnR2.5.

2.6.2. Liposomal Studies with ZnR2 Type Lipids

With the completion and characterization of ZnR2.2, it was immediately utilized for liposomal studies. Lipid ZnR2.2 was prepared at a 10 mM stock in chloroform and liposomes were formed by the same techniques from section 2.5.3. Liposomes of 0, 10, and 20% ZnR2.2 hydrated with MilliQ water were prepared at 2 mM and 0.033 mM dilute liposome samples, as previously described. Titration with aqueous $Zn(OAc)_2$ provided no release in any case, leading to a reevaluation of

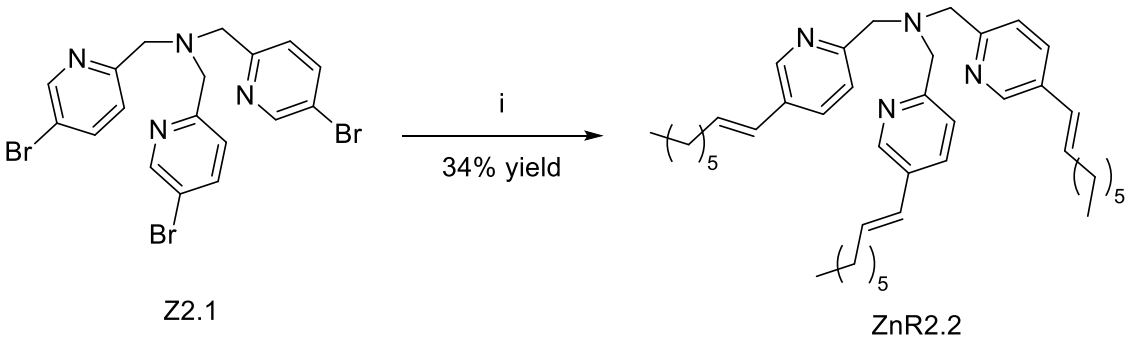

Figure 15. ***Synthesis of ZnR2.2***
Conditions: i) trans-octenylboronic acid, $Pd(PPh_3)_4$, K_2CO_3, DMF/toluene/H2O 100°C

the proposed release method. The draw of TPA was its selectivity for zinc over other divalent metal ions. This selectivity is attributed to the small binding pocket of the TPA core as compared to TPEN along with a more desirable pK_a.[79] This could be negatively impacting the conformational change aspect of this platform. The TPA unit would idealy be presented at the aqueous interface of the liposome surface where, based on hydrophilicity, the nitrogens of the pyridine rings along with the central tertiary nitrogen could be oriented upward, essentially preforming a binding pocket for zinc to fall in to (Figure 16). If this is the case, there would not be a large conformational change between bound and unbound states of the switch. This would explain the failure of both ZnR1 and ZnR2.2. There also exists a pH dependency of these lipid analogs. At low pH, 6.2 or below, a large portion of TPA becomes protonated.[79] As modeled in Figure 16, protonation of the central nitrogen of TPA will facilitate the preformation of the proposed zinc binding pocket, further dampening the conformational change aspect of these TPA based lipid analogs.

To determine if the lipids were capable of chelating zinc and to rule out a lack of binding as the reason for lack of release, UV-Vis studies were performed. Solutions of 40 μM of lipids ZnR1 and ZnR2.2 were prepared in pH 7.45 PIPES buffer. An initial scan of UV-Vis absorbance was taken. Then, a sample that was 40 μM in lipid and 200 μM in $ZnCl_2$ was prepared and UV-Vis spectra were collected at time 0, 10, and 20 minutes. ZnR1 did not exhibit a specific pattern in changes, further strengthening the previous assertion that its more electron withdrawn TPA core will not bind zinc strongly. However, ZnR2.2 showed a steady decrease in absorbance at ~283 nm. This can be attributed to the chelation of zinc decreasing the absorption of the TPA core.[79] This indicates that lipid ZnR2.2 is capable of chelating zinc, adding more weight to the argument that the presentation of TPA at the surface is preformed in an ideal conformation for the acceptance of zinc. Taking these results into consideration, a shift was made in

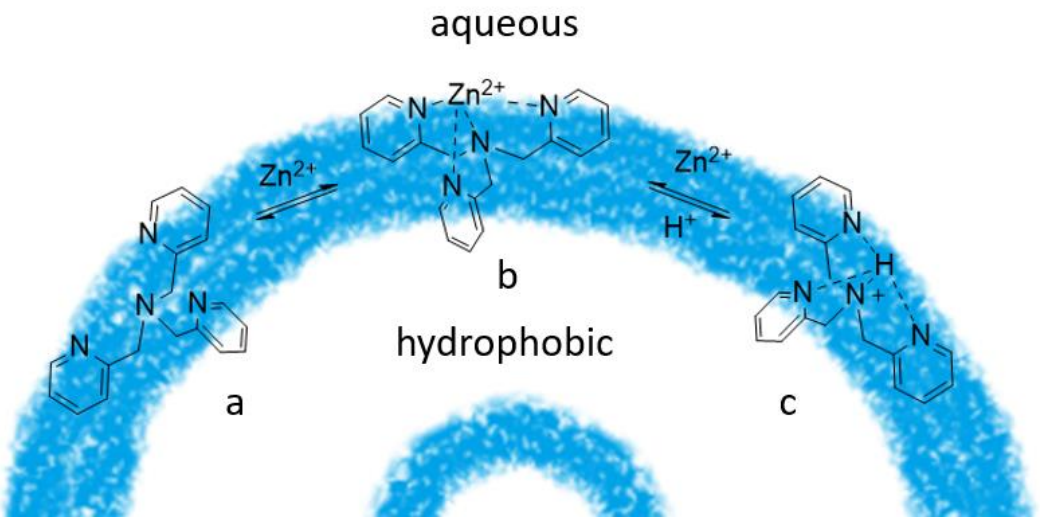

Figure 16. ***Optimal presentation of TPA core at the aqueous interface of the liposomal membrane***
All nitrogen units will be oriented upward to the aqueous interface, preforming a binding pocket for incoming Zn^{2+} ions (structure a). This may not lead to a large conformational change of the core upon chelation (structure b), thus dampening release. Protonation of the central TPA nitrogen may also lead to pre-organization of the pyridal units (structure c) strengthening the preformed binding pocket for zinc.

synthetic efforts to also target a different zinc chelator as the lipid core, as will be expanded on in the next section.

To further investigate the pH dependence of the binding ability of ZnR2.2, liposomes composed of 0, 25, 50 and 75% ZnR2.2 with PC were prepared in pH 7 PIPES buffer. Though the same thin film hydration and extrusion methods were followed as before, no fluorescence, by extension no encapsulated nile red lipophilic dye, was detected via fluorimetry experiments for any of the liposome formulations in either concentrated or dilute liposome samples. This led to the determination that PIPES buffer will not be suitable for liposome studies. Next, tris-buffered saline (TBS) at pH 8 was used to hydrate the lipid films. Liposomes of 0, 25, 50, 75, and 95% ZnR2.2 were formed at 2 mM lipid content as previously described and 100 µL of the liposome solution was titrated with aqueous 0.1 M $Zn(OAc)_2$ to a total concentration of 10 mM Zn^{2+}. Under these conditions, an increase in release was seen for the liposomes composed of 50% or more of lipid switch with PC when compared to control liposomes (Figure 17). While the release was not extensive, at only 13, 17, and 29% release for 50, 75, and 95% ZnR2.2, respectively with background release at 9% in absence of trigger lipid, these results indicated that lipid ZnR2.2 is able to induce membrane destabilization in the presence of increased concentrations of zinc ions. These preliminary results are indicative that pH control of the liposomal solution is important to the chelation ability of the TPA based lipid switches. From here, further changes to the liposome composition were studied to see the effects on dye release properties.

Phosphatidyl ethanolamine (PE) is a non membrane forming lipid, however, when mixed with other lipids it can form stable membranes. For the following studies, the incorporation of ZnR2.2 was held constant at 50% while the amounts of PE and PC were varied. PE was incorporated at 10, 25, and 50% with the remaining percentage being made up of PC. The lipid films were formed by the same protocol as the previous studies and hydrated with TBS. Of the given preparations, that

composed of 50% PE and 50% ZnR2.2 did not form liposomes. Titration data for the other liposome preparations is given in Figure 17. It was seen that incorporation of 25% PE was optimal for release with 41 % release seen for these liposomes. This was a large increase over liposomes containing 50% synthetic lipid in the absence of PE which saw only 13% release. It is assumed that the incorporation of PE predisposed the liposomes fusion and membrane disruption, making the small hypothesized conformational change previously postulated in Figure 16 a large enough factor to effect appreciable release. Still, a more effective conformational lipid switch was desired, so other lipid analogs were designed as will be discussed in the next section.

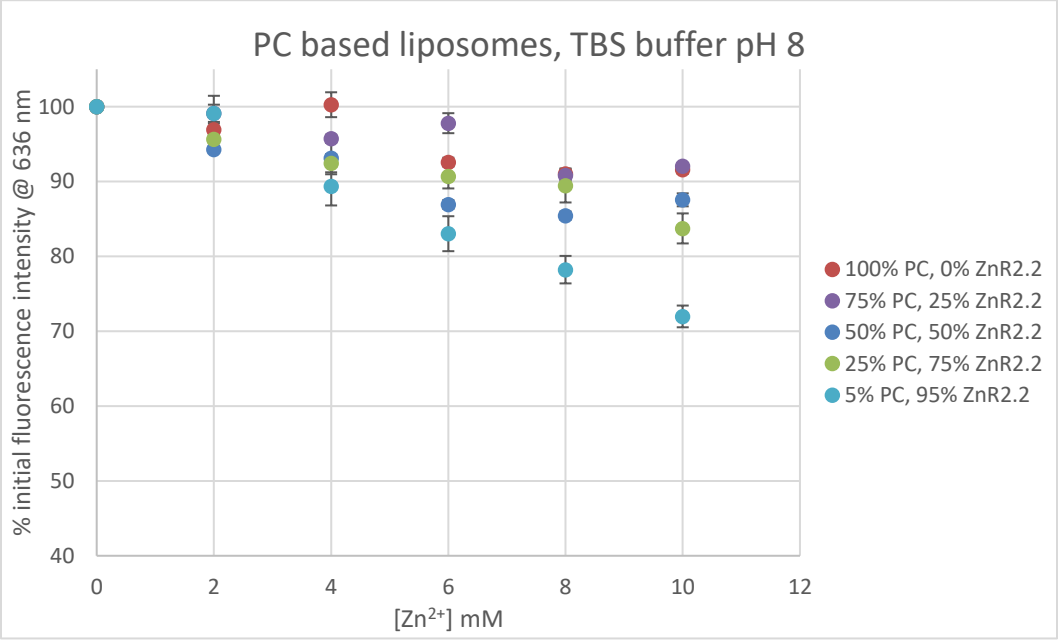

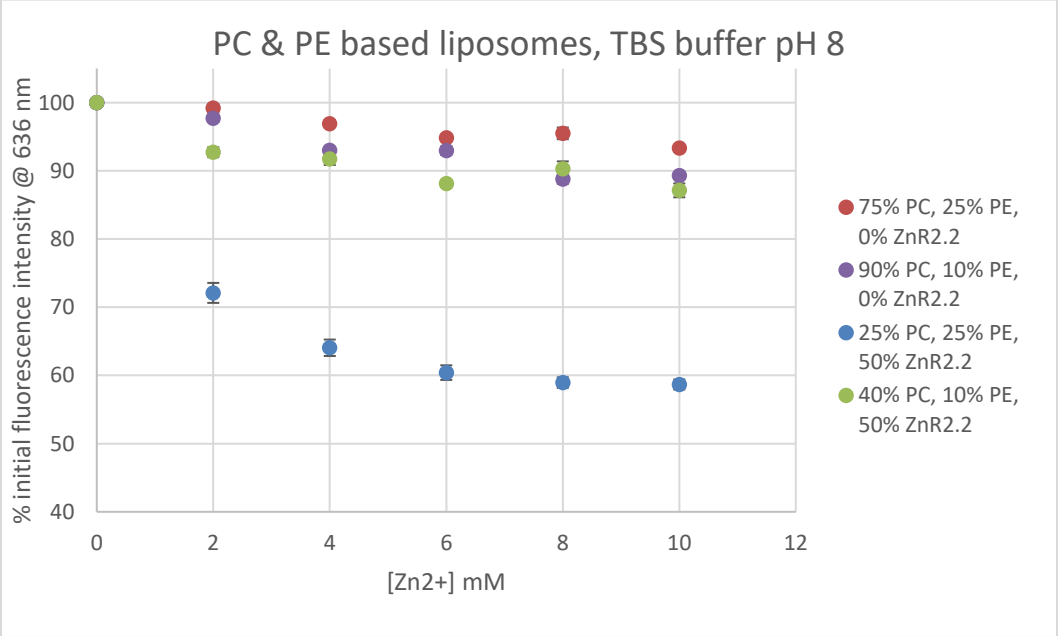

Figure 17. ***Dye release profile of lipid switch ZnR2.2***
TOP: Liposomes composed of PC and lipid analog ZnR2.2. Appreciable release was only seen at high percentages of ZnR2.2 where liposomes of 95% ZnR2.2 gave 29% release. BOTTOM: Incorporation of PE into the liposomal formulations decreased the required synthetic lipid content while increasing dye release. Liposomes of 25% PC, 25% PE, 50% ZnR2.2 gave 41% release.

2.7. Design and Synthesis of Zinc-Responsive Lipids of ZnR3 Type

With the limited release of the TPA based lipid switches, TPEN was next targeted as a lipid core ion chelator. It was hypothesized that due to the presentation of TPA at the surface of the liposomal membrane, there may not be a significant conformational change with chelation of zinc. The use of TPEN, however, could change that as it was envisaged that TPEN based lipids, when inserted into the membrane, would have greater separation between the pyridal units of the chelating core than those in the TPA based lipid analogs. Upon treatment with zinc, it is hypothesized that these units would have to come in closer proximity in order to properly chelate an ion (Figure 18). This should cause a large enough conformational change in the lipid skeleton to disturb the membrane thus causing release of cargo. As previously described, TPEN has a higher affinity for zinc (0.3 fM) as compared to TPA (10 pM) though it is less selective among other divalent metal cations.[79] This is also advantageous as the increased affinity will potentiate greater chelation ability. These structural and affinity differences will be beneficial to our goal of designing an effective lipid switch. Similar chemistry to that used to synthesize lipid ZnR2.2 will be utilized to form the TPEN core and attach a variety of alkyl tails to quickly and efficiently build a number of lipid skeletons. The targeted TPEN based lipids are shown in Figure 18.

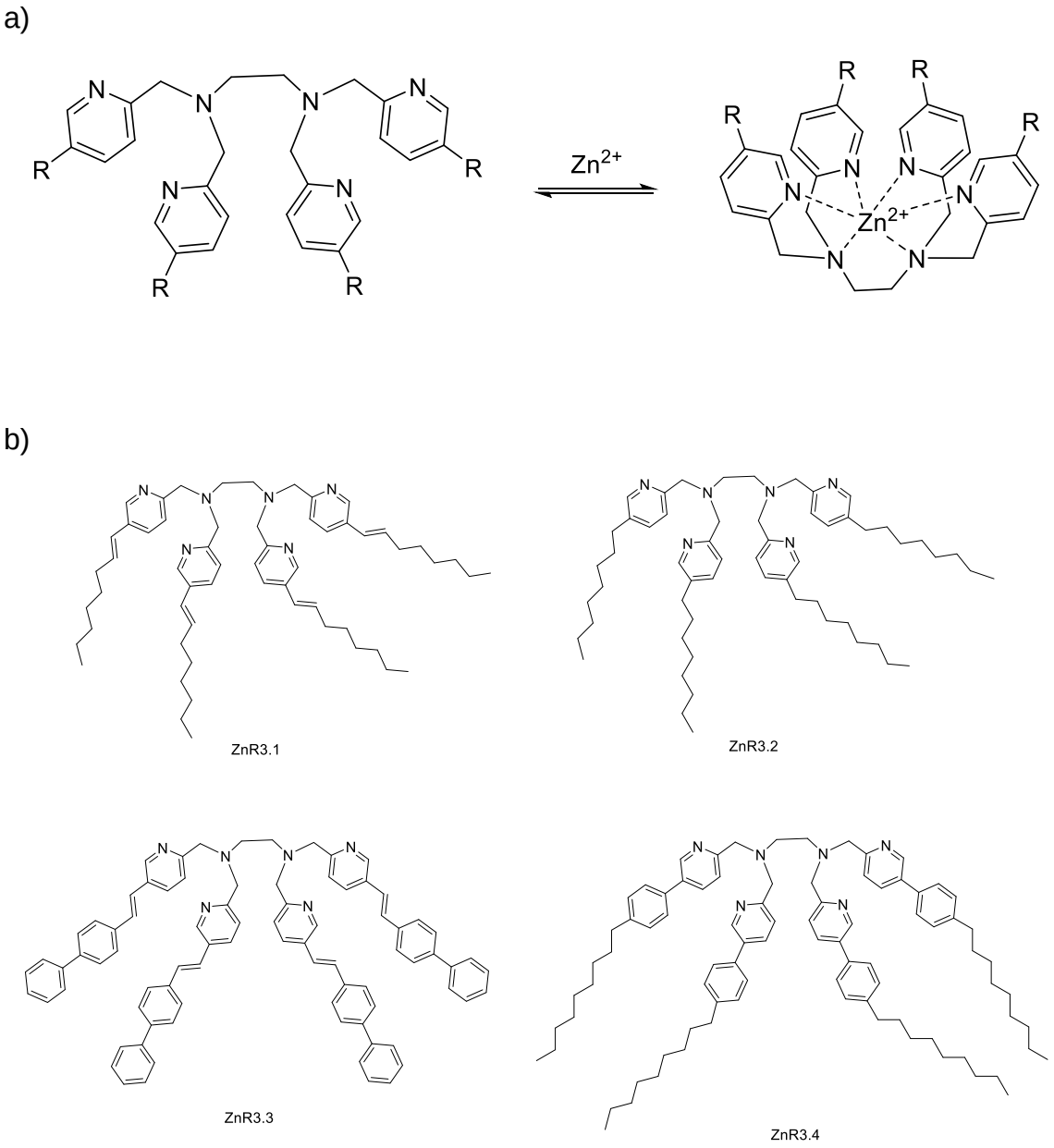

Figure 18. ***TPEN chelation of zinc and structures of lipid analogs ZnR3.1 – ZnR3.4***

a) A greater potential for conformational change and membrane disruption is hypothesized for TPEN based lipid switches as compared to TPA based lipid switches. R= alkyl tail. b) Target structures of TPEN lipid analogs designed similarly to ZnR2 type lipids. These lipids are based on a common TPEN zinc chelating core with a variety of possible alkyl tails.

2.7.1. Synthesis of ZnR3 Type Lipids

The synthesis of the TPEN core was pursued by multiple routes (Figure 19). The first route to the TPEN core began with the reduction of common starting material 5-bromo-2-pyridinecarboxaldehyde to transform the aldehyde functionality to an alcohol, Z3.1. This alcohol intermediate was then chlorinated to give intermediate Z3.2. Coupling of chloride Z3.2 with ethylenediamine was attempted with various basic conditions including NaOH[90] and K_2CO_3, neither of which successfully yielded the target TPEN unit Z3.3. Another route to intermediate Z3.3 included the stepwise formation of secondary amine Z3.4 through successive reductive aminations with ammonium acetate as the nitrogen source and sodium borohydride as the reducer. However, the initial primary amine was not recovered. A one pot reductive amination was also pursued utilizing a weaker hydride reducer in sodium triacetoxyborohydride which yielded tertiary amine Z2.1 as the main product rather than the desired secondary amine Z3.4. The next plausible route that was designed was to synthesize primary amine Z3.7 through an azide reduction and then couple that amine with the readily available aldehyde precursor through a reductive amination to give secondary amine Z3.4. This synthetic route began with alcohol intermediate Z3.1, synthesized as before, which was then activated by transformation into tosylate Z3.5. Substitution of the tosylate with sodium azide was successful in installing the required nitrogen unit. The azide can then be reduced via palladium catalyzed hydrogenation to give primary amine Z3.7. This will then be coupled with the readily available aldehyde to give secondary amine Z3.4. To construct the TPEN core, intermediate Z3.4 will be coupled with dibromoethane in a double substitution reaction to give common intermediate Z3.3. When the TEPN core intermediate is successfully synthesized it will be coupled with the desired boronic acid alkyl tail precursor to yield the target lipid analogs, ZnR3.1 – ZnR3.4. Lipid analog ZnR3.1 will be targeted first as it is analogous to ZnR2.2 which performed well in the TPA based studies. Facile switching of boronic acid functionality will provide quick access to the rest of the

.

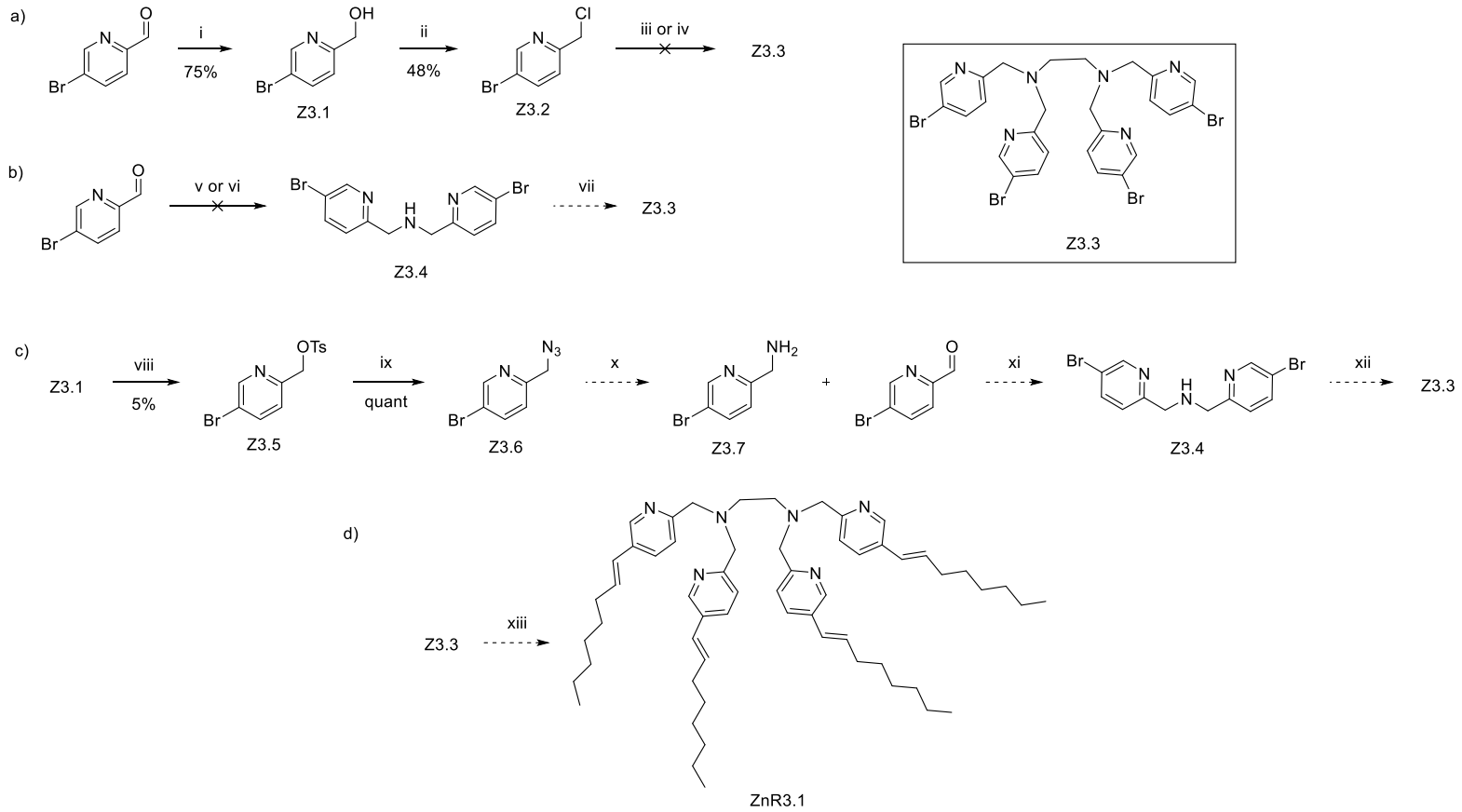

Figure 19. ***Synthetic routes toward TPEN based lipid analogs***

Various synthetic routes to synthetic intermediate Z3.3 and lipid analog ZnR3.1. Conditions: i) $NaBH_4$, EtOH, 0°C ii) $SOCl_2$, toluene iii) ethylenediamine, NaOH(aq), DCM[90] iv) ethylenediamine, K_2CO_3, MeCN v) NH_4OAc, $NaBH(OAc)_3$, DCM vi) 1) NH_4OAc, DCM, $NaBH_4$ 2) 5-bromo-2-pyridinecarboxaldehyde, DCM, $NaBH_4$ vii) 1,2-dibromoethane, K_2CO_3, MeCN viii) DMAP, TEA, *p*TsCl, DCM ix) NaN_3, DMF x) 10% Pd/C, H_2 xi) 5-bromo-2-pyridinecarboxaldehyde, EtOH, $NaBH_4$ xii) 1,2-dibromoethane, K_2CO_3, MeCN xiii) trans-octenylboronic acid, $Pd(PPh_3)_4$, K_2CO_3, DMF/toluene/H_2O

target lipid skeletons. As these targets are successfully synthesized, they will be applied in liposomal release studies to determine their release characteristics.

Upon completion of synthesis of the TPEN based lipid analogs the optimized dye release conditions as determined in the TPA based studies of section 2.6.2 will be applied with formation of 200 nm liposomes composed of trigger lipid, PC, and/or PE in TBS. The difference in pKa of TPEN as compared to TPA may influence the release profile and binding ability of the second set of analogs (ZnR3 type), so determination of the optimal conditions for each lipid type may be required. Taking all of the experimental optimization into account, the TPEN lipid switches are hypothesized to have a greater potential for release than their smaller TPA counterparts due to their higher propensity for conformational change upon ion chelation. The exact release profiles will be determined upon successful synthesis of each analog

2.8. Summary and Future Work

Molecular recognition as stimuli for the release of payload from a therapeutic liposome represents a new level of targeted therapeutics. The ability to harness a unique physiological aspect of a disease for treatment allows for less off target interactions and a more concise treatment. Toward this end, this work proposed a number of synthetic lipid switches for the recognition of zinc. Based on well-known zinc chelators, TPA and TPEN, it was envisioned that upon recognition of zinc there would be a conformational change within the lipid causing it to become a non-bilayer lipid. This would ideally destabilize the membrane and potentiate cargo release.

Currently, of the available completed lipid switches only ZnR2.2 causes cargo release. This required a significant amount of synthetic lipid which has been attributed to the way in which the TPA based lipids present themselves at the bilayer aqueous interface. It is hypothesized that the chelating nitrogens are

presented in such a way that they readily bind with zinc without having to rotate within the membrane. This setback was countered with the design of TPEN based lipid switches which have the potential for a greater conformational change upon chelation of zinc. Future work with this research will include completion of the synthesis of compounds ZnR2.3-ZnR2.5 and further liposomal studies of these lipid switches along with the completed lipid ZnR2.2. Furthermore, the completion of the synthesis of the panel of TPEN lipids ZnR3.1-Znr3.4 will provide a large panel of lipid switches for study of their cargo release profiles. Taken together, these lipid conformational switches will provide new insights into the possibilities of triggered liposomal release.

2.9. Synthetic Details and Compound Characterization

2.9.1. General Experimental Information

Reagents and solvents were generally purchased from Acros, Aldrich, or Fisher Scientific and used without further purification. PC (L-α-phosphatidylcholine, mixed isomers from chicken eggs) was purchased from Avanti Polar Lipids, Inc. Dry solvents were obtained from a Pure solvent delivery system purchased from Innovative Technology, Inc. Column chromatography was performed using 230-300 mesh silica gel purchased from Sorbent Technologies. NMR spectra were obtained using Varian Mercury Vx 300 MHz and Varian 500 MHz spectrometers. Mass spectra were obtained with JEOL DART-AccuTOF and Q-Star XL quadrupole time-of-flight hybrid mass spectrometers (Applied Biosystems, Foster City, CA). Liposome extruder and polycarbonate membranes were obtained from Avestin (Ottawa, Canada). Ultrapure water was purified via a Millipore water system. Fluorescence studies were performed using a Cary Eclipse Fluorescence Spectrophotometer.

2.9.2. Synthetic Details: Z1 Compounds

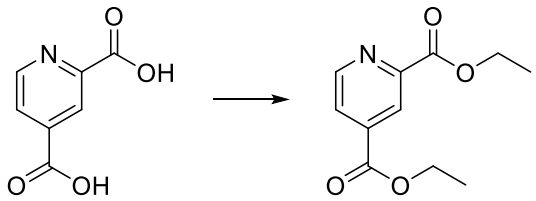

Z1.1

Diethylpyridine-2,4-dicarboxylate (Z1.1)[85]

Commercially available 2,4-pyridine dicarboxylic acid (150.0 mg, 0.90 mmol, 1.0 equiv) and *para*-toluenesolufonic acid (pTsOH, 342.6 mg, 1.80 mmol, 2.4 equiv) were dissolved in 15 mL EtOH and refluxed for 24 h. The reaction mixture was then subjected to rotary evaporation to remove the solvent. The residue was dissolved in 15 mL of $CHCl_3$ and washed with saturated $NaHCO_3$ (15 mL). The aqueous layer was extracted with 3 x 15 mL $CHCl_3$. The organics were combined, dried with $MgSO_4$, filtered, and the solvent was removed by rotary evaporation. Compound Z1.1 was obtained as a clear oil/ white solid (190.3 mg, 95% yield). ^1H NMR (300 MHz, $CDCl_3$): δ 0.96 (m, 6H), 3.99 (m, 4H), 7.53 (d, 1H, J = 5.29 Hz), 8.07 (s, 1H), 8.41 (d, 1H, J = 4.77 Hz) ^{13}C NMR (125 MHz, $CDCl_3$): δ 14.17, 14.29, 62.31, 62.3, 124.32, 126.02, 139.19, 149.14, 150.55, 164.23, 164.45. Molecular formula: $C_{12}H_{14}O_4$. DART-AccuTOF-Mass Spec: [M+1] predicted: 224.09173 [M+1] found: 224.08598

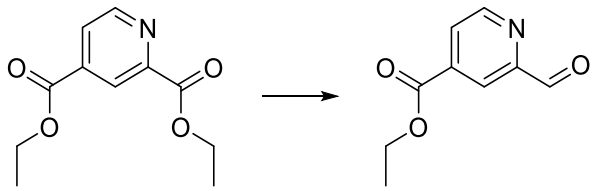

Z1.1 Z1.2

Ethyl 2-formylisonicotinate (Z1.2)[86]

Compound Z1.1 (597.5 mg, 2.69 mmol, 1.0 equiv) was dissolved in 20 mL dry THF under stirring and nitrogen atmosphere and then cooled to -78°C in a dry ice/ acetone bath. DIBAL-H (10.7 mL of a 1 M solution in hexane, 10.75 mmol, 4.0

equiv) was added dropwise to the cold, stirring solution. The reaction was stirred for 2.5 h at -78°C and then poured over ice cold acetic acid:deionized water (2 mL:10 mL) and stirred for 1 h. The pH of the solution was next brought to ~8 by adding saturated $NaHCO_3$. The resulting solution was extracted with 3 x 15 mL EtOAc and the organic layers were combined, washed with 20 mL saturated $NaHCO_3$, dried with $MgSO_4$, filtered, and the solvent was removed by rotary evaporation. The crude reaction mixture was purified via column chromatography with 10-25-50% EtOAc in hexane to provide Z1.2 as a white solid. (300.8 mg, 65% yield). ^1H NMR (300 MHz, $CDCl_3$): δ 1.39 (t, 3H, J = 7.20), 4.41 (q, 2H, J = 7.22 Hz), 8.05 (dd, 1H, J = 4.96 Hz, 1.67 Hz), 8.43 (s, 1H), 8.91 (dd, 1H, J = 4.87 Hz, 0.81 Hz), 10.10 (s,1H) ^{13}C NMR (75 MHz, $CDCl_3$): δ 14.13, 62.23, 120.84, 126.84, 139.12, 150.95, 153.62, 164.10, 192.52. Molecular formula: $C_{10}H_{10}O_3$. DART-AccuTOF-Mass Spec: [M+1] predicted: 180.06552 [M+1] found: 180.09109

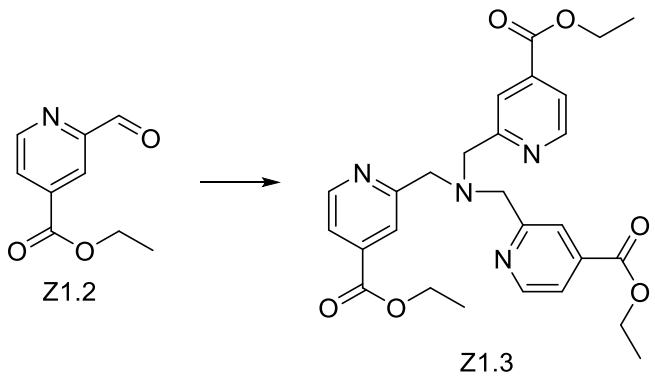

Triethyl 2,2',2''-(nitrilotris(methylene))triisonicotinate (Z1.3)[87]

Compound Z1.2 (301.0 mg, 1.70 mmol, 3.0 equiv) and NH_4OAc (43.2 mg, 0.48 mmol, 1.0 equiv) were dissolved in 7 mL dry DCM and the reaction was stirred under N_2 for 1 h. $NaBH(OAc)_3$ was added in 3 portions (120.1 mg, 0.57 mmol, 1.0 equiv per addition) and the reaction was stirred for 1 h in between each addition. After the final hydride addition, the reaction was allowed to stir overnight at rt under N_2. The solvent was removed under reduced pressure and the reaction residue was dissolved in 15 mL EtOAc and washed with 15 mL of 0.1 M KOH. The organic layer was dried with $MgSO_4$, filtered, and the solvent removed under reduced

pressure. Column chromatography with 0-10% MeOH:$CHCl_3$ gave 140.5 mg of the product as a clear oil (49% yield). ^1H NMR (300 MHz, $CDCl_3$): δ 1.40 (t, 9H, J = 6.66 Hz), 4.03 (s, 6H), 4.41 (q, 6H, J = 7.23 Hz), 7.69 (dd, 3H, J = 5.10 Hz, 1.51 Hz), 8.07 (s, 3H), 8.67 (dd, 3H, J = 5.05 Hz, 0.73 Hz) ^{13}C NMR (75 MHz, $CDCl_3$): δ 14.15, 60.04, 61.69, 121.25, 122.40, 138.25, 149.85, 160.14, 165.18 Molecular formula: $C_{27}H_{30}N_4O_6$. Q-Star XL quadrupole TOF-Mass Spec: [M+1] predicted: 507.22381 [M+1] found: 507.2337

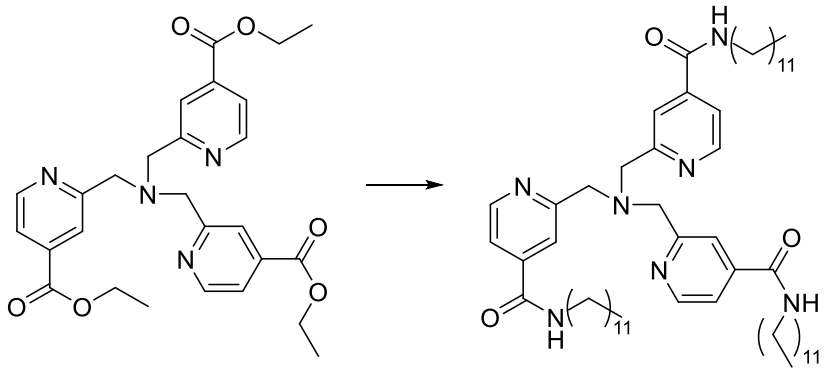

Z1.3 ZnR1

2,2',2''-(Nitrilotris(methylene))tris(*N*-dodecylisonicotinamide) (ZnR1)[88]

Dodecylamine (82.3 mg, 0.44 mmol, 18.0 equiv) was dissolved in 1 mL dry THF and the mixture was cooled to 0°C under N_2. DIBAL-H (422 µL of a 1 M in hexane solution, 0.42 mmol, 17.1 equiv) was added to the cooled solution and the mixture was stirred for 2 h while warming to rt. Triester Z1.3 (12.5 mg, 0.02 mmol, 1equiv) was dissolved in 0.5 mL THF with stirring under N_2. The previous activated amine solution was added dropwise to triester solution via cannula. The reaction was then brought to 50°C and stirred overnight under N_2. The reaction was then cooled to 0°C and quenched with 1 mL of 0.5 M $KHSO_4$. The reaction mixture was then extracted with 5mL DCM and the resulting aqueous layer was then extracted with 5mL of $CHCl_3$. The combined organic layers were washed with 10 mL saturated NaCl, dried with $MgSO_4$, filtered, and dried via rotary evaporation. Column chromatography with 0-60% EtOAc:hexane followed by 10% MeOH:$CHCl_3$ gave

ZnR1 as a yellow oil (3.1 mg, 17% yield). ^{1}H NMR (300 MHz, $CDCl_3$): δ 0.71 (t, 9H, J = 7.07 Hz), 1.10 (s, 54H), 1.49 (m, 6H), 3.25 (m, 6H), 3.88 (s, 6H), 7.47 (d, 3H, J = 4.38 Hz), 7.79 (s, 3H), 8.23 (bs, 3H), 8.41 (d, 3H, J = 4.97 Hz) Molecular formula: $C_{57}H_{93}N_7O_3$. Q-Star XL quadrupole TOF-Mass Spec: [M+Na] predicted: 946.72321 [M+Na] found: 946.7208

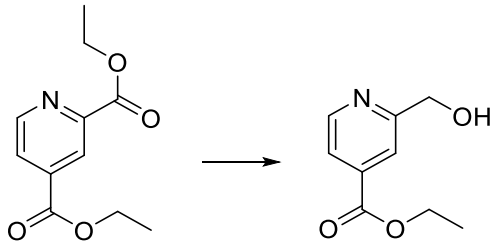

Z1.1 Z1.4

Ethyl 2-(hydroxymethyl)isonicotinate (Z1.4)[85]

Compound Z1.1 (636.0 mg, 2.86 mmol, 1.0 equiv) was dissolved in 10 mL dry, degassed EtOH. The solution was cooled below 0°C in an ice/salt bath with stirring. $NaBH_4$ (64.7 mg, 1.71 mmol, 0.6 equiv) was added in small portions to the cooled solution to maintain temperature of -10 to 0°C. Then, freshly crushed anhydrous $CaCl_2$ (310.7 mg, 2.86 mmol, 1.0 equiv) was slowly added to the cold reaction. The reaction was allowed to stir for 3 h at 0°C under N_2 after addition of all reagents. After 3 h of reacting, the pH of the solution was adjusted to 6 with 1 N HCl. Next the solution was filtered to remove solid salts and condensed under reduced pressure. Column chromatography with 10-100% EtOAc:hexanes yielded Z1.4 as a white solid (344.6 mg, 68% yield). ^{1}H NMR (500 MHz, $CDCl_3$): δ 1.41 (t, 3H, J = 7.54 Hz), 3.57, (bs, 1H), 4.41, (q, 2H, J = 7.24 Hz), 4.83, (s, 2H), 7.76 (d, 1H, J = 4.92 Hz), 7.82 (s, 1H), 8.69 (d, 1H, J = 4.99 Hz) ^{13}C NMR (125 MHz, $CDCl_3$): δ 14.18, 61.88, 64.20, 119.75, 121.58, 138.40, 149.30, 160.20, 164.96 Molecular formula: $C_{10}H_{12}O_3$. DART-AccuTOF-Mass Spec: [M+1] predicted: 182.08117 [M+1] found:182.21761

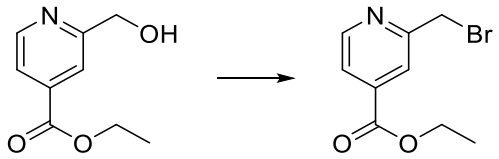

Ethyl 2-(bromomethyl)isonicotinate (Z1.5)

Compound Z1.4 (181.2 mg, 1.01 mmol, 1.0 equiv) was dissolved in 4mL dry DCM. PBr_3 (1.4 mL, 14.89 mmol, 14.74 equiv) was added and the reaction was stirred for 6 h at rt under nitrogen. Next, the reaction was cooled in an ice bath and 1.5 mL methanol was added dropwise to quench any excess PBr_3. The reaction mixture was washed three times with water, dried with $MgSO_4$, and the solvent was removed via rotary evaporation without the application of heat. Column chromatography with 10-25% EtOAc:hexane yielded Z1.5 as a clear oil (60.2 mg, quant). Compound Z1.5 was found to quickly decompose to a purple oil unless stored at -80°C. ^{1}H NMR (300 MHz, $CDCl_3$): δ 1.41 (t, 3H, J = 7.09 Hz), 4.41 (q, 2H, J = 7.16 Hz), 4.60 (s, 2H), 7.76 (d, 1H, J = 4.49 Hz), 7.98 (s, 1H), 8.72 (s, 1H) ^{13}C NMR (75 MHz, $CDCl_3$): δ 14.19, 33.18, 61.98, 109.99, 122.24, 138.89, 150.44, 157.90, 164.62. Molecular formula: $C_{10}H_{11}BrO_2$. DART-AccuTOF-Mass Spec: [M+1] predicted: 243.99677, 245.99472 [M+1] found: 243.99381, 245.98980

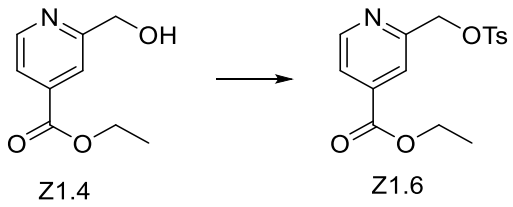

Ethyl 2-((tosyloxy)methyl)isonicotinate (Z1.6)

Compound Z1.4 (20.0 mg, 0.11 mmol, 1.0 equiv), DMAP (2.4 mg, 0.02 mmol, 0.2 equiv), and TEA (16.5 µL, 0.22 mmol, 2.0 equiv) were dissolved in 5 mL dry DCM. pTsCl (41.9 mg, 0.22 mmol, 2.0 equiv) was added and the reaction was stirred overnight under N_2. Next, the reaction was diluted with 5 mL DCM and washed twice with 10 mL 1 N HCl. The aqueous layer was extracted with 3 x 10 mL DCM.

The organic layers were combined, dried with $MgSO_4$, filtered, and the solvent was removed by rotary evaporation. Purification via column chromatography with 10-75% EtOAc:hexane gave compound Z1.6 as a white solid (17.9 mg, 49% yield). ^1H NMR (300 MHz, $CDCl_3$): δ 1.42 (t, 3H, J = 7.16 Hz), 2.44 (s,3H), 4.42 (q, 2H, J = 7.20 Hz), 5.19 (s, 2H), 7.34 (d, 2H, J = 8.11 Hz), 7.78 (dd, 1H, J = 5.08 Hz, 1.58 Hz), 7.84 (td, 2H, J = 8.39 Hz, 1.99 Hz), 7.92 (s, 1H), 8.66 (d, 1H, J = 4.91 Hz) ^{13}C NMR (125 MHz, $CDCl_3$): δ 14.19, 21.63, 62.09, 70.99, 121.30, 122.76, 128.10, 129.95, 132.54, 139.13, 145.19, 149.75, 154.69, 164.42 Molecular formula: $C_{17}H_{18}O_5S$.

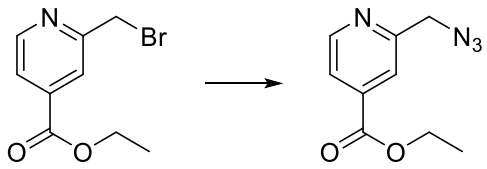

Z1.5 Z1.7

Ethyl 2-(azidomethyl)isonicotinate (Z1.7)

Compound Z1.5 (30.5 mg, 0.13 mmol, 1.0 equiv) and NaN_3 (24.4 mg, 0.38 mmol, 3 equiv) were dissolved in 5 mL of dry DMF. The reaction was then heated to 85°C and allowed to stir overnight. Next the reaction was diluted with 20 mL of EtOAc and the solvent was removed via rotary evaporation. The reaction residue was dissolved in 10 mL EtOAc and washed with 10 mL water. The aqueous layer was then extracted with 3 x 7 mL EtOAc. The combined organic layers were washed with 5 x 10 mL ice cold water, 1 x 20 mL saturated NaCl, and then dried with $MgSO_4$. Then the reaction was filtered and the solvent was removed via rotary evaporation. The target compound was obtained in a quantitative yield as a yellow oil (25.8 mg). The same reaction conditions applied to Z1.6 also gave a quantitative transformation to Z1.7. ^1H NMR (300 MHz, $CDCl_3$): δ 1.42 (t, 3H, J = 7.04 Hz), 4.43, (q, 2H, J = 7.11 Hz), 4.57, (s, 2H), 7.81 (dd, 1H, J = 5.03 Hz, 1.44 Hz), 7.90 (s, 1H), 8.75 (dd, 1H, J = 5.02 Hz, 0.74 Hz). ^{13}C NMR (125 MHz, $CDCl_3$): δ 14.18, 55.42, 61.96, 121.15, 121.16, 138.78, 150.43, 156.91, 164.78. Molecular

formula: $C_{10}H_{11}N_3O_2$. DART-AccuTOF-Mass Spec: [M+1] predicted: 207.08765 [M+1] found: 207.09040

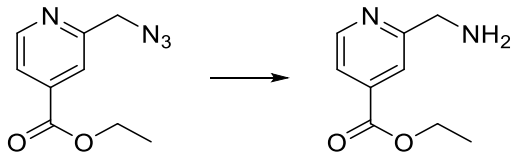

Z1.7 Z1.8

Ethyl 2-(aminomethyl)isonicotinate (Z1.8)

Compound Z1.7 (12.3 mg, 0.06 mmol, 1.0 equiv) was dissolved in 5 mL of EtOAc. 10% Pd/C (2.5 mg, 20% wt of azide, 0.002 mmol Pd) was added to the reaction flask and the atmosphere was replaced with H_2. After 1 hour of stirring, the atmosphere was replaced with N_2 and a second addition of Pd/C (0.8 mg, 5% wt of azide, 0.0008 mmol Pd) was added and the atmosphere replaced with H_2. The reaction was allowed to stir overnight under hydrogen atmosphere. Next, the reaction was filtered through celite to remove the palladium catalyst and the solvent was removed via rotary evaporation. The crude reaction mixture was purified via column chromatography with 5-25% MeOH:$CHCl_3$ and compound Z1.8 was collected as a yellow oil (4.7 mg, 40% yield). The product gave a yellow spot by ninhydrin stain on TLC. ^{1}H NMR (500 MHz, MeOD): δ 1.40 (t, 3H, J = 7.09 Hz), 4.10 (bs, 2H), 4.42 (q, 2H, J = 7.19 Hz), 7.82 (d, 1H, J = 4.48 Hz), 7.96 (s, 1H), 8.71 (d, 1H, J = 4.65 Hz). Molecular formula: $C_{10}H_{13}NO_2$. DART-AccuTOF-Mass Spec: [M+1] predicted: 181.09715 [M+1] found: 181.10196

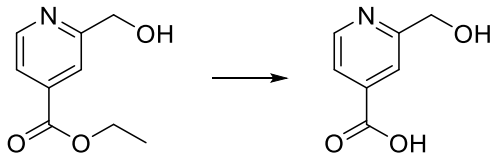

Z1.4 Z1.10

2-(Hydroxymethyl)isonicotinic acid (Z1.10)

Compound Z1.4 (15.6 mg, 0.09 mmol, 1.0 equiv) was dissolved in 6 mL THF:H2O (1:1 v/v). Freshly ground KOH (14.5 mg, 0.26 mmol, 3.0 equiv) was added to the stirring reaction. Next, the reaction mixture was heated at reflux (100°C) for 20 h. The reaction was then allowed to cool to rt and then further cooled in an ice bath. The pH of the solution was adjusted to ~4-5 with 3 N HNO_3. The solvent was then removed via rotary evaporation. The solid residue remaining in the flask was washed with 3 x 10 mL portions of EtOH. The ethanol washes were transferred to a clean flask and the solvent was removed under reduced pressure. The resulting residue was dissolved in hot isopropanol and filtered. Removal of solvent under reduced pressure gave compound Z1.10 as a white solid (12.2 mg, 93% yield). ^{1}H NMR (300 MHz, $CDCl_3$/MeOD): δ 4.59 (s, 2H), 7.57 (dd, 1H, J = 5.20 Hz, 1.50 Hz), 7.80 (s, 1H), 8.37 (d, 1H, J = 5.26 Hz). Molecuar formula: $C_8H_8O_3$. DART-AccuTOF-Mass Spec: [M+1] predicted: 154.04987 [M+1] found: 154.04561

2.9.3. Synthetic Details: Z2 Compounds

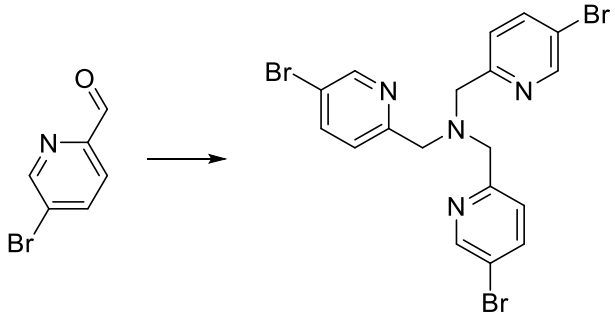

Z2.1

Tris((5-bromopyridin-2-yl)methyl)amine (Z2.1)[87]

5-Bromo-2-pyridinecarboxaldehyde (1.50 g, 8.06 mmol, 3.0 equiv) and NH_4OAc (207.2 mg, 2.69 mmol, 1 equiv) were dissolved in 25 mL of dry DCM and stirred for 1 hour. 3 equivalents of $NaBH(OAc)_3$ were added in 1 equiv portions (565.2 mg, 2.69 mmol, per addition) with 1 h of stirring between each addition. The reaction was left to stir overnight and then the solvent was removed under vacuum, and the residue was dissolved in 30 mL EtOAc. The reaction was washed with 20 mL 0.1 M KOH three times, dried with $MgSO_4$, filtered, and the solvent

removed by rotary evaporation. Recrystallization twice from 50:50 THF:hexane and rinsing with cold hexane gave the product as a white needlelike solid (1.35 g, 96% yield). ^{1}H NMR (300 MHz, $CDCl_3$): δ 3.81 (s, 6H), 7.40 (d, 3H, J = 8.36 Hz), 7.76 (dd, 3H, J = 8.22 Hz, 2.25 Hz), 8.59 (d, 3H, J = 2.31 Hz) ^{13}C NMR (75 MHz, $CDCl_3$): δ 59.26, 119.17, 124.44, 139.05, 150.22, 157.40. Molecular formula: $C_{18}H_{15}Br_3N_4$. DART-AccuTOF-Mass Spec: [M+1] predicted: 526.88991, 528.88787 [M+1] found: 526.91788, 528.83407

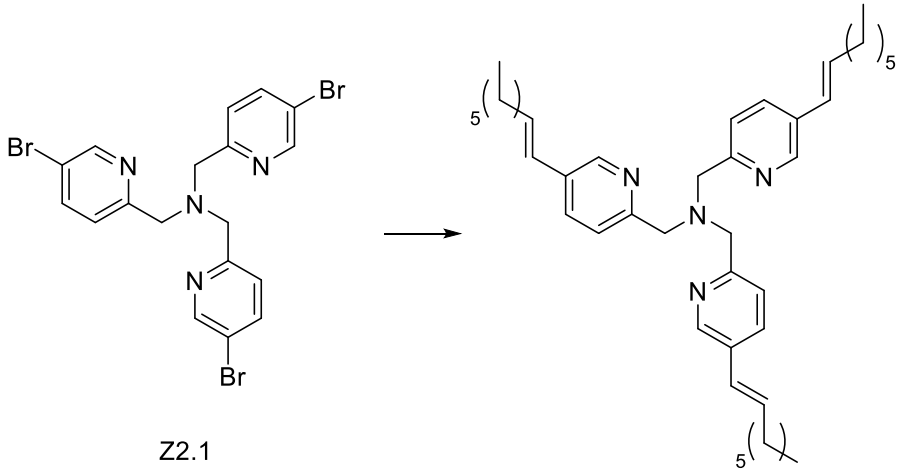

Z2.1 ZnR2.2

Tris((5-((E)-oct-1-en-1-yl)pyridin-2-yl)methyl)amine (ZnR2.2)[87]

Compound Z2.1 (25.0 mg, 0.05 mmol, 1.0 equiv), trans-octenylboronic acid (44.0 mg, 0.28 mmol, 6.0 equiv), and K_2CO_3 (45.5 mg, 0.33 mmol, 7.0 equiv) were dissolved in a 4:2:1 mixture of DMF:toluene:deionized water under Ar. $Pd(PPh_3)_4$ (3.8 mg, 7 mol%) was added and the atmosphere of the reaction vessel was evacuated and replaced with Ar three times. Next, the reaction was heated at 100°C for 48 h, followed by removal of the solvent by rotary evaporation. The reaction residue was dissolved in 15 mL EtOAc and was washed with 3 x 15 mL water. The organic layer was dried with $MgSO_4$, filtered, and the solvent was removed by rotary evaporation. Column chromatography with 0-10% MeOH:$CHCl_3$ gave the product as a yellow oil (9.9 mg, 34% yield). ^{1}H NMR (300 MHz, $CDCl_3$): δ 0.89 (t, 9H, J = 6.79 Hz), 1.30 (s, 18H), 1.45 (quint, 6H, J = 7.26),

2.21 (q, 4H, J = 6.80 Hz), 3.83 (s, 6H), 6.28 (m, 6H), 7.46 (d, 3H, J = 8.09 Hz), 7.62 (dd, 3H, J = 8.04 Hz, 2.28 Hz), 8.45 (d, 3H, J = 1.80 Hz) ^{13}C NMR (75 MHz, $CDCl_3$): δ 14.07, 22.59, 28.87, 29.14, 31.69, 33.13, 59.58, 122.86, 126.00, 131.95, 132.89, 133.27, 147.07. Molecular formula: $C_{42}H_{60}N_4$. DART-AccuTOF-Mass Spec: [M+1] predicted: 621.48907 [M+1] found: 621.43042

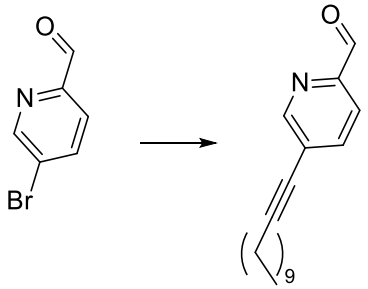

Z2.2

5-(Dodec-1-yn-1-yl)picolinaldehyde (Z2.2)

5-Bromo-2-pyridinecarboxaldehyde (50.0 mg, 0.27 mmol, 1.0 equiv), 1-dodecyne (36.3 μL, 0.27 mmol, 1.0 equiv), CuI (0.5 mg, 0.003 mmol, 1 mol% of bromide), and $PdCl_2(PPh_3)_2$ (5.7 mg, 0.008 mmol, 3 mol% of bromide) were dissolved in 2 mL of a mixture of dry, degassed DMF:TEA (5:1). The reaction vessel was flushed with N_2 and stirred overnight at 65°C. The reaction was then cooled and diluted with 15 mL of water. The mixture was extracted with 15 mL EtOAc and the organic layer was washed twice with 10 mL water, once with 10 mL saturated NaCl, was dried with $MgSO_4$, filtered, and the solvent was removed under reduced pressure. Purification via column chromatography with 0-2% EtOAc:hexane yielded Z2.2 as a yellow oil (40.3 mg, 55% yield). ^{1}H NMR (300 MHz, $CDCl_3$): *δ* 0.86 (t, 3H, J = 6.87 Hz), 1.26 (s, 12H), 1.44 (quint, 2H, J = 7.28 Hz), 1.62 (quint, 2H, J = 7.13 Hz), 2.45 (t, 3H, J = 6.99 Hz), 7.80 (dd, 1H, J = 8.16 Hz, 1.72 Hz), 7.87 (d, 1H, J = 8.02 Hz), 8.73 (s, 1H), 10.04 (s, 1H). ^{13}C NMR (75 MHz, $CDCl_3$): *δ* 4.08, 19.61, 22.65, 28.33, 28.91, 29.08, 29.28, 29.48, 29.54, 31.95, 98.55, 120.88, 125.76, 139.25, 150.43, 152.55, 192.60. Molecular formula: $C_{18}H_{25}NO$. DART-AccuTOF-Mass Spec: [M+1] predicted: 272.20089 [M+1] found: 272.08493

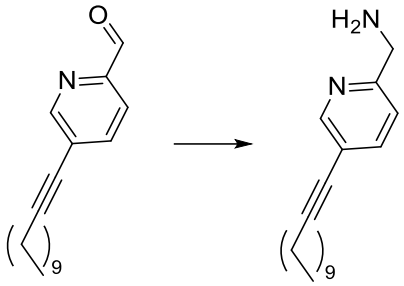

Z2.2 Z2.3

(5-(Dodec-1-yn-1-yl)pyridin-2-yl)methanamine (Z2.3)[87]

Compound Z2.2 (21.7 mg, 0.08 mmol, 3.0 equiv) and NH_4OAc (2.3 mg, 0.03 mmol, 1 equiv) were dissolved in 2 mL of dry DCM and stirred for 1 h. 3 equivalents of $NaBH(OAc)_3$ were added in 1 equivalent portions (6.4 mg, 0.03 mmol per addition) with 1 hour of stirring between each addition. The reaction was left to stir overnight and then the solvent was removed under vacuum, and the residue was dissolved in 7 mL EtOAc. The reaction was washed with 7 mL 0.1 M KOH three times, dried with $MgSO_4$, filtered, and the solvent removed by rotary evaporation. Column chromatography with 10-50% EtOAc:hexane gave Z2.3 as the major product (though tertiary amine ZnR1 was the desired product) as a white solid (11.7 mg, quant). ^1H NMR (300 MHz, $CDCl_3$): δ 0.88 (t, 3H, J = 6.81 Hz), 1.27 (s, 12H), 1.44 (m, 2H, J = 6.96 Hz), 1.61 (quint, 2H, J = 7.13 Hz), 2.42 (t, 2H, J = 6.99 Hz), 4.74 (s, 2H), 7.18 (d, 1H, J = 8.08 Hz), 7.67 (d, 1H, J = 8.38 Hz), 8.56 (s, 1H). Molecular formula: $C_{18}H_{28}N_2$.

2.9.4. Synthetic Details: Z3 Compounds

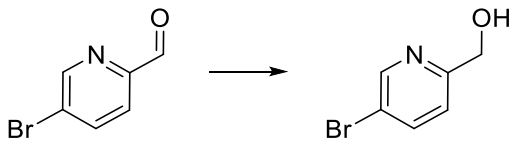

Z3.1

5-bromo-2-pyridinecarboxaldehyde (1.0 g, 5.38 mmol, 1.0 equiv) was dissolved in 20 mL of EtOH and the solution was cooled to 0°C. $NaBH_4$ (1.1 g, 28.22 mmol, 5.3 equiv) was added in small portions to the cooled solution to maintain a temperature of 0°C and then the reaction was stirred for 4 h at rt. Next, the solvent was removed via rotary evaporation and the resulting residue was dissolved in 20 mL of DCM and was washed three times with 20 mL of water. The organic layer was then dried with $MgSO_4$, filtered, and the solvent removed under rotary evaporation. Z3.1 was recovered as a white solid without further purification (757.2 mg, 75% yield) ^{1}H NMR (300 MHz, $CDCl_3$): δ 3.14 (bs, 1H), 4.73 (s, 2H), 7.20 (d, 1H, J = 8.29 Hz), 7.82 (dd, 1H, J = 8.33 Hz, 2.31 Hz), 8.62 (d, 1H, 2.17 Hz) ^{13}C NMR (75 MHz, $CDCl_3$): δ 63.88, 119.07, 121.76, 139.38, 149.59, 157.71 Molecular formula: C_6H_6BrNO

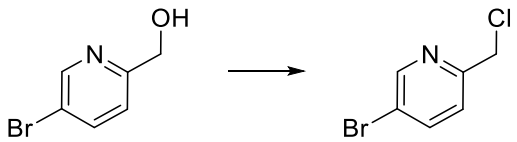

Z3.1 Z3.2

Z3.1 (757.2 mg, 4.03 mmol, 1.0 equiv) was dissolved in 20 mL of dry toluene. $SOCl_2$ (877.0 µL, 12.09 mmol, 3.0 equiv) was added dropwise to the solution of alcohol Z3.1 in toluene and allowed to stir for 3 h at rt then quenched with 20 mL of saturated $NaHCO_3$, extracted three times with 20 mL of DCM, and the combined organic fractions were dried with $MgSO_4$, filtered, and the solvent was removed via rotary evaporation. Column chromatography with 10-50% acetone:hexane gave compound Z3.2 as a pale yellow oil (396.5 mg, 48% yield) ^{1}H NMR (300 MHz, $CDCl_3$): δ 4.57 (s, 2H), 7.31 (d, 1H, J = 8.38 Hz), 7.77 (dd, 1H, J = 8.33 Hz, 2.47 Hz), 8.56 (dd, 1H, J = 2.42 Hz, 0.57 Hz) ^{13}C NMR (75 MHz, $CDCl_3$): δ 45.94, 120.08, 124.05, 139.56, 150.43, 155.08 Molecular formula: C_6H_5BrClN

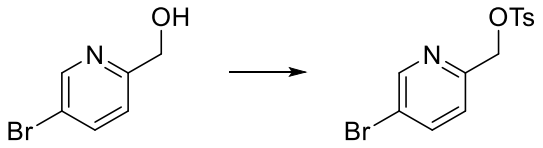

Z3.1 Z3.5

Z3.1 (565.4 mg, 3.00 mmol, 1.0 equiv), DMAP (73.5 mg, 0.60 mmol, 0.2 equiv), and TEA (836.3 uL, 6.00 mmol, 2.0 equiv) were dissolved in 30 mL dry DCM then *p*TsCl (1.1 g, 6.00 mmol, 2.0 equiv) was added and the reaction was stirred under N_2 overnight. Then, the reaction was transferred to a separatory funnel, washed twice with 20 mL 1N HCl, and the aqueous fractions washed thrice with 20 mL DCM. The organic fractions were combined, dried with $MgSO_4$, filtered, and the solvent was removed under reduced pressure. Column chromatography with 10-50% EtOAc:hexane gave the desired product as a white solid (5% yield). ^{1}H NMR (300 MHz, $CDCl_3$): δ 2.44 (s, 3H), 5.09 (s, 2H), 7.33 (m, 3H), 7.81 (d, 1H, J = 8.33 Hz), 8.56 (s, 1H) ^{13}C NMR (75 MHz, $CDCl_3$): δ 21.64, 71.00, 120.42, 123.19, 128.04, 129.94, 132.63, 139.50, 145.19, 150.38, 152.35 Molecular formula: $C_{13}H_{12}BrNO_3S$

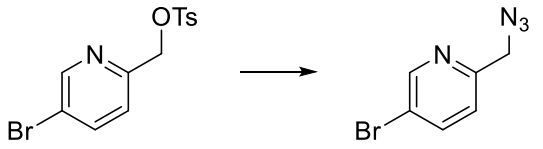

Z3.5 Z3.6

Z3.5 (47.5 mg, 0.14 mmol, 1.0 equiv) and NaN_3 (27.1 mg, 0.42 mmol, 3.0 equiv) were dissolved in 10 mL of dry DMF and stirred at 85°C under nitrogen overnight. Then the reaction was diluted with 60 mL EtOAc and then the solvent was removed by rotary evaporation. The resulting residue was dissolved in 25 mL EtOAc, washed with 25 mL of water, then the aqueous layer was extracted three times with 20 mL of EtOAc. The combined EtOAc fractions were washed five times with ice water, once with 20 mL of saturated NaCl, dried with $MgSO_4$, filtered, and the solvent was removed via rotary evaporation. Azide product Z3.6 was used as a

yellow-orange solid without further purification for the next reaction (quant). ^{1}H NMR (300 MHz, $CDCl_3$) δ 4.45 (s, 2H), 7.25 (d, 1H, J = 8.11 Hz, overlaps with solvent $CDCl_3$ peak), 7.84 (dd, 1H, J = 8.32 Hz, 2.36 Hz), 8.65 (d, 1H, J = 2.26 Hz) ^{13}C NMR (75 MHz, $CDCl_3$): δ 29.68, 54.99, 119.98, 123.18, 139.57, 150.73, 154.29 Molecular formula: $C_6H_5BrN_4$

LIST OF REFERENCES

1. Brazdova, B.; Zhang, N.; Samoshin, V. V.; Guo, X., trans-2-Aminocyclohexanol as a pH-sensitive conformational switch in lipid amphiphiles. *Chemical Communications* **2008,** (39), 4774-4776.
2. Viricel, W.; Mbarek, A.; Leblond, J., Switchable Lipids: Conformational Change for Fast pH-Triggered Cytoplasmic Delivery. *Angewandte Chemie International Edition* **2015,** *54* (43), 12743-12747.
3. Plum, L. M.; Rink, L.; Haase, H., The Essential Toxin: Impact of Zinc on Human Health. *International Journal of Environmental Research and Public Health* **2010,** *7* (4), 1342-1365.
4. Grattan, B. J.; Freake, H. C., Zinc and Cancer: Implications for LIV-1 in Breast Cancer. *Nutrients* **2012,** *4* (7), 648.
5. Murakami, M.; Hirano, T., Intracellular zinc homeostasis and zinc signaling. *Cancer Science* **2008,** *99* (8), 1515-1522.
6. Li, M.; Zhang, Y.; Liu, Z.; Bharadwaj, U.; Wang, H.; Wang, X.; Zhang, S.; Liuzzi, J. P.; Chang, S.-M.; Cousins, R. J.; Fisher, W. E.; Brunicardi, F. C.; Logsdon, C. D.; Chen, C.; Yao, Q., Aberrant expression of zinc transporter ZIP4 (SLC39A4) significantly contributes to human pancreatic cancer pathogenesis and progression. *Proceedings of the National Academy of Sciences* **2007,** *104* (47), 18636-18641.
7. Regland, B.; Lehmann, W.; Abedini, I.; Blennow, K.; Jonsson, M.; Karlsson, I.; Sjögren, M.; Wallin, A.; Xilinas, M.; Gottfries, C. G., Treatment of Alzheimer's Disease with Clioquinol. *Dementia and Geriatric Cognitive Disorders* **2001,** *12* (6), 408-414.
8. Ritchie, C. W.; Bush, A. I.; Mackinnon, A.; et al., Metal-protein attenuation with iodochlorhydroxyquin (clioquinol) targeting aβ amyloid deposition and toxicity in alzheimer disease: A pilot phase 2 clinical trial. *Archives of Neurology* **2003,** *60* (12), 1685-1691.
9. Luckey, M., *Membrane Structural Biology*. 2 ed.; Cambridge University Press: 2014.
10. Cell Membranes.
11. Wymann, M. P.; Schneiter, R., Lipid signalling in disease. *Nature Reviews Molecular Cell Biology* **2008,** *9* (2), 162-176.
12. Kumar, A.; Baycin-Hizal, D.; Zhang, Y.; Bowen, M. A.; Betenbaugh, M. J., Cellular traffic cops: the interplay between lipids and proteins regulates vesicular formation, trafficking, and signaling in mammalian cells. *Current Opinion in Biotechnology* **2015,** *36*, 215-221.
13. Bhardwaj, N.; Stahelin, R. V.; Langlois, R. E.; Cho, W.; Lu, H., Structural Bioinformatics Prediction of Membrane-binding Proteins. *Journal of Molecular Biology* **2006,** *359* (2), 486-495.
14. Waddington, Kirsty E.; Jury, Elizabeth C., Manipulating membrane lipid profiles to restore T-cell function in autoimmunity. *Biochemical Society Transactions* **2015,** *43* (4), 745-751.

15. Best, M. D.; Rowland, M. M.; Bostic, H. E., Exploiting Bioorthogonal Chemistry to Elucidate Protein–Lipid Binding Interactions and Other Biological Roles of Phospholipids. *Accounts of Chemical Research* **2011,** *44* (9), 686-698.
16. Lee, A. G., Biological membranes: the importance of molecular detail. *Trends in Biochemical Sciences* **2011,** *36* (9), 493-500.
17. Smith, M. D.; Gong, D.; Sudhafar, C. G.; Reno, J. C.; Stahelin, R. V.; Best, M. D., Synthesis and Convenient Functionalization of Azide-Labeled Diacylglycerol Analogues for Modular Access to Biologically Active Lipid Probes. *Bioconjugate Chemistry* **2008,** *19*, 1855-1863.
18. Hurley, J. H.; Misra, S., Signaling and Subcellular Targeting by Membrane-Binding Domains. *Annual Review of Biophysics and Biomolecular Structure* **2000,** *29* (1), 49-79.
19. Carrasco, S.; Mérida, I., Diacylglycerol, when simplicity becomes complex. *Trends in Biochemical Sciences* **2007,** *32* (1), 27-36.
20. Best, M. D.; Zhang, H.; Prestwich, G. D., Inositol polyphosphates, diphosphoinositol polyphosphates and phosphatidylinositol polyphosphate lipids: Structure, synthesis, and development of probes for studying biological activity. *Natural Product Reports* **2010,** *27* (10), 1403-1430.
21. Yeung, T.; Gilbert, G. E.; Shi, J.; Silvius, J.; Kapus, A.; Grinstein, S., Membrane phosphatidylserine regulates surface charge and protein localization. *Science* **2008,** *319* (5860), 210-213.
22. Balla, T., Phosphoinositides: Tiny lipids with giant impact on cell regulation. *Physiological Reviews* **2013,** *93* (3), 1019-1137.
23. Bangham, A. D.; De Gier, J.; Greville, G. D., Osmotic properties and water permeability of phospholipid liquid crystals. *Chemistry and Physics of Lipids* **1967,** *1* (3), 225-246.
24. Pattni, B. S.; Chupin, V. V.; Torchilin, V. P., New Developments in Liposomal Drug Delivery. *Chemical Reviews* **2015,** *115* (19), 10938-10966.
25. Immordino, M. L.; Dosio, F.; Cattel, L., Stealth liposomes: review of the basic science, rationale, and clinical applications, existing and potential. *International Journal of Nanomedicine* **2006,** *1* (3), 297-315.
26. England, C. G.; Im, H.-J.; Feng, L.; Chen, F.; Graves, S. A.; Hernandez, R.; Orbay, H.; Xu, C.; Cho, S. Y.; Nickles, R. J.; Liu, Z.; Lee, D. S.; Cai, W., Re-assessing the Enhanced Permeability and Retention Effect in Peripheral Arterial Disease using Radiolabeled Long Circulating Nanoparticles. *Biomaterials* **2016,** *100*, 101-109.
27. Crielaard, B. J.; Lammers, T.; Schiffelers, R. M.; Storm, G., Drug targeting systems for inflammatory disease: One for all, all for one. *Journal of Controlled Release* **2012,** *161* (2), 225-234.
28. Nakamura, Y.; Mochida, A.; Choyke, P. L.; Kobayashi, H., Nanodrug Delivery: Is the Enhanced Permeability and Retention Effect Sufficient for Curing Cancer? *Bioconjugate Chemistry* **2016,** *27* (10), 2225-2238.

29. Allen, T. M., The use of glycolipids and hydrophilic polymers in avoiding rapid uptake of liposomes by the mononuclear phagocyte system. *Advanced Drug Delivery Reviews* **1994,** *13* (3), 285-309.
30. Sousa, I.; Rodrigues, F.; Prazeres, H.; Lima, R. T.; Soares, P., Liposomal therapies in oncology: does one size fit all? *Cancer Chemotherapy and Pharmacology* **2018,** *82* (5), 741-755.
31. Klibanov, A. L.; Maruyama, K.; Torchilin, V. P.; Huang, L., Amphipathic polyethyleneglycols effectively prolong the circulation time of liposomes. *FEBS letters* **1990,** *268* (1), 235-7.
32. Polymers & Polymerizable Lipids. https://avantilipids.com/product-category/polymers-polymerizable-lipids (accessed Oct 20, 2018).
33. Kube, S.; Hersch, N.; Naumovska, E.; Gensch, T.; Hendriks, J.; Franzen, A.; Landvogt, L.; Siebrasse, J.-P.; Kubitscheck, U.; Hoffmann, B.; Merkel, R.; Csiszár, A., Fusogenic Liposomes as Nanocarriers for the Delivery of Intracellular Proteins. *Langmuir* **2017,** *33* (4), 1051-1059.
34. Kuang, H.; Ku, S. H.; Kokkoli, E., The design of peptide-amphiphiles as functional ligands for liposomal anticancer drug and gene delivery. *Advanced Drug Delivery Reviews* **2017,** *110-111*, 80-101.
35. Liu, Z.; Xiong, M.; Gong, J.; Zhang, Y.; Bai, N.; Luo, Y.; Li, L.; Wei, Y.; Liu, Y.; Tan, X.; Xiang, R., Legumain protease-activated TAT-liposome cargo for targeting tumours and their microenvironment. *Nature Communications* **2014,** *5*, 4280.
36. Yang, Y.; Yang, Y.; Xie, X.; Cai, X.; Mei, X., Preparation and characterization of photo-responsive cell-penetrating peptide-mediated nanostructured lipid carrier. *Journal of Drug Targeting* **2014,** *22* (10), 891-900.
37. Yang, Y.; Yang, Y.; Xie, X.; Cai, X.; Wang, Z.; Gong, W.; Zhang, H.; Li, Y.; Mei, X., A near-infrared two-photon-sensitive peptide-mediated liposomal delivery system. *Colloids and Surfaces B: Biointerfaces* **2015,** *128*, 427-438.
38. Xie, X.; Yang, Y.; Yang, Y.; Mei, X., Photolabile-caged peptide-conjugated liposomes for siRNA delivery. *Journal of Drug Targeting* **2015,** *23* (9), 789-799.
39. Hilgenbrink, A. R.; Low, P. S., Folate Receptor-Mediated Drug Targeting: From Therapeutics to Diagnostics. *Journal of Pharmaceutical Sciences* **2005,** *94* (10), 2135-2146.
40. Toffoli, G.; Cernigoi, C.; Russo, A.; Gallo, A.; Bagnoli, M.; Boiocchi, M., Overexpression of folate binding protein in ovarian cancers. *International journal of cancer* **1997,** *74* (2), 193-8.
41. Soe, Z. C.; Thapa, R. K.; Ou, W.; Gautam, M.; Nguyen, H. T.; Jin, S. G.; Ku, S. K.; Oh, K. T.; Choi, H.-G.; Yong, C. S.; Kim, J. O., Folate receptor-mediated celastrol and irinotecan combination delivery using liposomes for effective chemotherapy. *Colloids and Surfaces B: Biointerfaces* **2018,** *170*, 718-728.
42. Scomparin, A.; Salmaso, S.; Eldar-Boock, A.; Ben-Shushan, D.; Ferber, S.; Tiram, G.; Shmeeda, H.; Landa-Rouben, N.; Leor, J.; Caliceti, P.; Gabizon, A.; Satchi-Fainaro, R., A comparative study of folate receptor-targeted

doxorubicin delivery systems: Dosing regimens and therapeutic index. *Journal of Controlled Release* **2015,** *208*, 106-120.
43. Zwicke, G. L.; Mansoori, G. A.; Jeffery, C. J., Utilizing the folate receptor for active targeting of cancer nanotherapeutics.
44. Leamon, C. P.; Cooper, S. R.; Hardee, G. E., Folate-Liposome-Mediated Antisense Oligodeoxynucleotide Targeting to Cancer Cells: Evaluation in Vitro and in Vivo. *Bioconjugate Chemistry* **2003,** *14* (4), 738-747.
45. Li, X.; Rao, X.; Cai, L.; Liu, X.; Wang, H.; Wu, W.; Zhu, C.; Chen, M.; Wang, P. G.; Yi, W., Targeting Tumor Cells by Natural Anti-Carbohydrate Antibodies Using Rhamnose-Functionalized Liposomes. *ACS Chemical Biology* **2016,** *11* (5), 1205-1209.
46. Merino, M.; Zalba, S.; Garrido, M. J., Immunoliposomes in clinical oncology: State of the art and future perspectives. *Journal of Controlled Release* **2018,** *275*, 162-176.
47. Wang, Y.; Liu, F.; Wang, Q.; Xiang, H.; Jin, H.; Li, H.; Mao, S., A novel immunoliposome mediated by CD123 antibody targeting to acute myeloid leukemia cells. *International Journal of Pharmaceutics* **2017,** *529* (1), 531-542.
48. Kuşoğlu, A.; Biray Avcı, Ç., Cancer stem cells: A brief review of the current status. *Gene* **2019,** *681*, 80-85.
49. Arabi, L.; Badiee, A.; Mosaffa, F.; Jaafari, M. R., Targeting CD44 expressing cancer cells with anti-CD44 monoclonal antibody improves cellular uptake and antitumor efficacy of liposomal doxorubicin. *Journal of Controlled Release* **2015,** *220*, 275-286.
50. Li, Q.; Tang, Q.; Zhang, P.; Wang, Z.; Zhao, T.; Zhou, J.; Li, H.; Ding, Q.; Li, W.; Hu, F.; Du, Y.; Yuan, H.; Chen, S.; Gao, J.; Zhan, J.; You, J., Human epidermal growth factor receptor-2 antibodies enhance the specificity and anticancer activity of light-sensitive doxorubicin-labeled liposomes. *Biomaterials* **2015,** *57*, 1-11.
51. Luo, D.; Li, N.; Carter, K. A.; Lin, C.; Geng, J.; Shao, S.; Huang, W.-C.; Qin, Y.; Atilla-Gokcumen, G. E.; Lovell, J. F., Rapid Light-Triggered Drug Release in Liposomes Containing Small Amounts of Unsaturated and Porphyrin–Phospholipids. *Small* **2016,** *12* (22), 3039-3047.
52. Carter, K. A.; Shao, S.; Hoopes, M. I.; Luo, D.; Ahsan, B.; Grigoryants, V. M.; Song, W.; Huang, H.; Zhang, G.; Pandey, R. K.; Geng, J.; Pfeifer, B. A.; Scholes, C. P.; Ortega, J.; Karttunen, M.; Lovell, J. F., Porphyrin–phospholipid liposomes permeabilized by near-infrared light. *Nature Communications* **2014,** *5*, 3546.
53. Sine, J.; Urban, C.; Thayer, D.; Charron, H.; Valim, N.; Tata, D. B.; Schiff, R.; Blumenthal, R.; Joshi, A.; Puri, A., Photo activation of HPPH encapsulated in “Pocket” liposomes triggers multiple drug release and tumor cell killing in mouse breast cancer xenografts. *International Journal of Nanomedicine* **2015,** *10*, 125-145.
54. Bayer, A. M.; Alam, S.; Mattern-Schain, S. I.; Best, M. D., Triggered liposomal release through a synthetic phosphatidylcholine analogue bearing a

photocleavable moiety embedded within the sn-2 acyl chain. *Chemistry* **2014,** *20* (12), 3350-7.
55. Alam, S.; Alves, D. S.; Whitehead, S. A.; Bayer, A. M.; McNitt, C. D.; Popik, V. V.; Barrera, F. N.; Best, M. D., A clickable and photocleavable lipid analogue for cell membrane delivery and release. *Bioconjugate Chemistry* **2015,** *26* (6), 1021-31.
56. Ta, T.; Convertine, A. J.; Reyes, C. R.; Stayton, P. S.; Porter, T. M., Thermosensitive Liposomes Modified with Poly(N-isopropylacrylamide-co-propylacrylic acid) Copolymers for Triggered Release of Doxorubicin. *Biomacromolecules* **2010,** *11* (8), 1915-1920.
57. Wong, P. T.; Choi, S. K., Mechanisms of Drug Release in Nanotherapeutic Delivery Systems. *Chemical Reviews* **2015,** *115* (9), 3388-3432.
58. Harris, A. L., Hypoxia — a key regulatory factor in tumour growth. *Nature Reviews Cancer* **2002,** *2*, 38.
59. Monteiro, L. O. F.; Malachias, Â.; Pound-Lana, G.; Magalhães-Paniago, R.; Mosqueira, V. C. F.; Oliveira, M. C.; de Barros, A. L. B.; Leite, E. A., Paclitaxel-Loaded pH-Sensitive Liposome: New Insights on Structural and Physicochemical Characterization. *Langmuir* **2018,** *34* (20), 5728-5737.
60. Zheng, Y.; Liu, X.; Samoshina, N. M.; Samoshin, V. V.; Franz, A. H.; Guo, X., Fliposomes: trans-2-aminocyclohexanol-based amphiphiles as pH-sensitive conformational switches of liposome membrane – a structure-activity relationship study. *Chemistry and Physics of Lipids* **2018,** *210*, 129-141.
61. Shin, **2012**.
62. Guo, X.; Szoka, F. C., Jr., Steric stabilization of fusogenic liposomes by a low-pH sensitive PEG--diortho ester--lipid conjugate. *Bioconjugate Chemistry* **2001,** *12* (2), 291-300.
63. Kale, A. A.; Torchilin, V. P., Design, Synthesis and Characterization of pH-Sensitive PEG-PE Conjugates for Stimuli-Sensitive Pharmaceutical Nanocarriers: The Effect of Substitutes at the Hydrazone Linkage on the pH-Stability of PEG-PE Conjugates. *Bioconjugate Chemistry* **2007,** *18* (2), 363-370.
64. Chi, Y.; Yin, X.; Sun, K.; Feng, S.; Liu, J.; Chen, D.; Guo, C.; Wu, Z., Redox-sensitive and hyaluronic acid functionalized liposomes for cytoplasmic drug delivery to osteosarcoma in animal models. *Journal of Controlled Release* **2017,** *261*, 113-125.
65. Fu, H.; Shi, K.; Hu, G.; Yang, Y.; Kuang, Q.; Lu, L.; Zhang, L.; Chen, W.; Dong, M.; Chen, Y.; He, Q., Tumor-Targeted Paclitaxel Delivery and Enhanced Penetration Using TAT-Decorated Liposomes Comprising Redox-Responsive Poly(Ethylene Glycol). *Journal of Pharmaceutical Sciences* **2015,** *104* (3), 1160-1173.
66. Tang, J.; Zhang, L.; Gao, H.; Liu, Y.; Zhang, Q.; Ran, R.; Zhang, Z.; He, Q., Co-delivery of doxorubicin and P-gp inhibitor by a reduction-sensitive liposome to overcome multidrug resistance, enhance anti-tumor efficiency and reduce toxicity. *Drug Delivery* **2016,** *23* (4), 1130-1143.

67. Fouladi, F.; Steffen, K. J.; Mallik, S., Enzyme-Responsive Liposomes for the Delivery of Anticancer Drugs. *Bioconjugate Chemistry* **2017,** *28* (4), 857-868.
68. Mock, J. N.; Costyn, L. J.; Wilding, S. L.; Arnold, R. D.; Cummings, B. S., Evidence for distinct mechanisms of uptake and antitumor activity of secretory phospholipase A2 responsive liposome in prostate cancer. *Integrative biology : quantitative biosciences from nano to macro* **2013,** *5* (1), 172-82.
69. Zhu, L.; Kate, P.; Torchilin, V. P., Matrix metalloprotease 2-responsive multifunctional liposomal nanocarrier for enhanced tumor targeting. *ACS Nano* **2012,** *6* (4), 3491-8.
70. Andreini, C.; Banci, L.; Bertini, I.; Rosato, A., Counting the Zinc-Proteins Encoded in the Human Genome. *Journal of Proteome Research* **2006,** *5* (1), 196-201.
71. Hancock, S. M.; Bush, A. I.; Adlard, P. A., The Clinical Implications of Impaired Zinc Signaling in the Brain. In *Zinc Signals in Cellular Functions and Disorders*, Fukada, T.; Kambe, T., Eds. Springer Japan: Tokyo, 2014; pp 183-196.
72. Nishida, K.; Yamasaki, S., Zinc Signaling by “Zinc Wave”. In *Zinc Signals in Cellular Functions and Disorders*, Fukada, T.; Kambe, T., Eds. Springer Japan: Tokyo, 2014; pp 89-109.
73. Kambe, T., Introduction: “Zinc Signaling”–The Blossoming Field of Zinc Biology. In *Zinc Signals in Cellular Functions and Disorders*, Fukada, T.; Kambe, T., Eds. Springer Japan: Tokyo, 2014; pp 1-5.
74. Lou, J.; Carr, A. J.; Watson, A. J.; Mattern-Schain, S. I.; Best, M. D., Calcium-Responsive Liposomes via a Synthetic Lipid Switch. *Chemistry – A European Journal* **2018,** *24* (14), 3599-3607.
75. Lou, J.; Zhang, X.; Best, M. D., Lipid Switches: Stimuli-Responsive Liposomes via Conformational Isomerism Driven by Molecular Recognition. *Chemistry* **2018**.
76. Zhang, X.; Alves, D. S.; Lou, J.; Hill, S. D.; Barrera, F. N.; Best, M. D., Boronic acid liposomes for cellular delivery and content release driven by carbohydrate binding. *Chemical Communications* **2018,** *54* (48), 6169-6172.
77. Grynkiewicz, G.; Poenie, M.; Tsien, R. Y., A new generation of Ca2+ indicators with greatly improved fluorescence properties. *The Journal of Biological Chemistry* **1985,** *260* (6), 3440-50.
78. Takeuchi, J.; Ohkubo, A.; Yuasa, H., A Ring-Flippable Sugar as a Stimuli-Responsive Component of Liposomes. *Chemistry – An Asian Journal* **2015,** *10* (3), 586-594.
79. Huang, Z.; Zhang, X.-a.; Bosch, M.; Smith, S.; Lippard, S. J., Tris(2-pyridylmethyl)amine (TPA) as a membrane-permeable chelator for interception of biological mobile zinc(). *Metallomics : Integrated Biometal Science* **2013,** *5* (6), 648-655.
80. Irving, H.; Williams, R. J. P., 637. The stability of transition-metal complexes. *Journal of the Chemical Society (Resumed)* **1953,** (0), 3192-3210.

81. Maruyama, S.; Kikuchi, K.; Hirano, T.; Urano, Y.; Nagano, T., A Novel, Cell-Permeable, Fluorescent Probe for Ratiometric Imaging of Zinc Ion. *Journal of the American Chemical Society* **2002,** *124* (36), 10650-10651.
82. Royzen, M.; Durandin, A.; Young, V. G.; Geacintov, N. E.; Canary, J. W., A Sensitive Probe for the Detection of Zn(II) by Time-Resolved Fluorescence. *Journal of the American Chemical Society* **2006,** *128* (12), 3854-3855.
83. Woodroofe, C. C.; Masalha, R.; Barnes, K. R.; Frederickson, C. J.; Lippard, S. J., Membrane-Permeable and -Impermeable Sensors of the Zinpyr Family and Their Application to Imaging of Hippocampal Zinc In Vivo. *Chemistry & Biology* **2004,** *11* (12), 1659-1666.
84. Tomat, E.; Lippard, S. J., Imaging mobile zinc in biology. *Current Opinion in Chemical Biology* **2010,** *14* (2), 225-230.
85. Takahiko, K.; Ken-ichi, H.; Shin-ya, I.; Fumito, T.; Yoshinori, N.; Masaki, K.; Yuji, O.; Yuichirou, H.; Kei, O.; Yoshihisa, M.; Shunichi, F., Synthesis and Characterization of Mononuclear Ruthenium(III) Pyridylamine Complexes and Mechanistic Insights into Their Catalytic Alkane Functionalization with m-Chloroperbenzoic Acid. *Chemistry – A European Journal* **2007,** *13* (29), 8212-8222.
86. Swahn, B.-M.; Kolmodin, K.; Karlström, S.; von Berg, S.; Söderman, P.; Holenz, J.; Berg, S.; Lindström, J.; Sundström, M.; Turek, D.; Kihlström, J.; Slivo, C.; Andersson, L.; Pyring, D.; Rotticci, D.; Öhberg, L.; Kers, A.; Bogar, K.; von Kieseritzky, F.; Bergh, M.; Olsson, L.-L.; Janson, J.; Eketjäll, S.; Georgievska, B.; Jeppsson, F.; Fälting, J., Design and Synthesis of β-Site Amyloid Precursor Protein Cleaving Enzyme (BACE1) Inhibitors with in Vivo Brain Reduction of β-Amyloid Peptides. *Journal of Medicinal Chemistry* **2012,** *55* (21), 9346-9361.
87. Bravin, C.; Badetti, E.; Scaramuzzo, F. A.; Licini, G.; Zonta, C., Triggering Assembly and Disassembly of a Supramolecular Cage. *Journal of the American Chemical Society* **2017,** *139* (18), 6456-6460.
88. Huang, P.-Q.; Zheng, X.; Deng, X.-M., DIBAL–H–H2NR and DIBAL–H–HNR1R2·HCl complexes for efficient conversion of lactones and esters to amides. *Tetrahedron Letters* **2001,** *42* (51), 9039-9041.
89. Kim, B. R.; Lee, H.-G.; Kang, S.-B.; Sung, G. H.; Kim, J.-J.; Park, J. K.; Lee, S.-G.; Yoon, Y.-J., tert-Butoxide-Assisted Amidation of Esters under Green Conditions. *Synthesis* **2012,** *44* (01), 42-50.
90. Tang, H.; Arulsamy, N.; Radosz, M.; Shen, Y.; Tsarevsky, N. V.; Braunecker, W. A.; Tang, W.; Matyjaszewski, K., Highly Active Copper-Based Catalyst for Atom Transfer Radical Polymerization. *Journal of the American Chemical Society* **2006,** *128* (50), 16277-16285.

APPENDIX

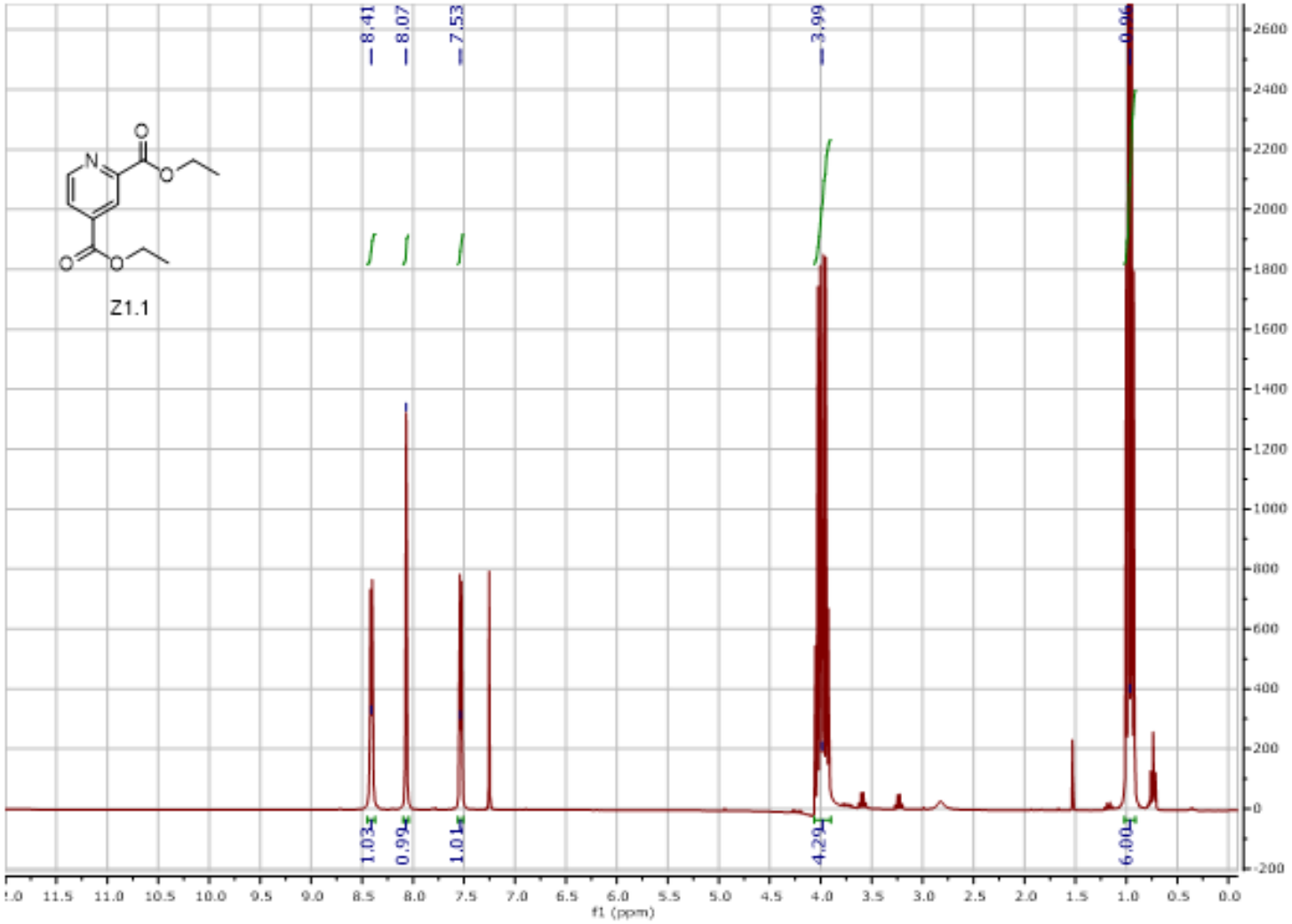

Spectrum 1: ^{1}H NMR (300 MHz, $CDCl_3$) Compound Z1.1

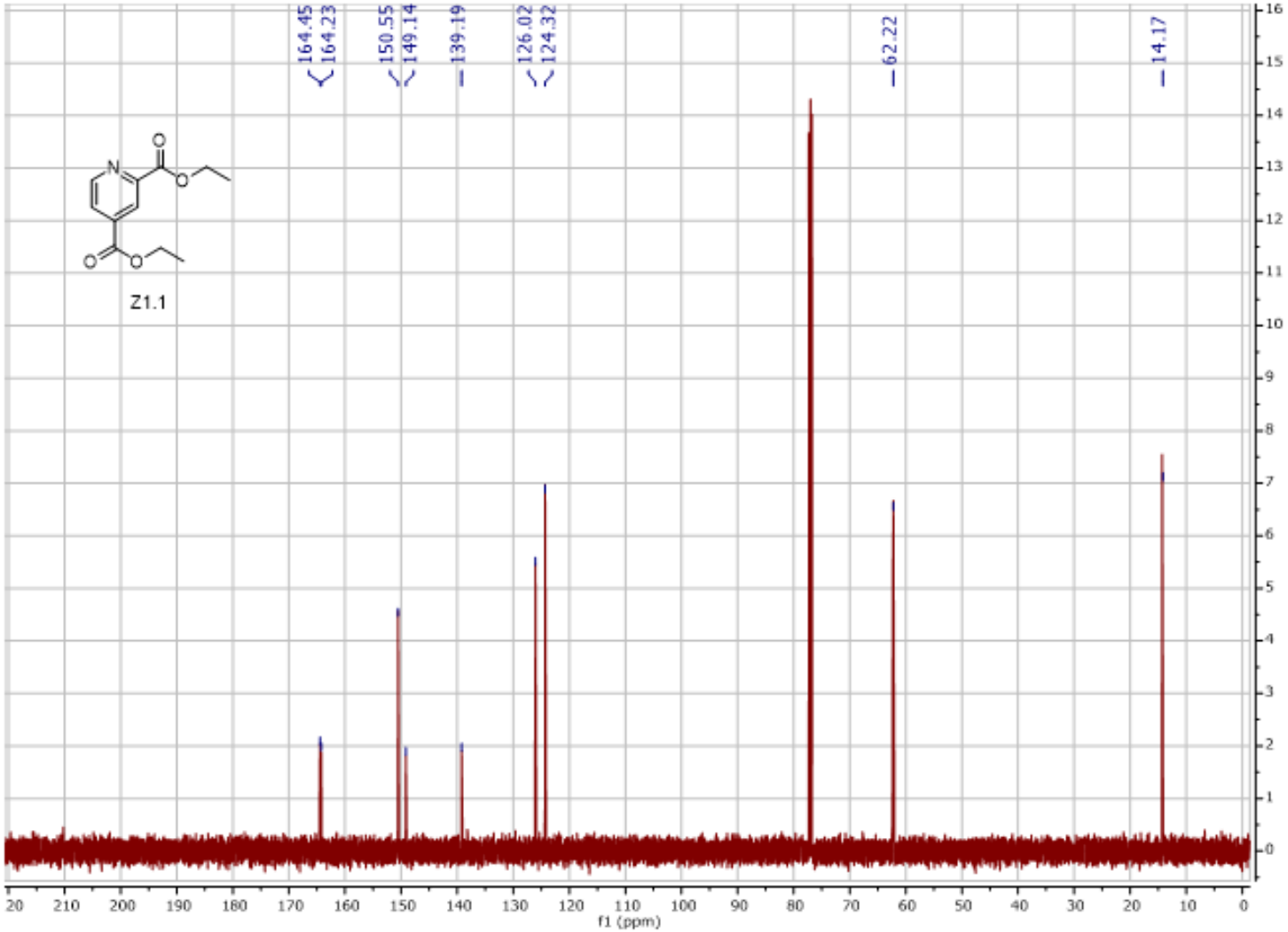

Spectrum 2: ^{13}C NMR (75 MHz, $CDCl_3$) Compound Z1.1

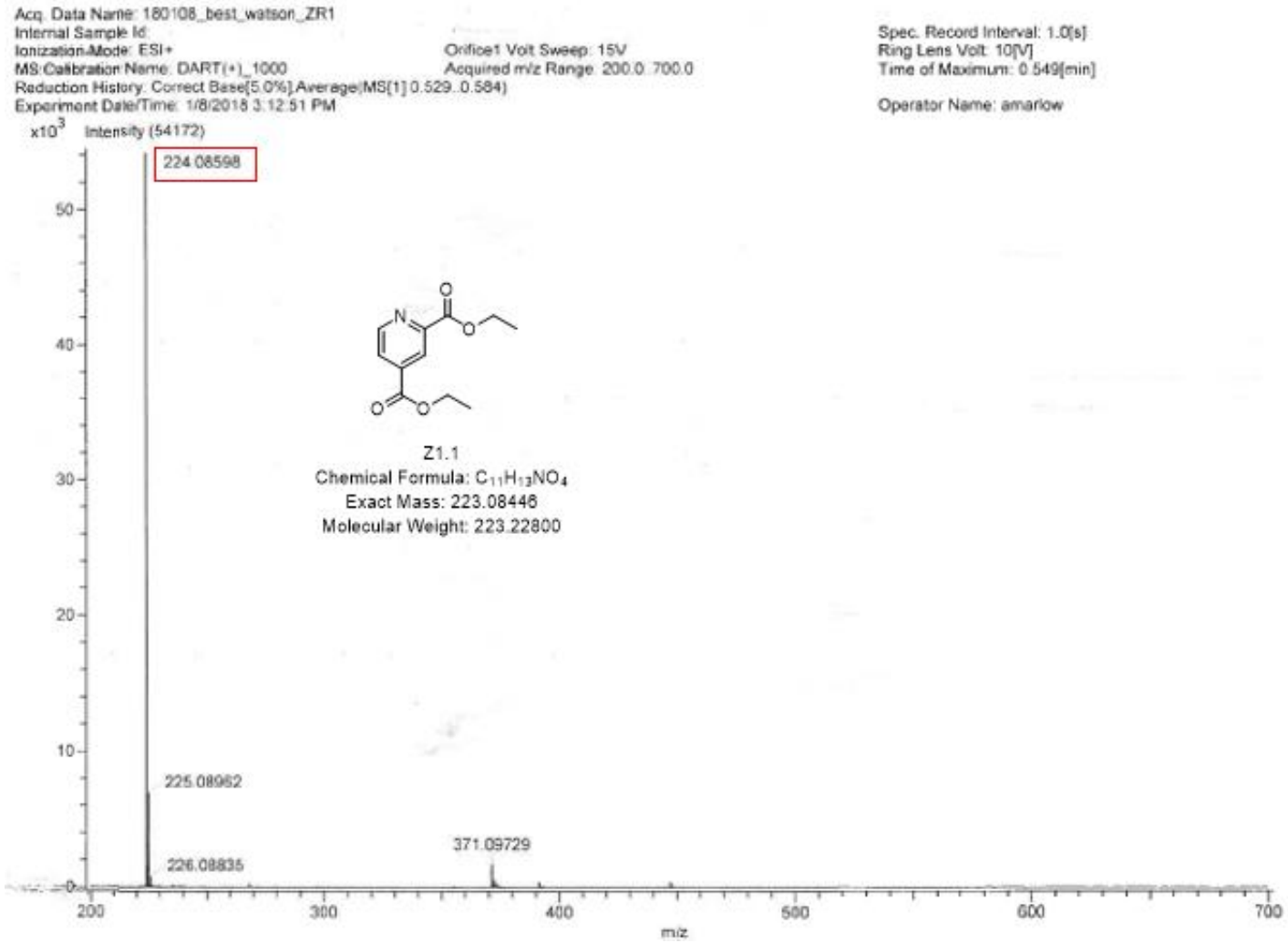

Spectrum 3: Mass Spectrum (JEOL DART-AccuTOF Mass Spectometer) Compound Z1.1 [M+1] predicted: 224.09173 [M+1] found: 224.08598

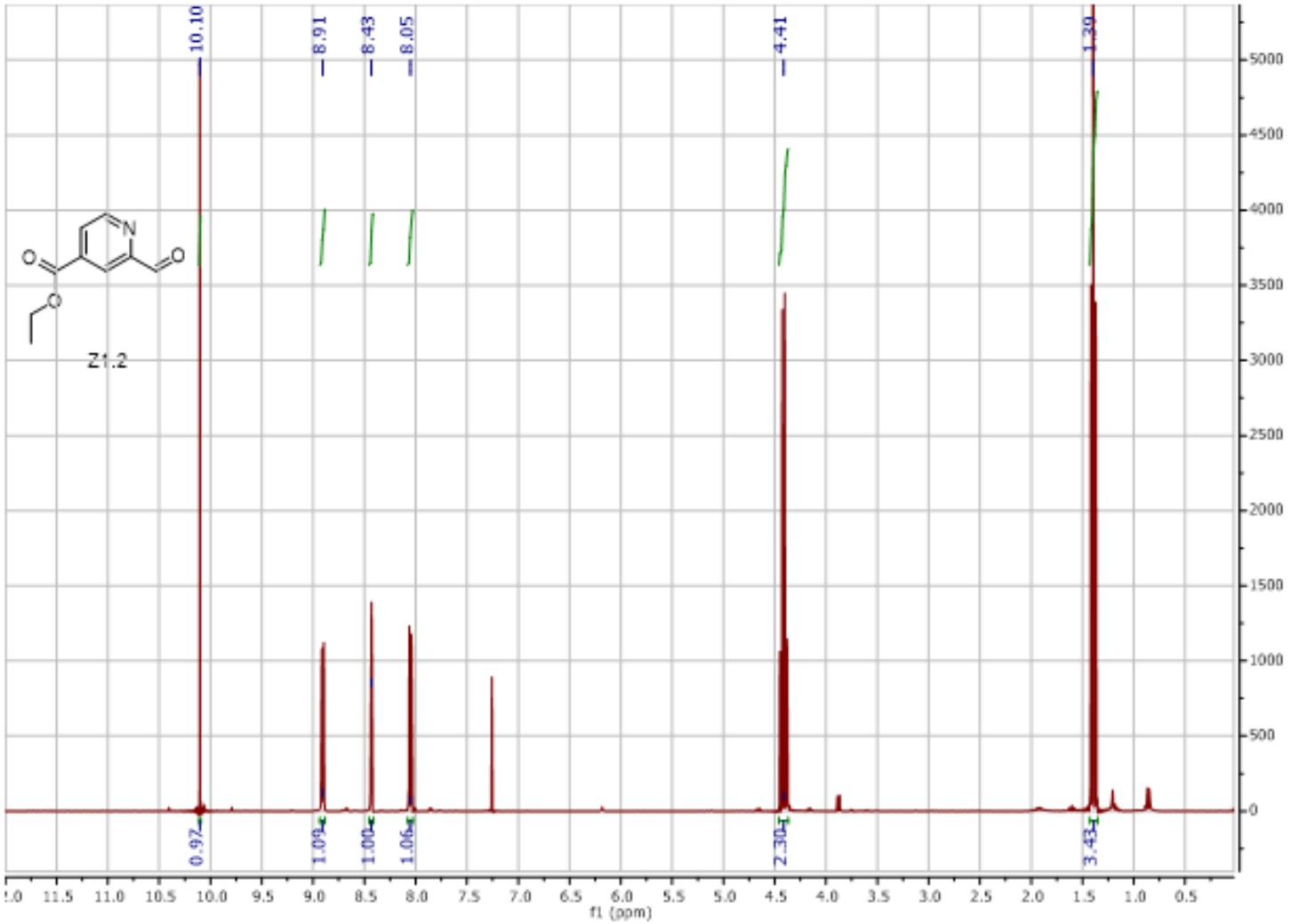

Spectrum 4: ^{1}H NMR (300 MHz, $CDCl_3$) Compound Z1.2

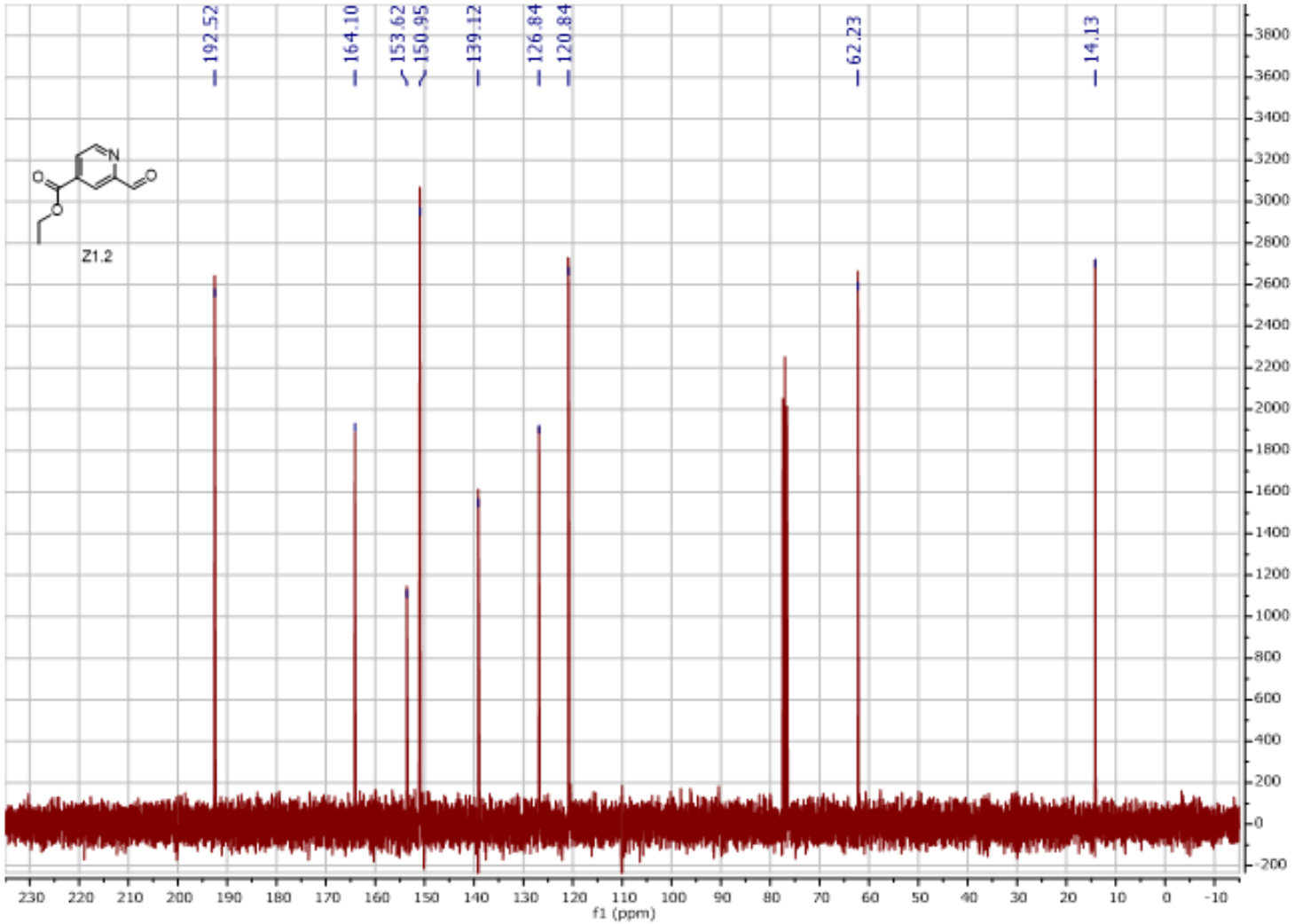

Spectrum 5: ^{13}C NMR (75 MHz, $CDCl_3$) Compound Z1.2

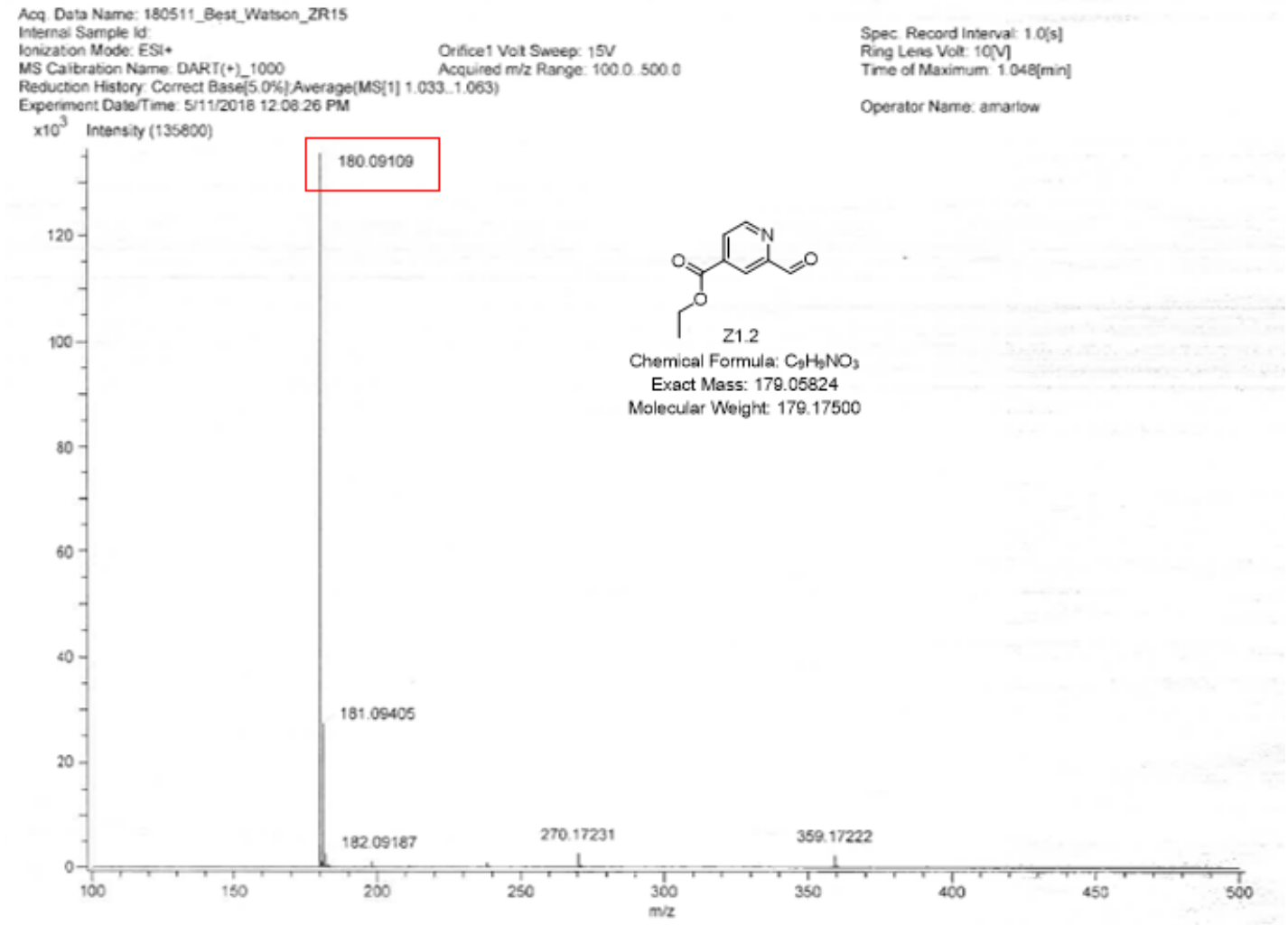

Spectra 6: Mass Spectrum (JEOL DART-AccuTOF Mass Spectometer) Compound Z1.2 [M+1] predicted: 180.06552 [M+1] found: 180.09109

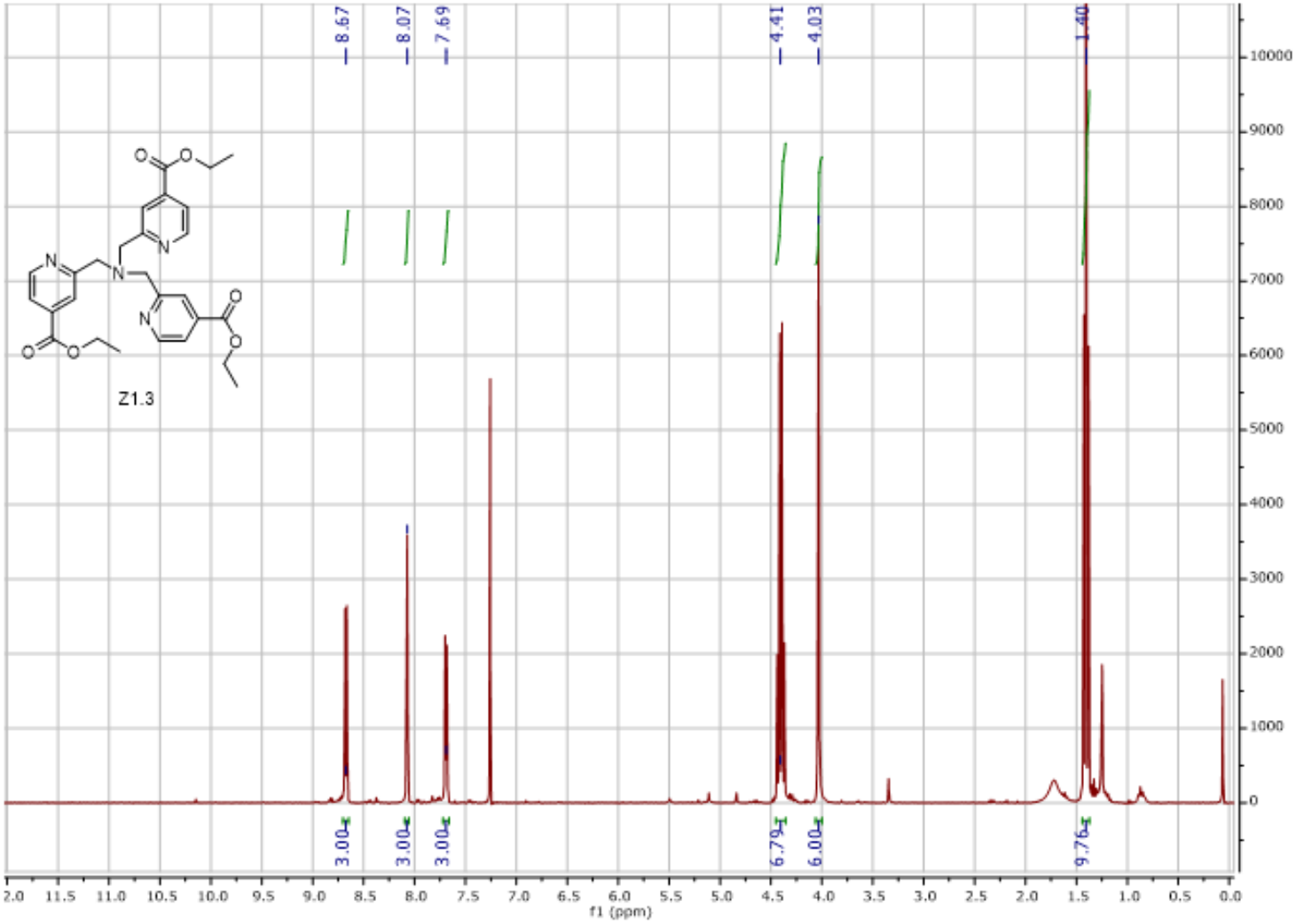

Spectrum 7: ^{1}H NMR (300 MHz, $CDCl_3$) Compound Z1.3

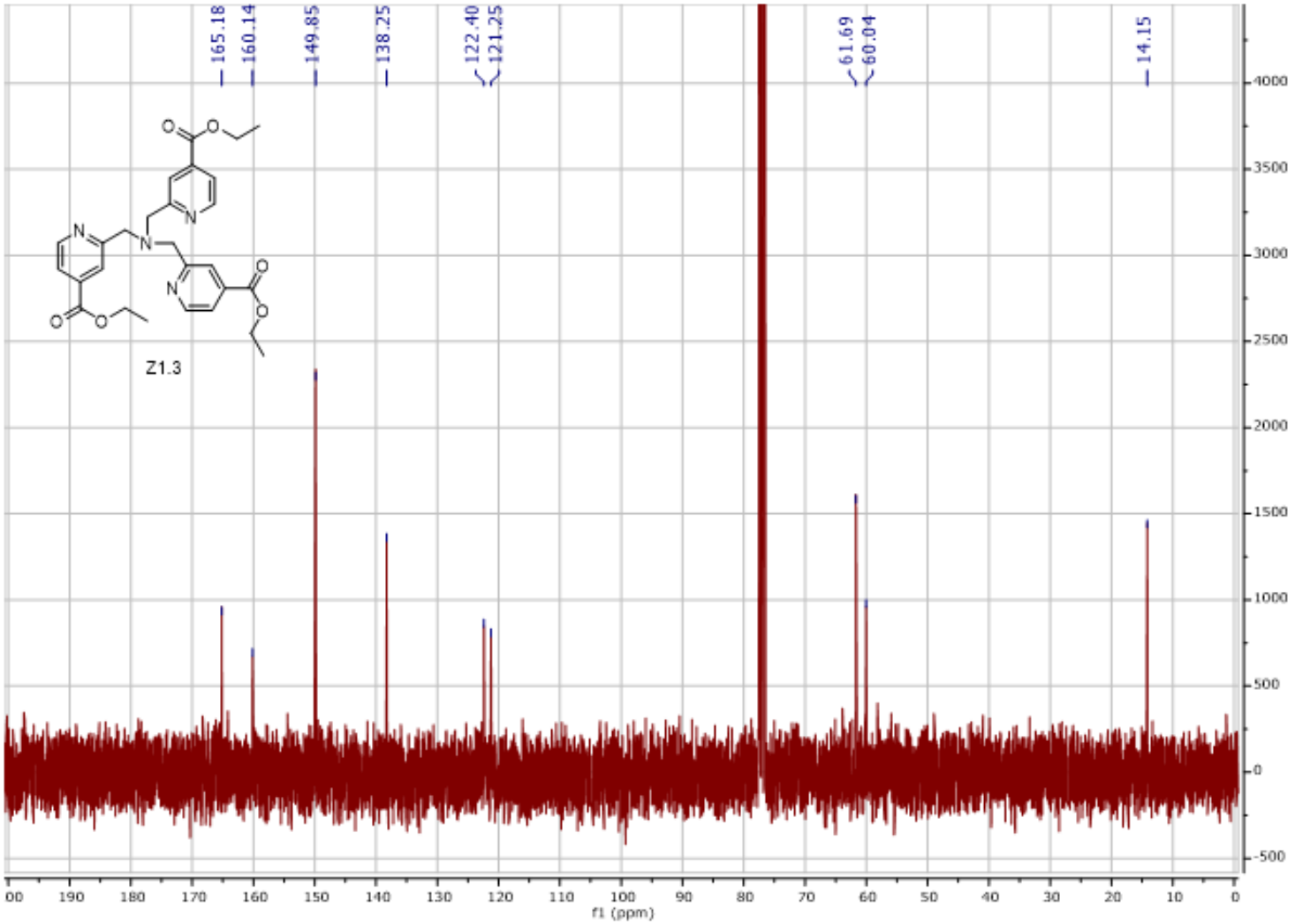

Spectra 8: ^{13}C NMR (75 MHz, $CDCl_3$) Compound Z1.

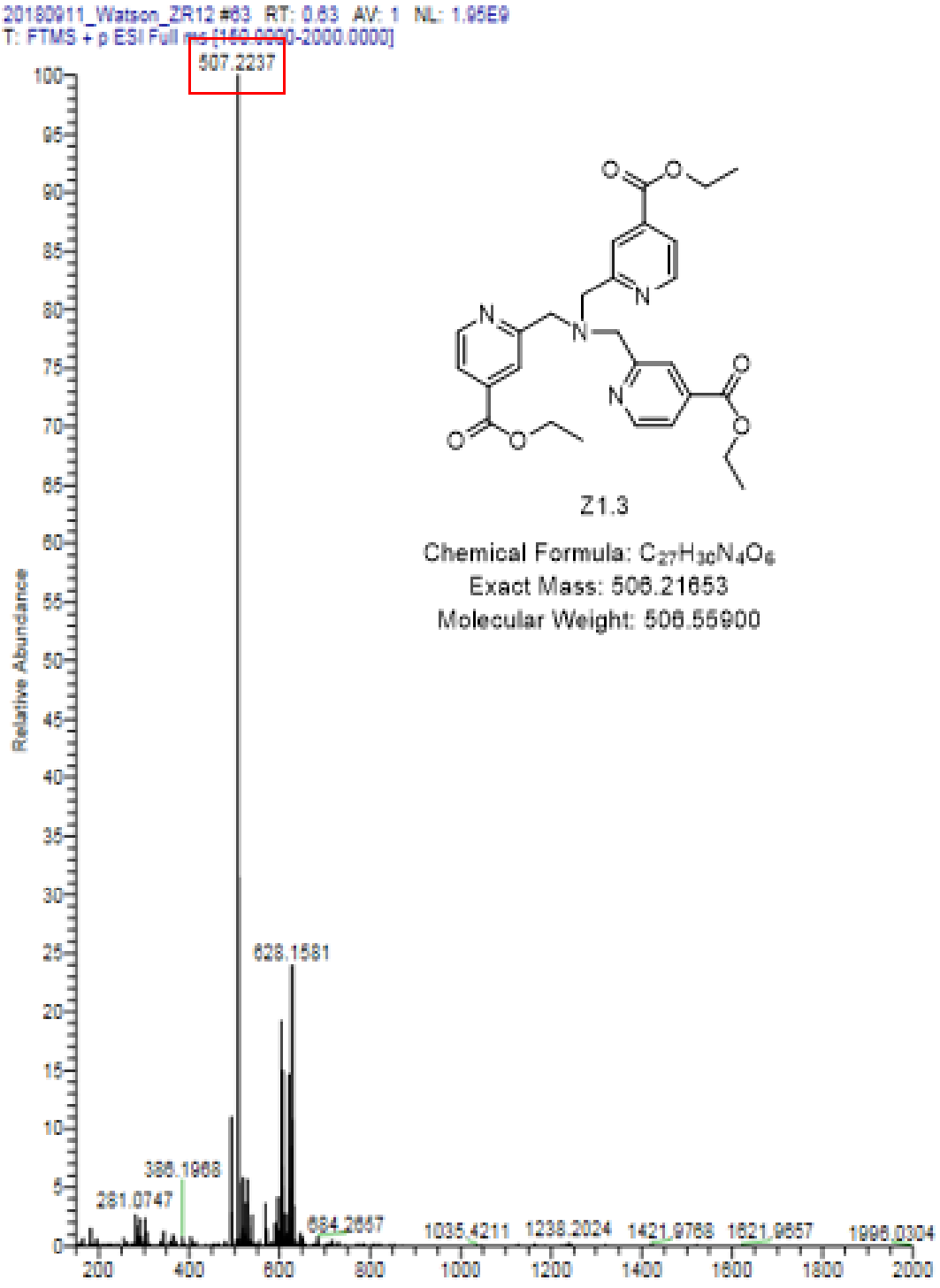

Spectrum 9: Mass specturm (Q-Star XL quadrupole time-of-flight hybrid mass spectrometer) Compound Z1.3 [M+1] predicted: 507.22381 [M+1] found: 507.233

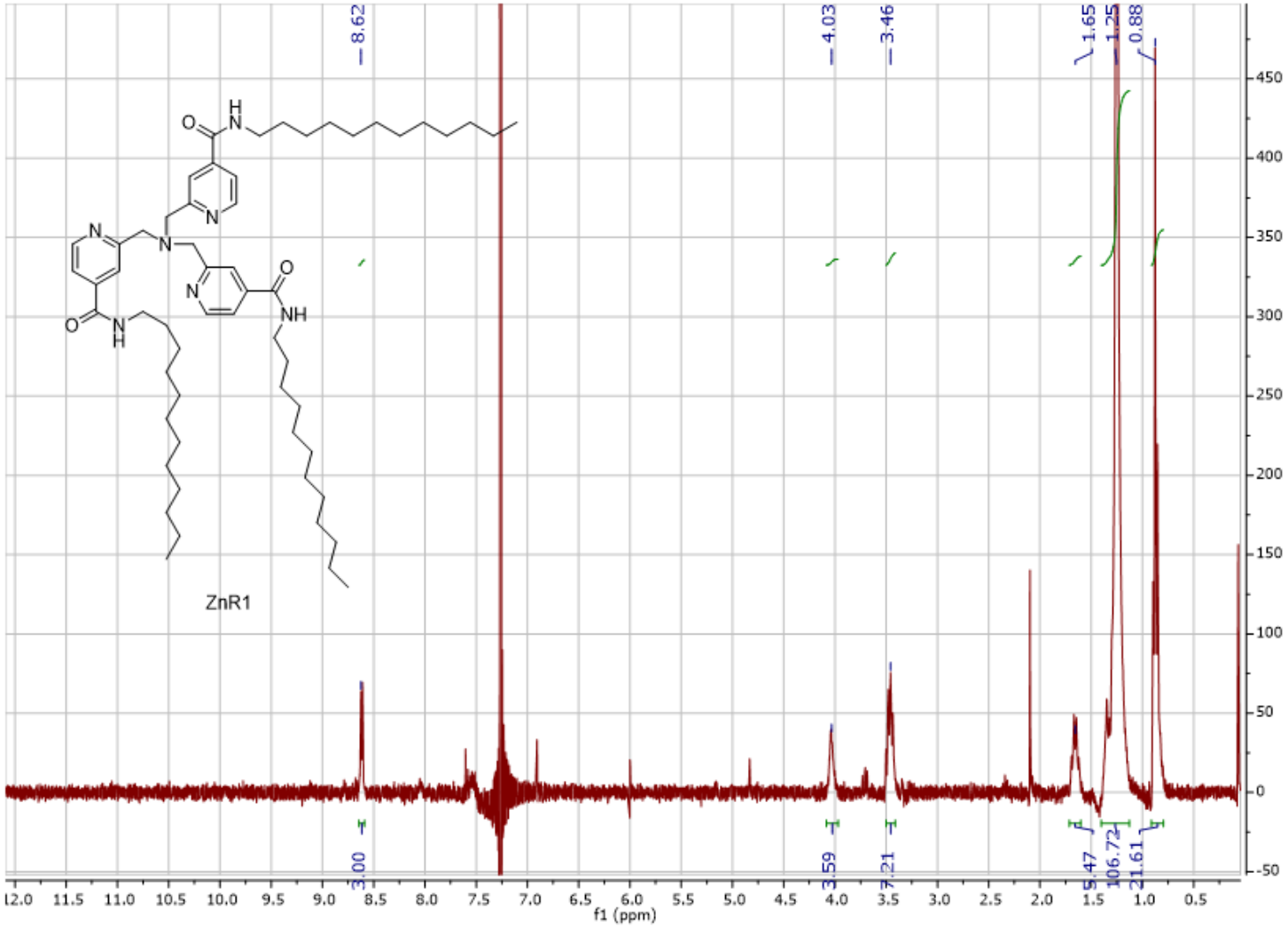

Spectrum 10: ^{1}H NMR (300MHz, $CDCl_3$) ZnR1. The aromatic region is muted in $CDCl_3$

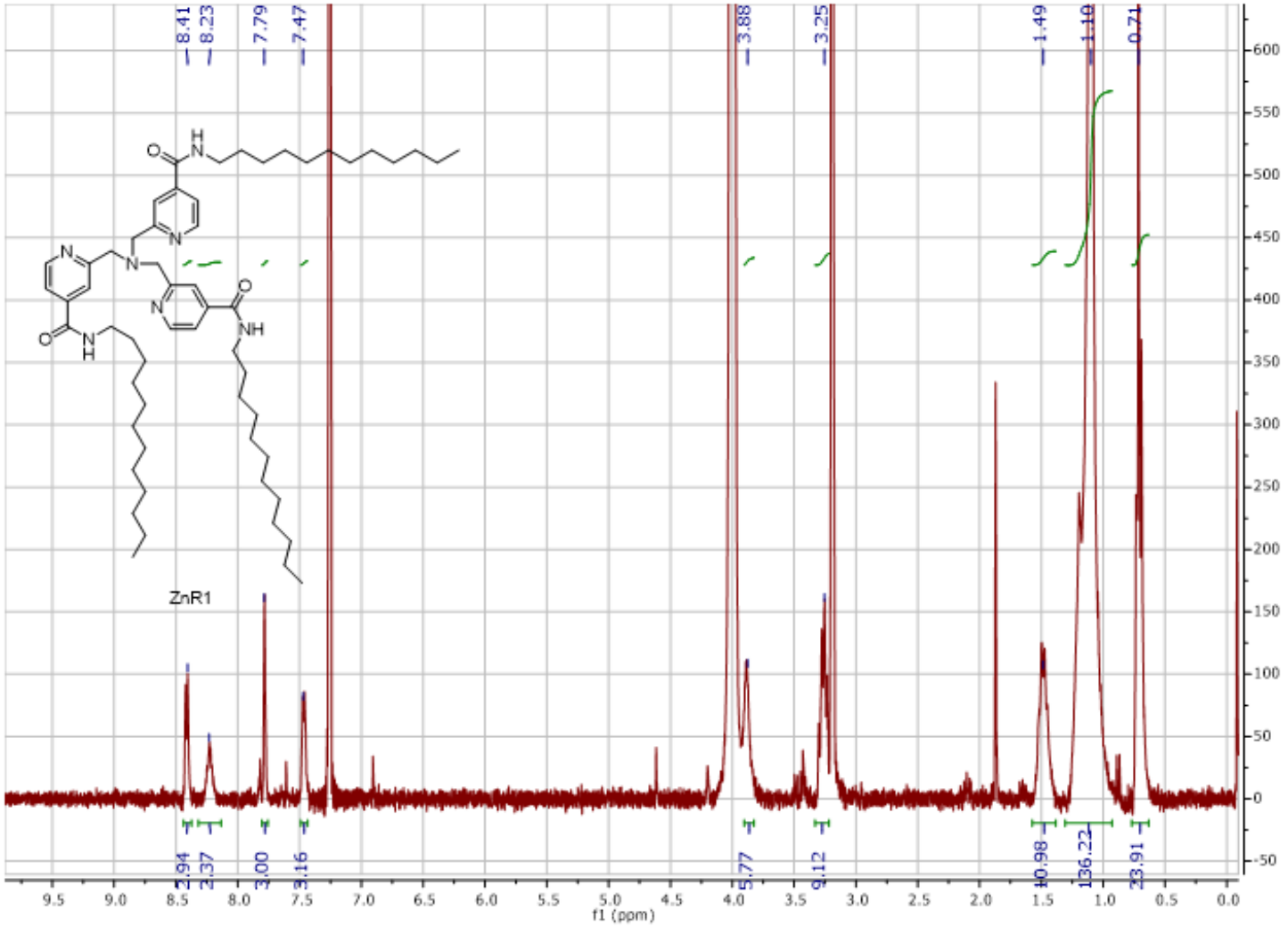

Spectrum 11: ^{1}H NMR (300 MHz, $CDCl_3$/MeOD) Compound ZnR1. The alkyl region integrates higher than the aromatic region (polar headgroup) as is common with lipid samples in NMR analysis.

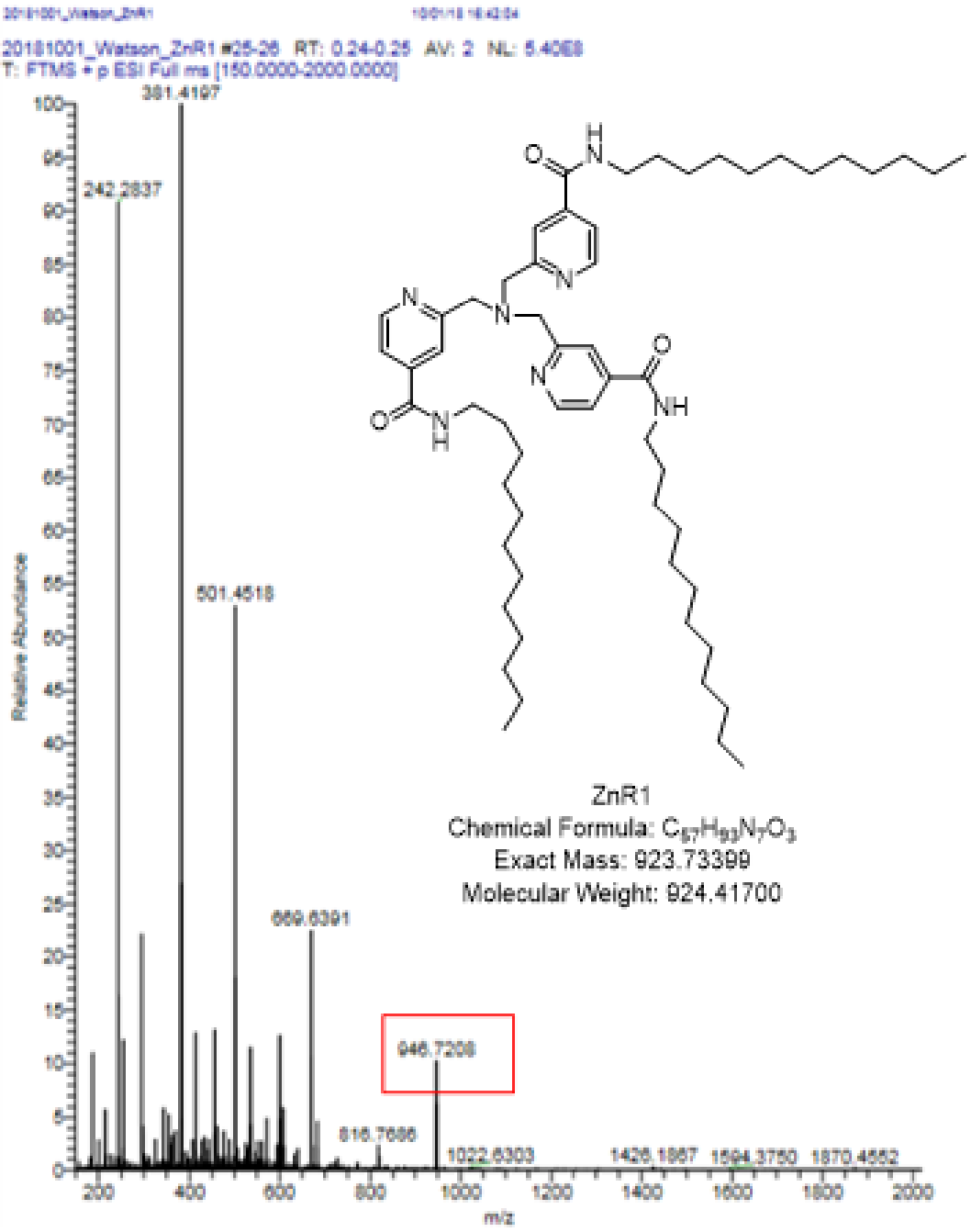

Spectrum 12: Mass specturm (Q-Star XL quadrupole time-of-flight hybrid mass spectrometer) Compound ZnR1. [M+Na] predicted: 946.72321 [M+Na] found: 946.7208

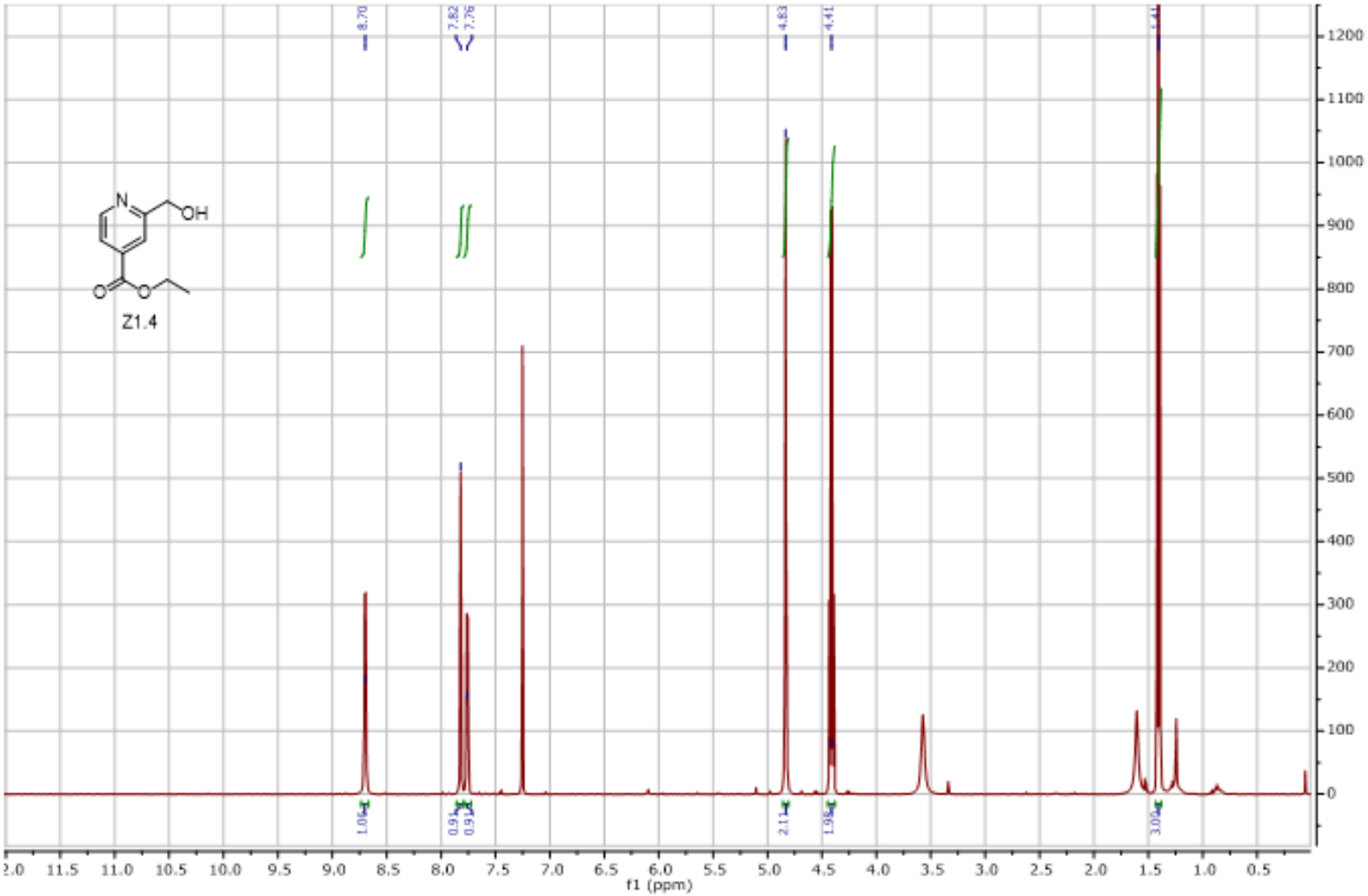

Spectrum 13: ^{1}H NMR (300 MHz, $CDCl_3$) Compound Z1.4

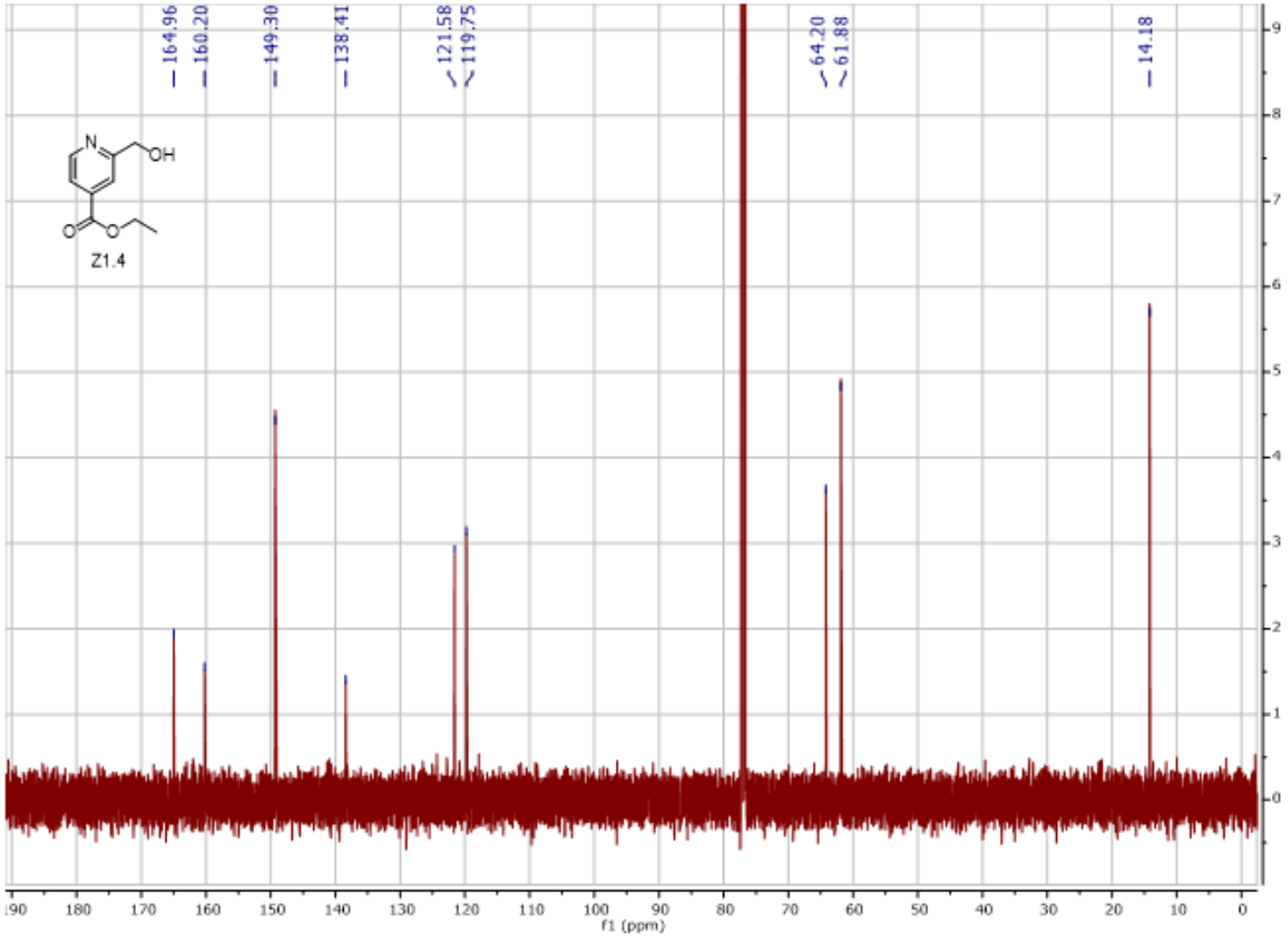

Spectrum 14: ^{13}C NMR: (75 MHz, $CDCl_3$) Z1.4

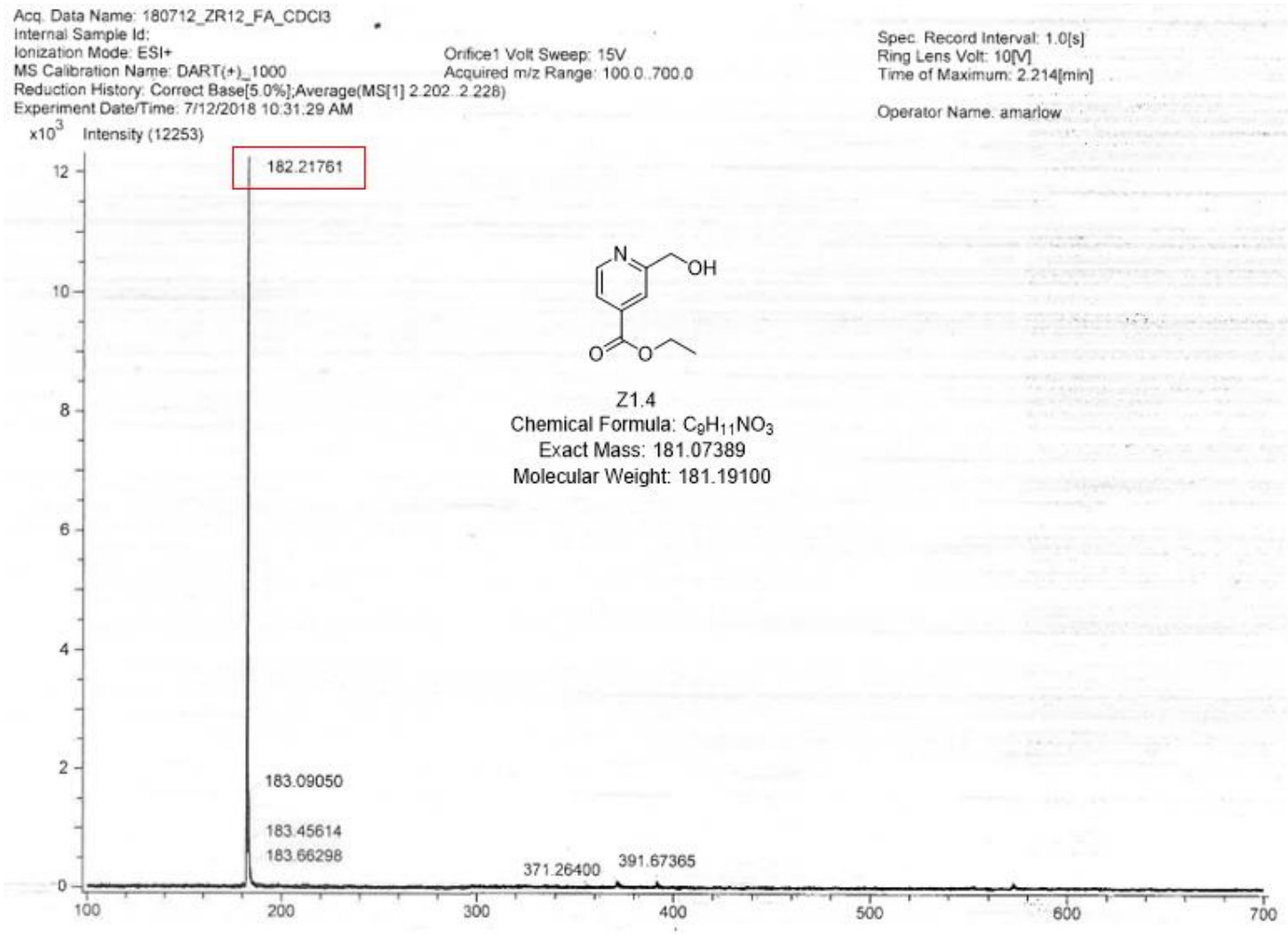

Spectrum 15: Mass Spectrum (JEOL DART-AccuTOF Mass Spectometer) Compound Z1.4 [M+1] predicted: 182.08117 [M+1] found:182.21761

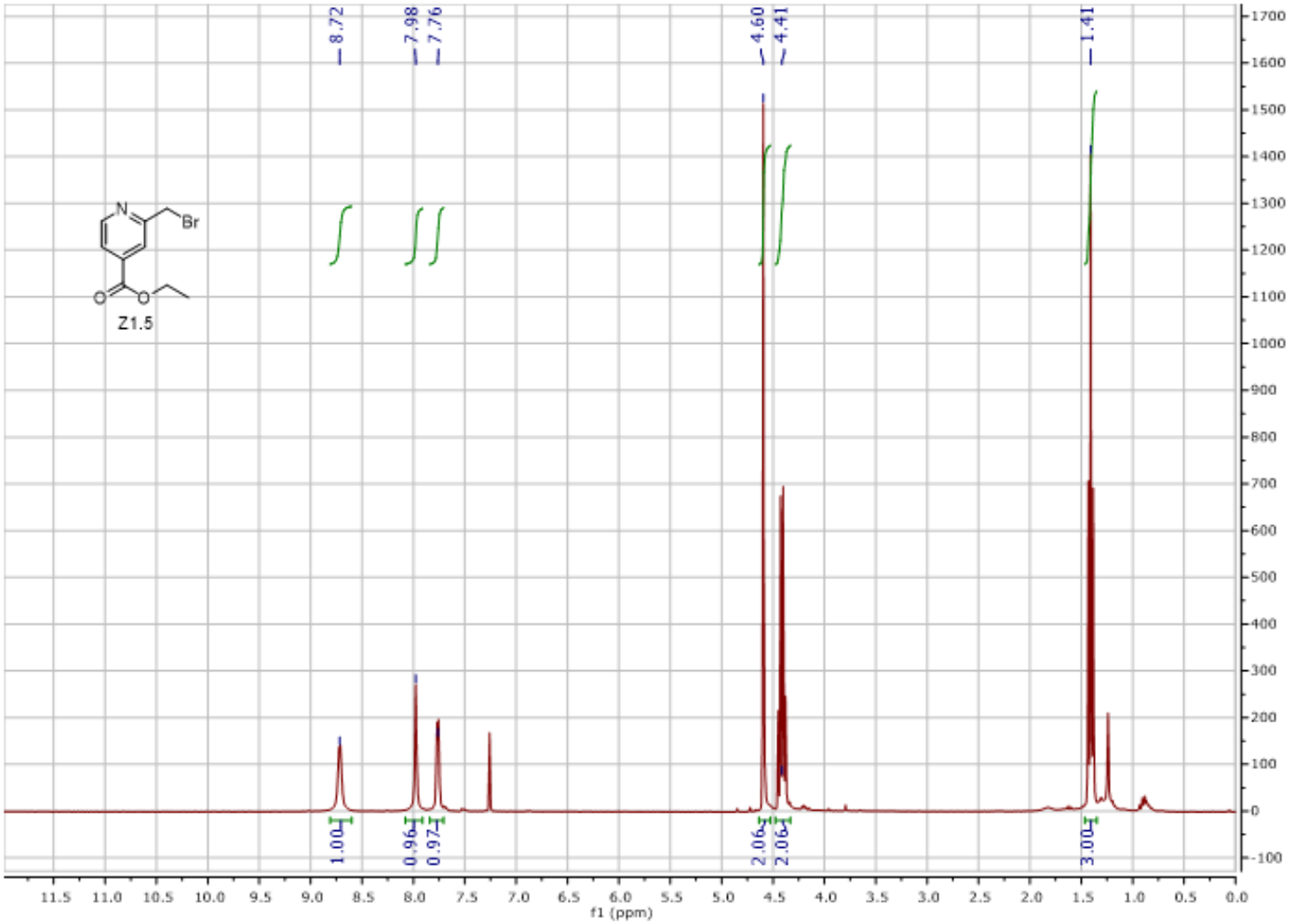

Spectrum 16: ^{1}H NMR (300 MHz, $CDCl_3$) Compound Z1.5

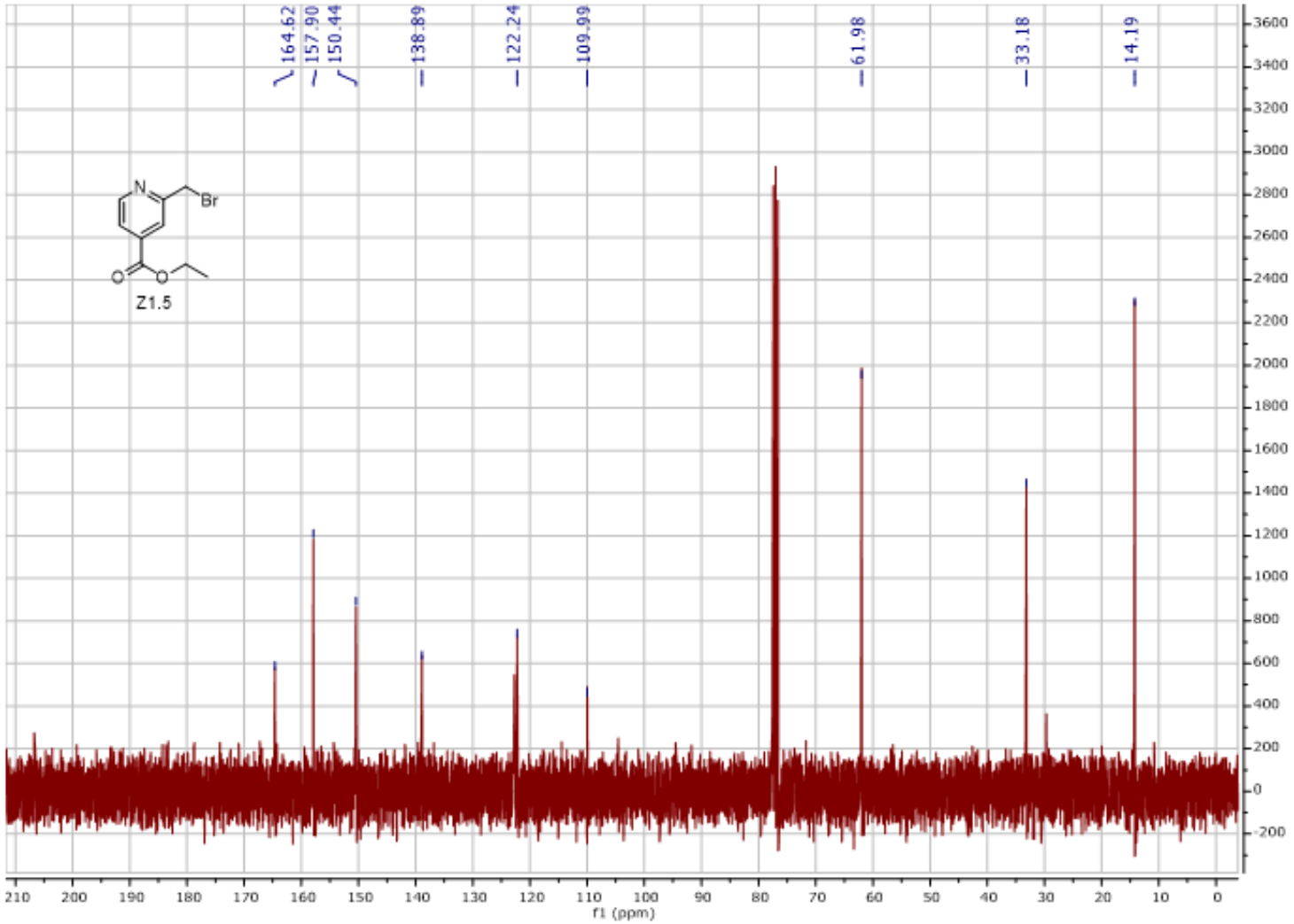

Spectrum 17: ^{13}C NMR (75 MHz, $CDCl_3$) Compound Z1.5

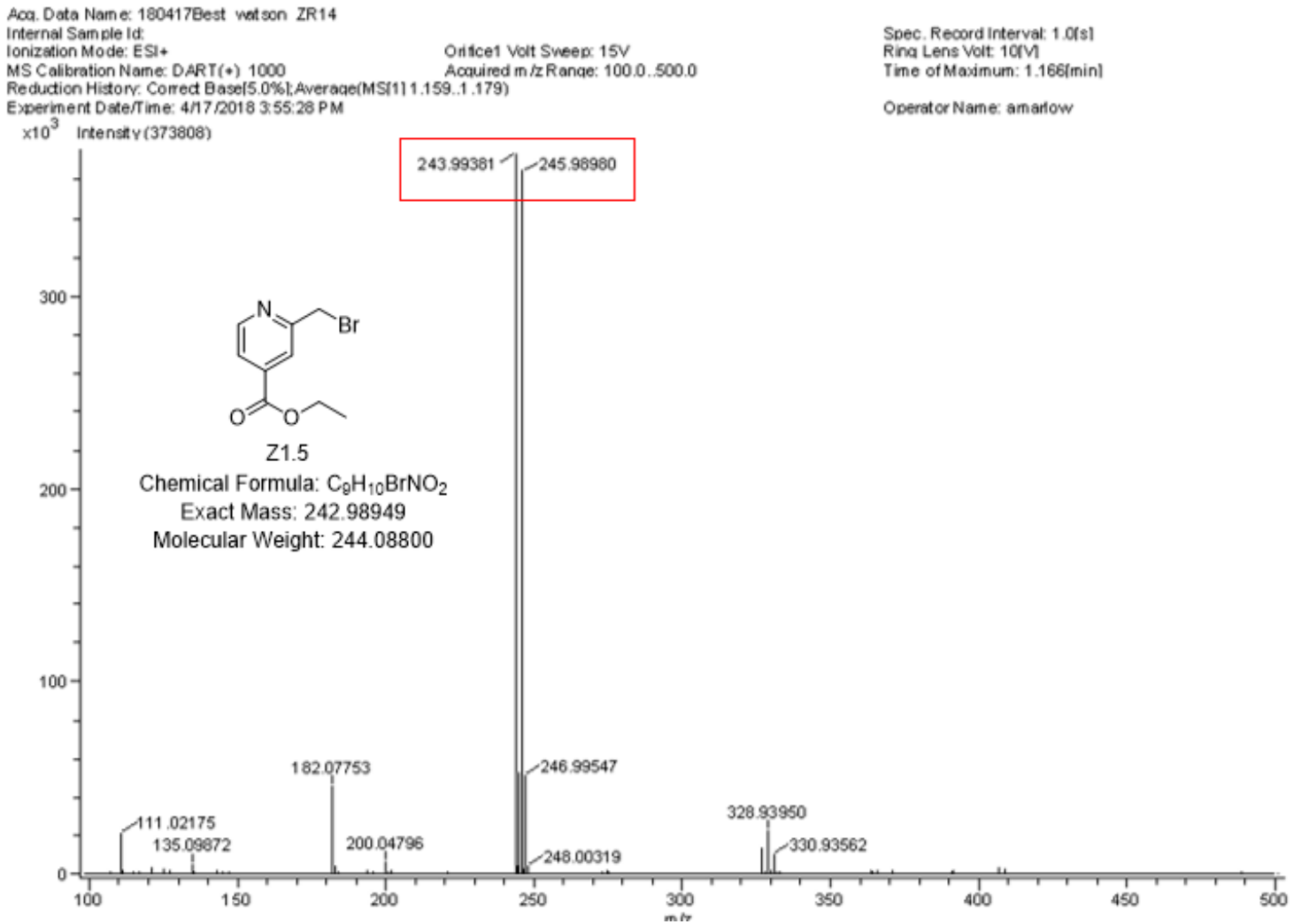

Spectrum 18: Mass Spectrum (JEOL DART-AccuTOF Mass Spectometer) Compound Z1.5 [M+1] predicted: 243.99677, 245.99472 [M+1] found: 243.99381, 245.98980

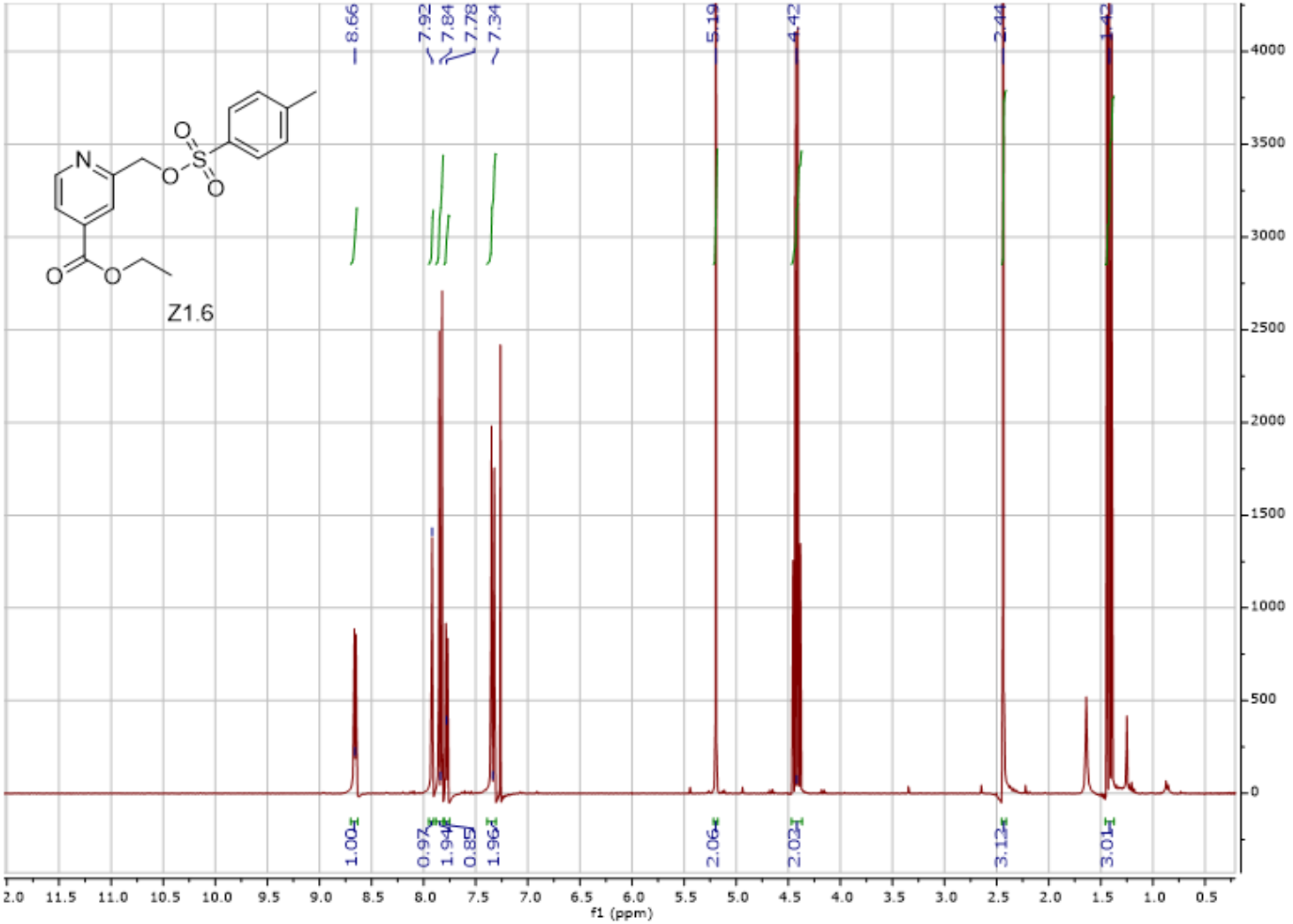

Spectrum 19: ^{1}H NMR (300 MHz, $CDCl_3$) Compound Z1.6

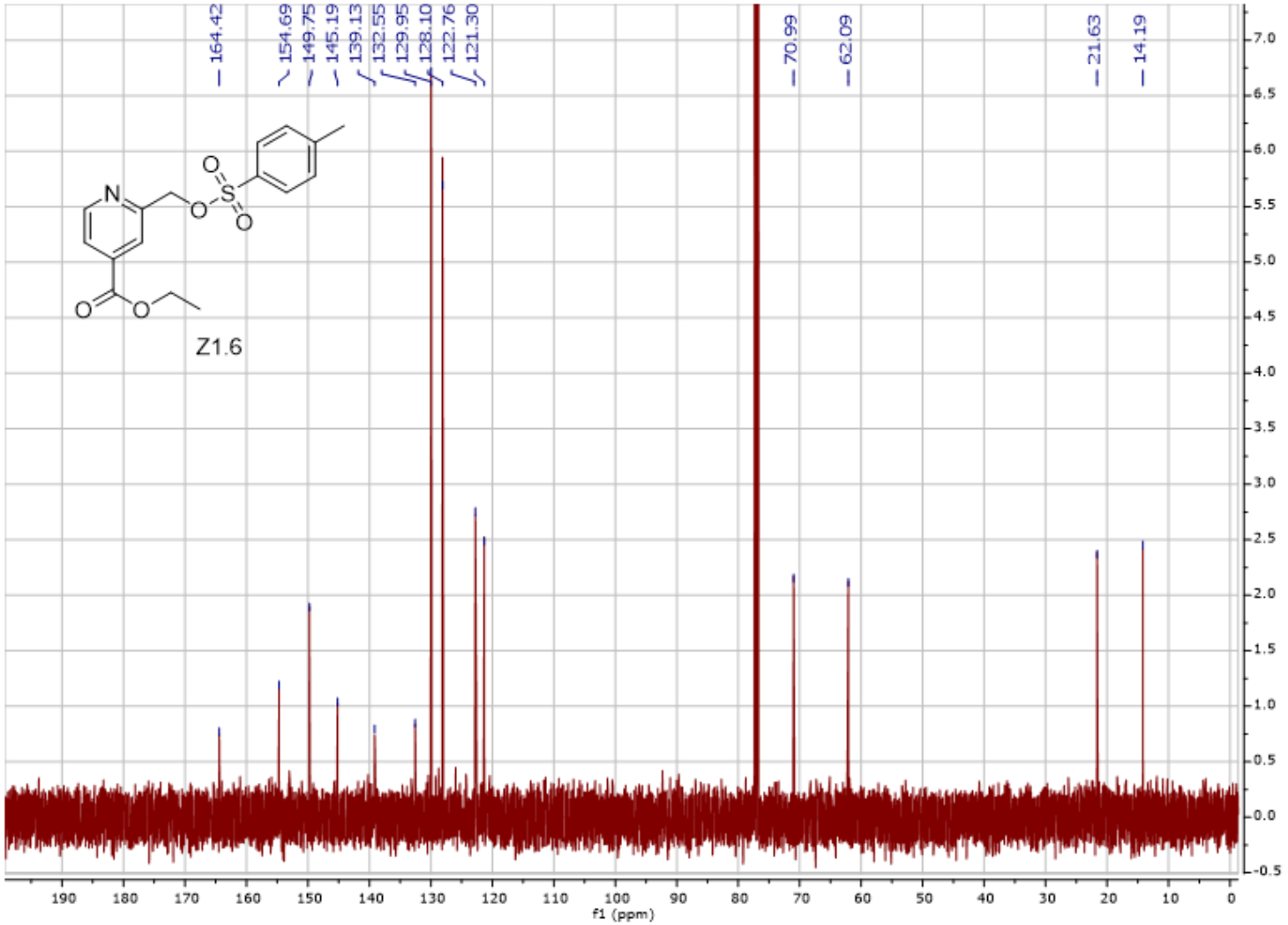

Spectrum 20: ^{13}C NMR (75 MHz, $CDCl_3$) Compound Z1.6

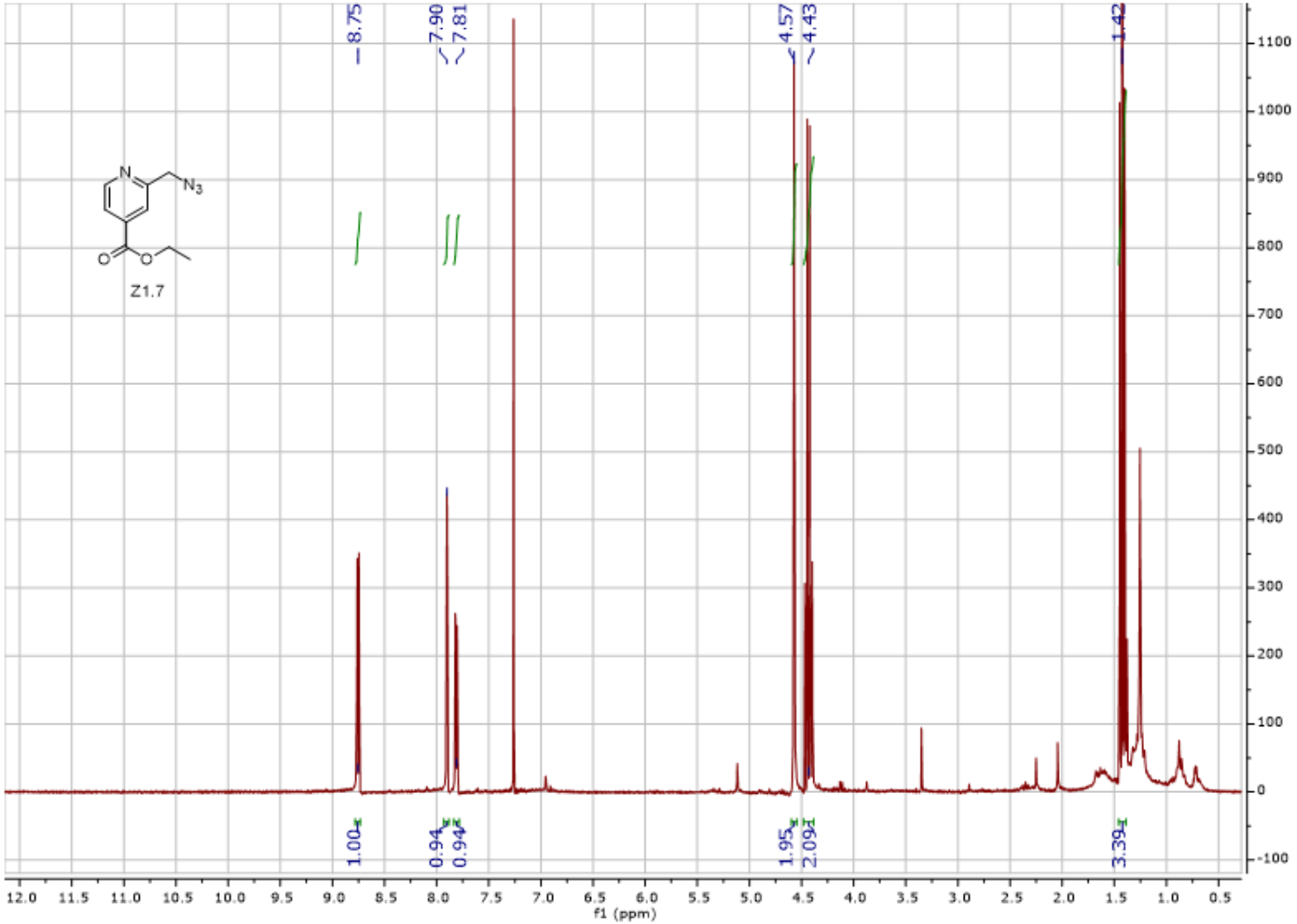

Spectrum 21: ^{1}H NMR (300 MHz, $CDCl_3$) Compound Z1.7

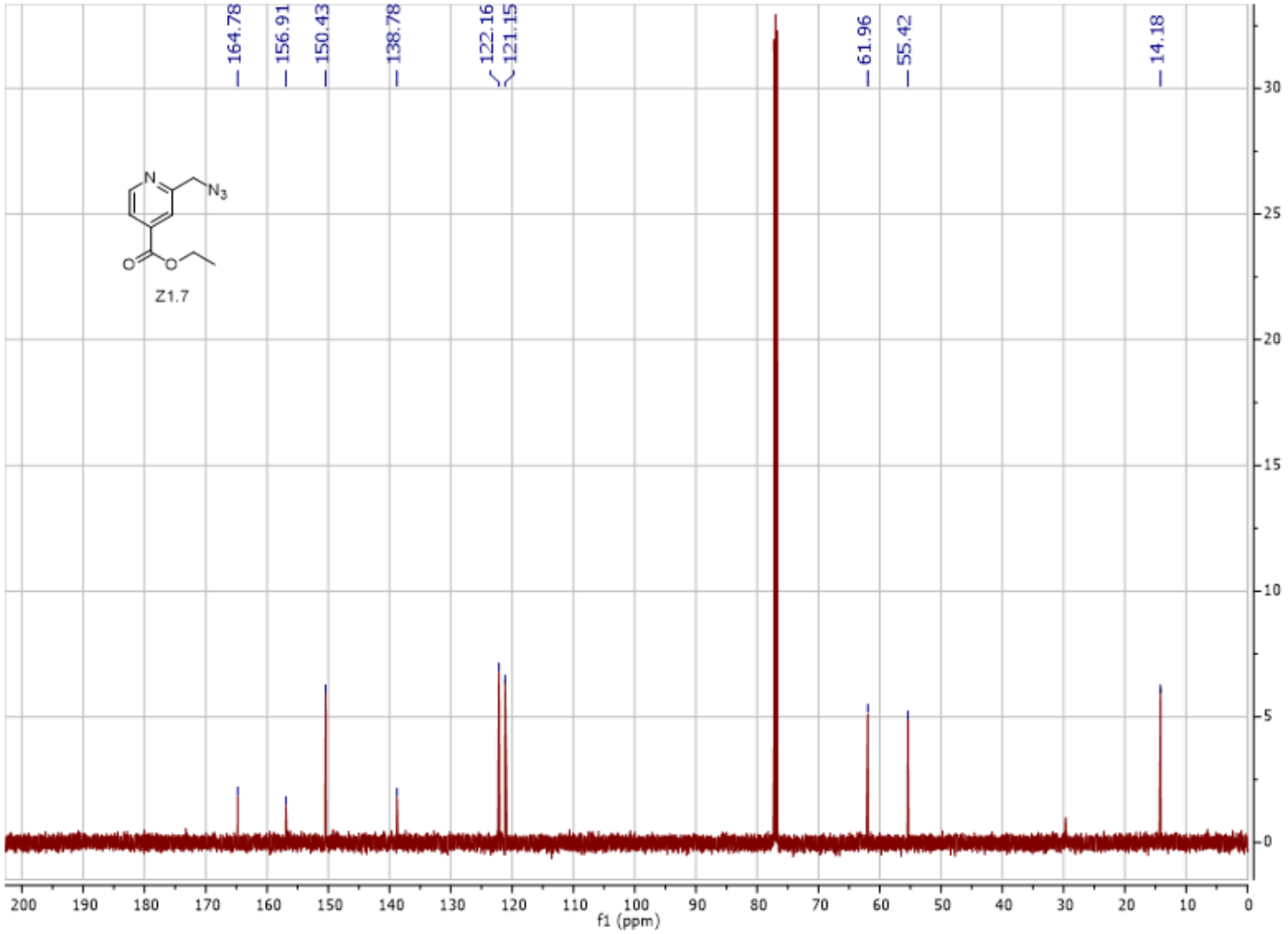

Spectrum 21: ^{13}C NMR (75 MHz, $CDCl_3$) Compound Z1.7

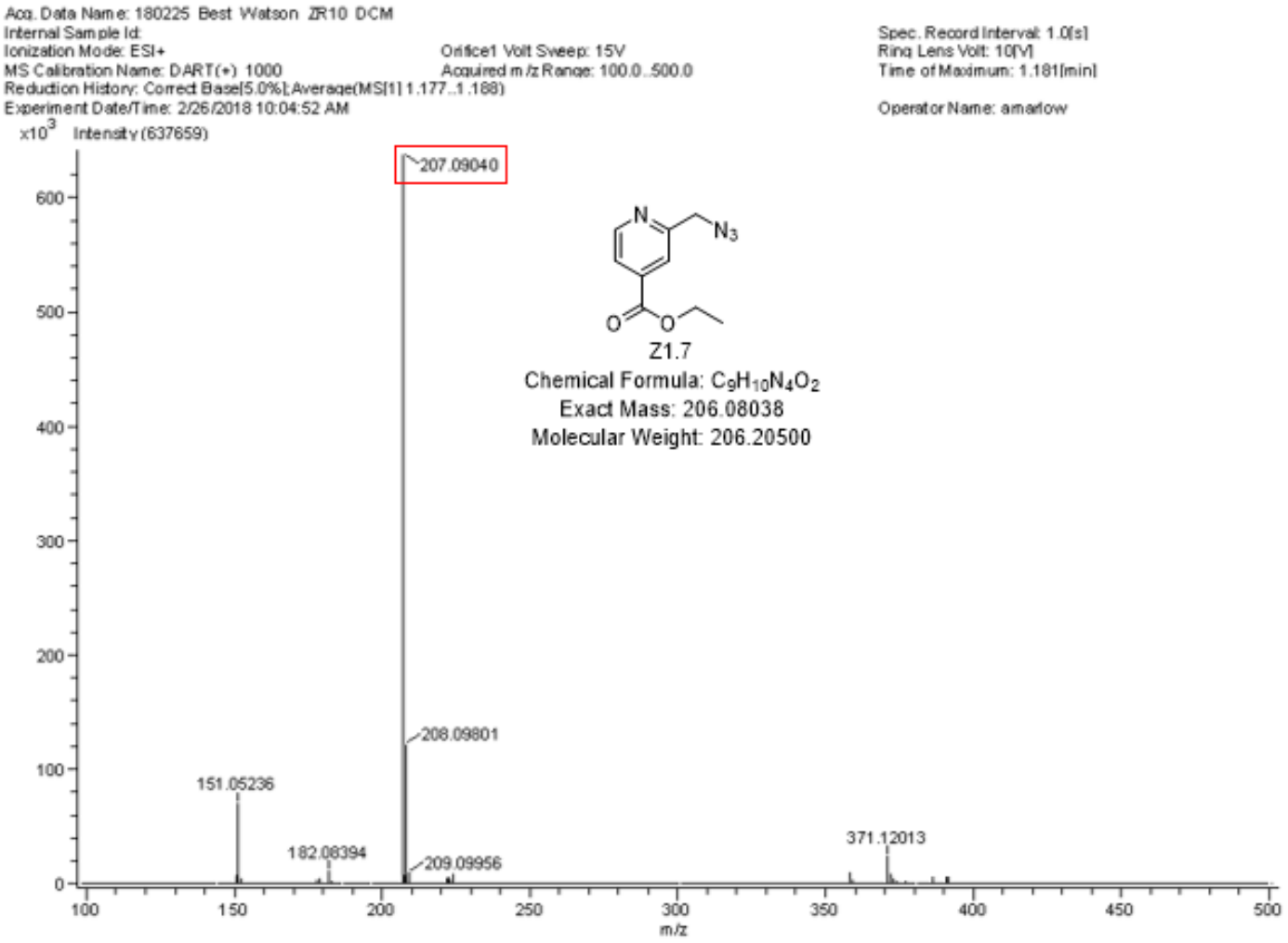

Spectrum 23: Mass Spectrum (JEOL DART-AccuTOF Mass Spectometer) Compound Z1.7 [M+1] predicted: 207.08765 [M+1] found: 207.09040

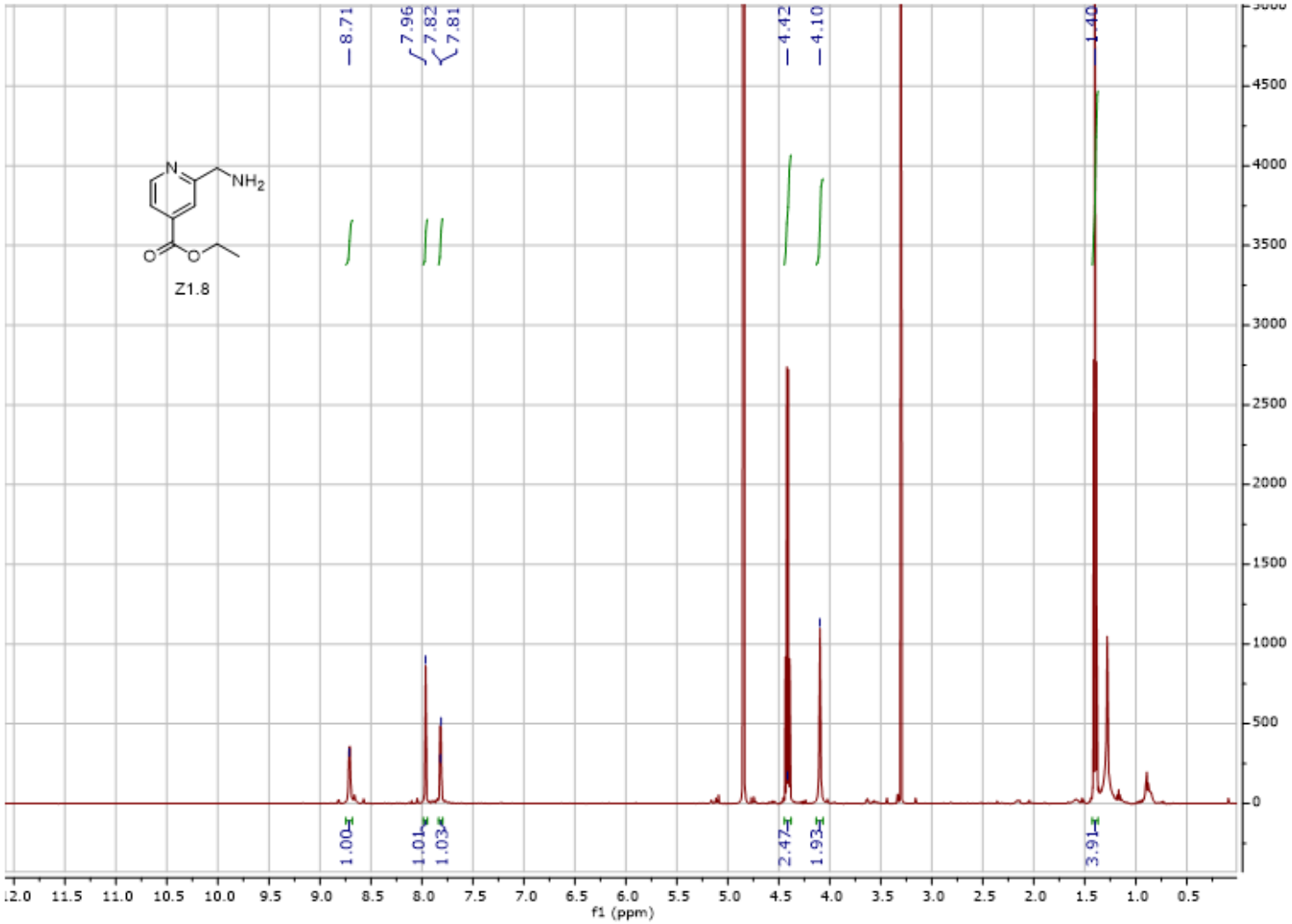

Spectrum 24: ^{1}H NMR (300 MHz, MeOD) Compound Z1.8

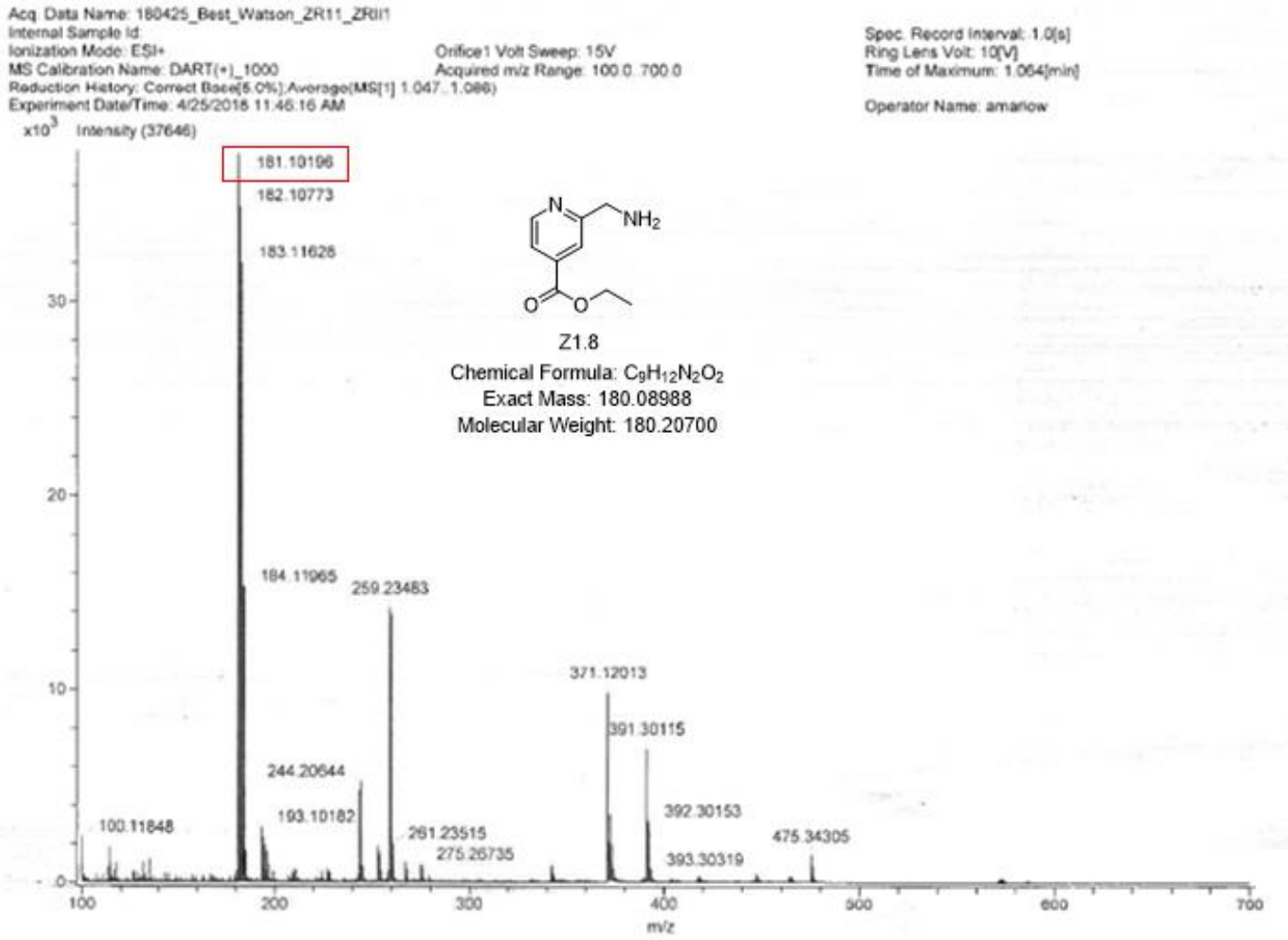

Spectrum 25: Mass Spectrum (JEOL DART-AccuTOF Mass Spectometer) Compound Z1.8 [M+1] predicted: 181.09715 [M+1] found: 181.10196

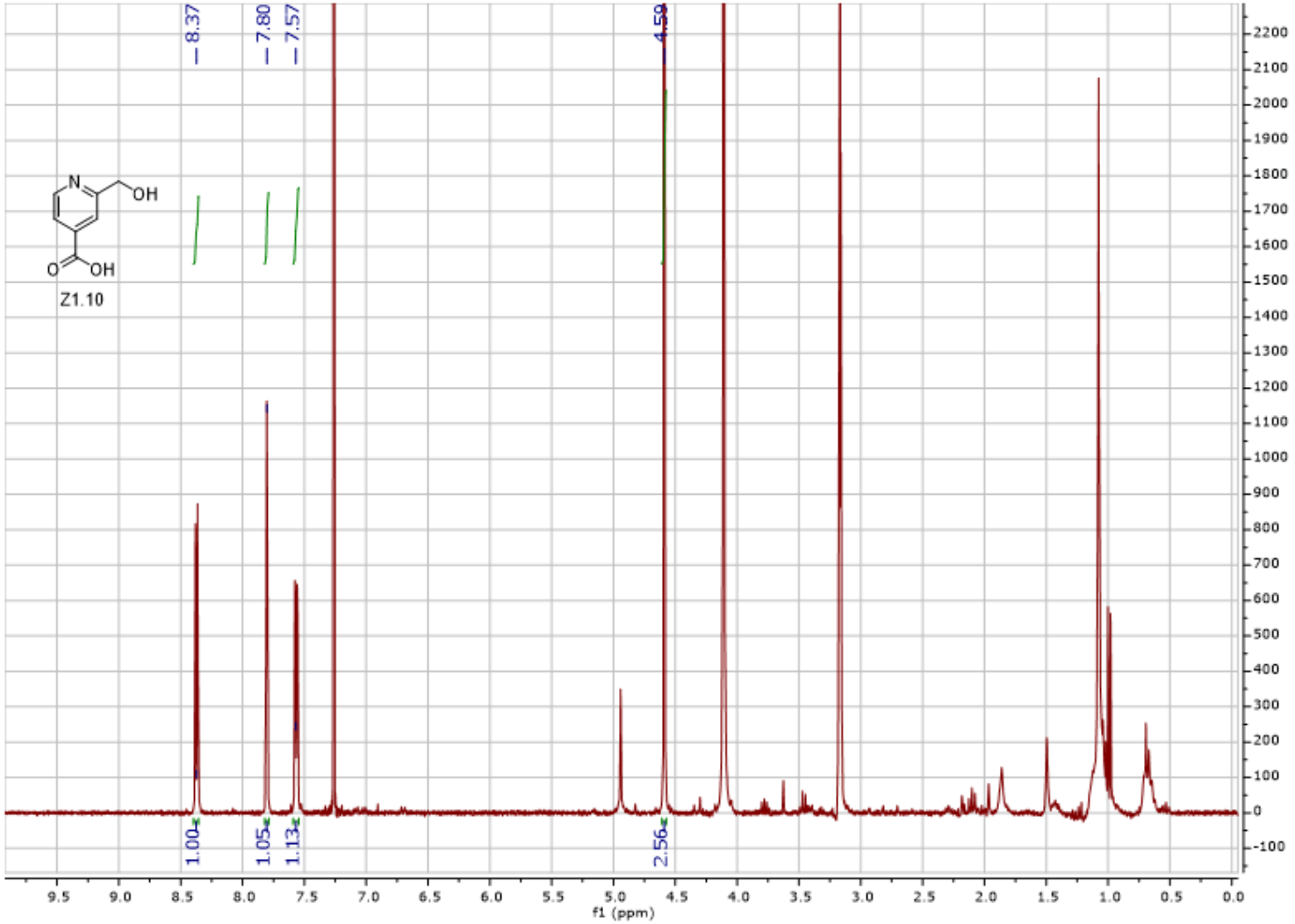

Spectrum 26: ^{1}H NMR (300 MHz, MeOD) Compound Z1.10

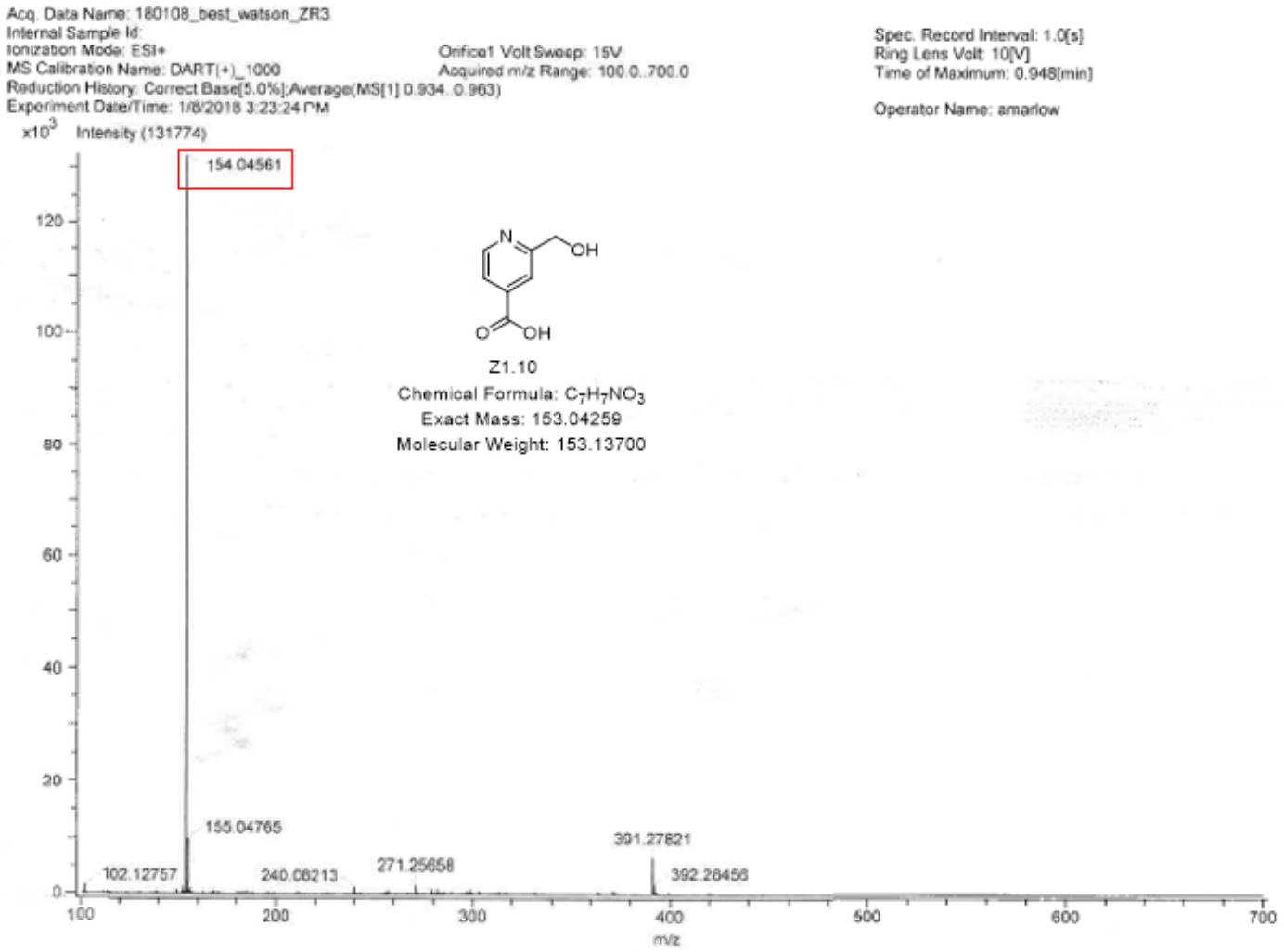

Spectrum 27: Mass Spectrum (JEOL DART-AccuTOF Mass Spectometer) Compound Z1.10 [M+1] predicted: 154.04987 [M+1] found: 154.04561

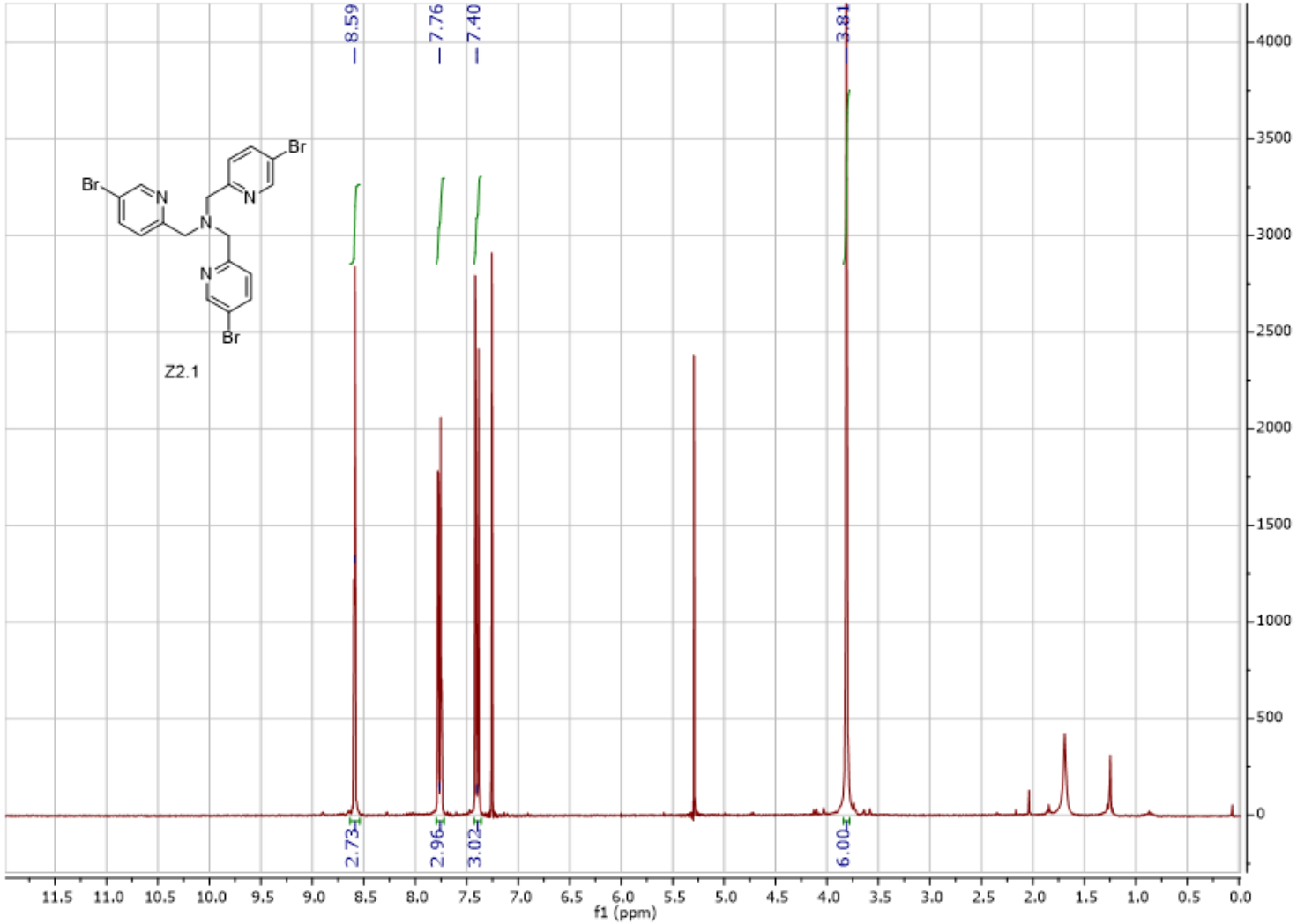

Spectrum 28: ^{1}H NMR (300 MHz, $CDCl_3$) Compound Z2.1

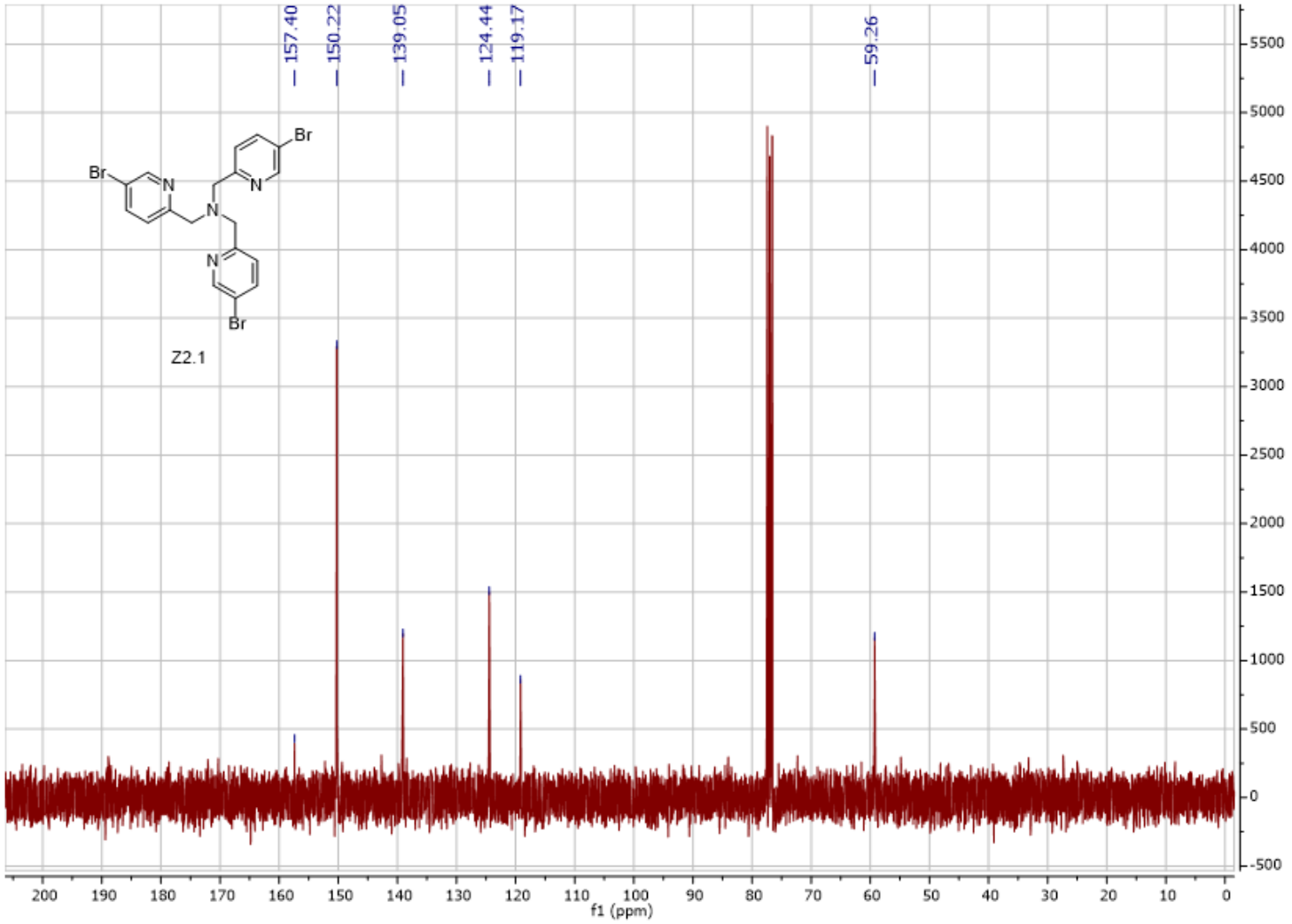

Spectrum 29: ^{13}C NMR (300 MHz, $CDCl_3$) Compound Z2.1

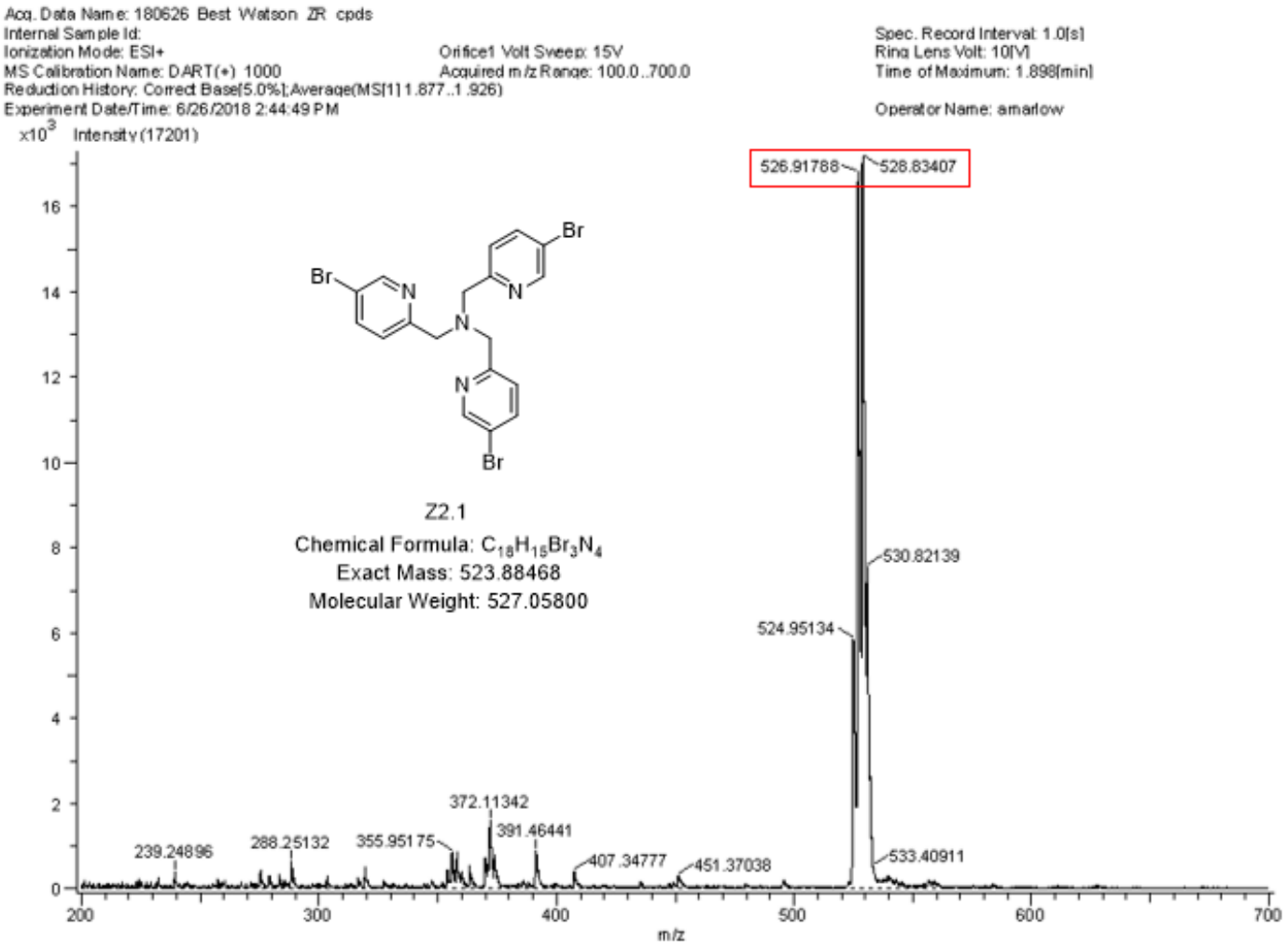

Spectrum 30: Mass Spectrum (JEOL DART-AccuTOF Mass Spectometer) Compound Z2.1 [M+1] predicted: 526.88991, 528.88787 [M+1] found: 526.91788, 528.83407

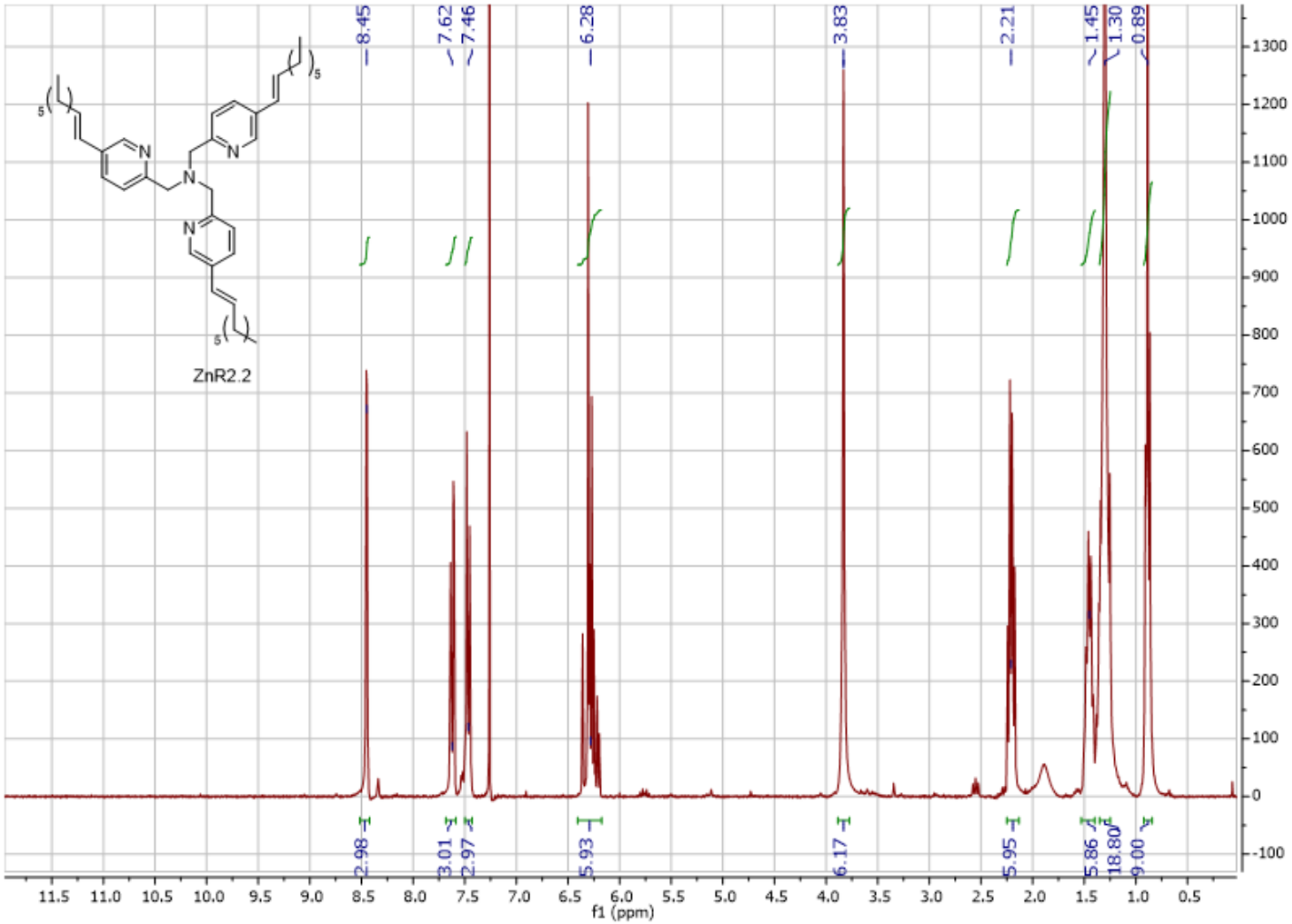

Spectrum 31: ^{1}H NMR (300 MHz, $CDCl_3$) Compund ZnR2.2

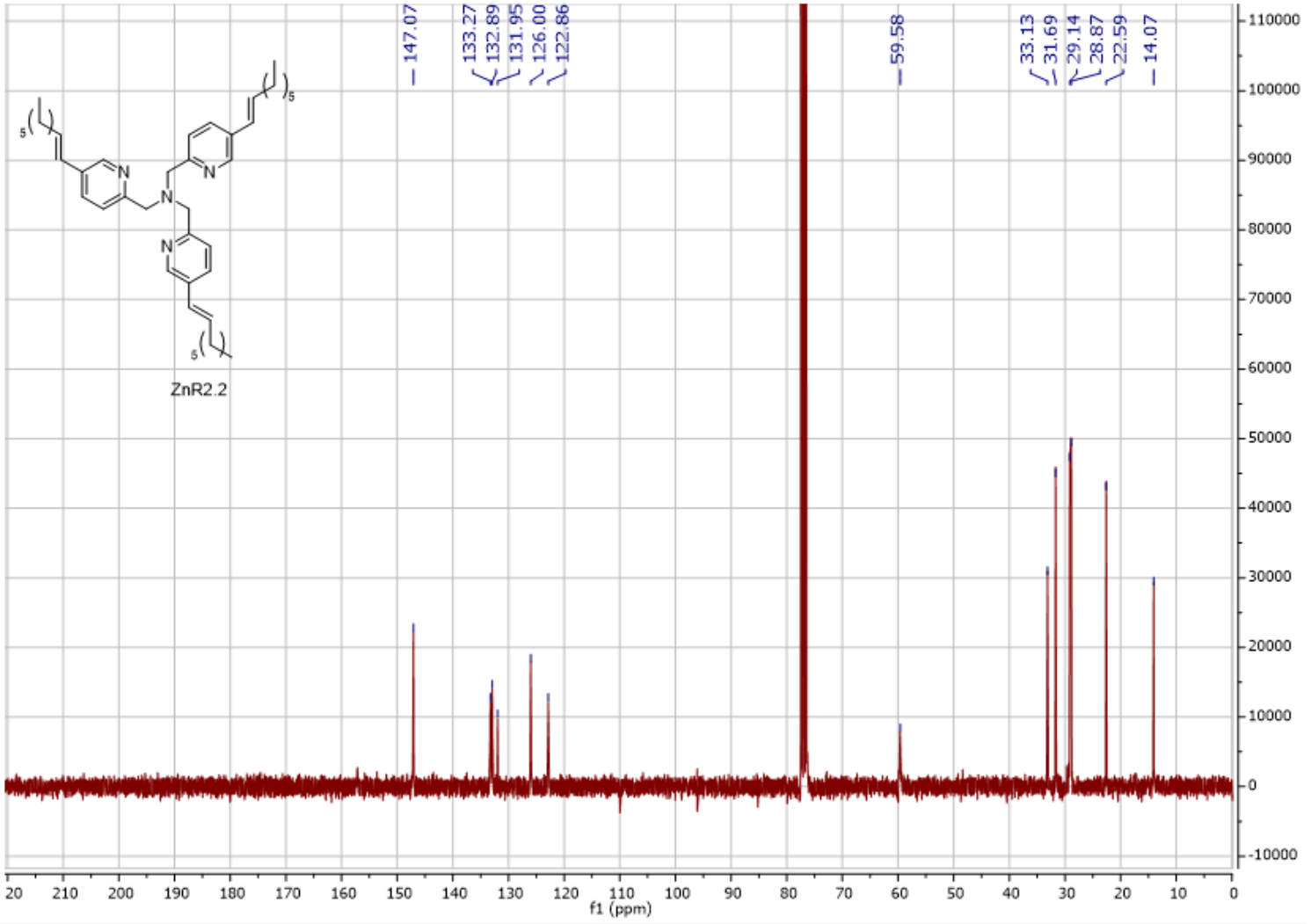

Spectrum 32: ^{13}C NMR (75 MHz, $CDCl_3$) Compund ZnR2.2

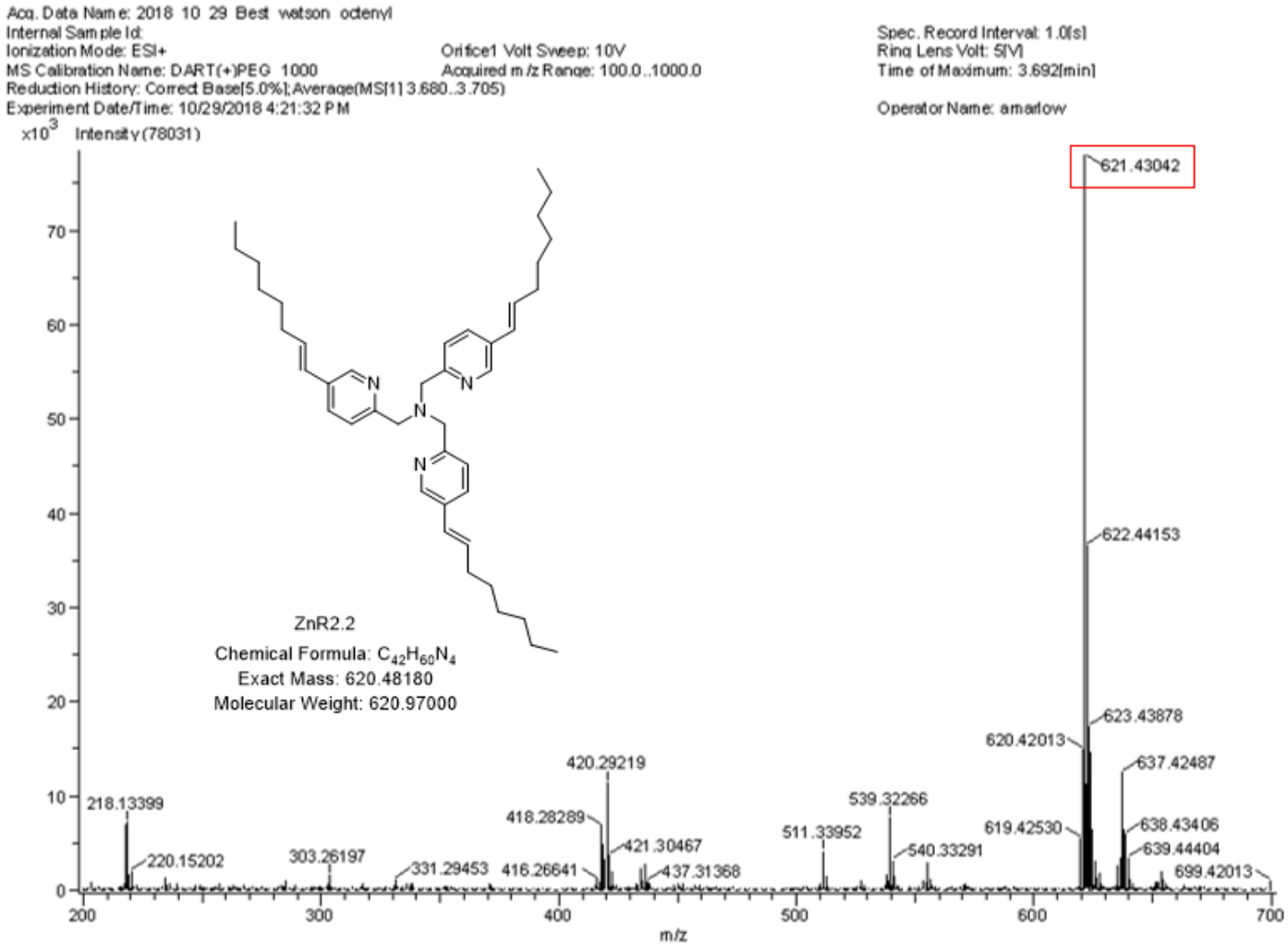

Spectrum 33: Mass Spectrum (JEOL DART-AccuTOF Mass Spectometer) Compund ZnR2.2 [M+1] predicted: 621.48907 [M+1] found: 621.43042

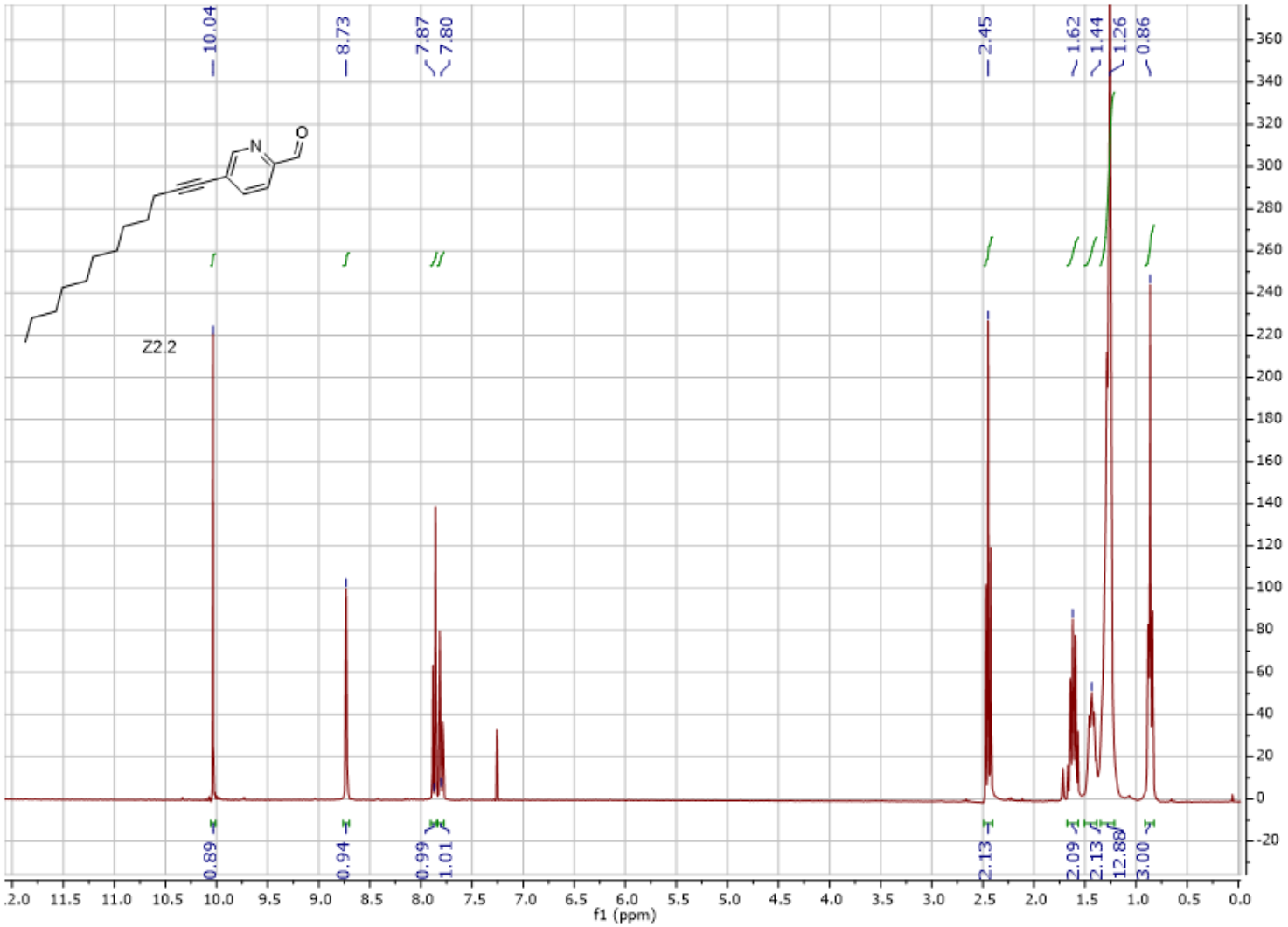

Spectrum 34: ^{1}H NMR (300 MHz, $CDCl_3$) Compound Z2.2

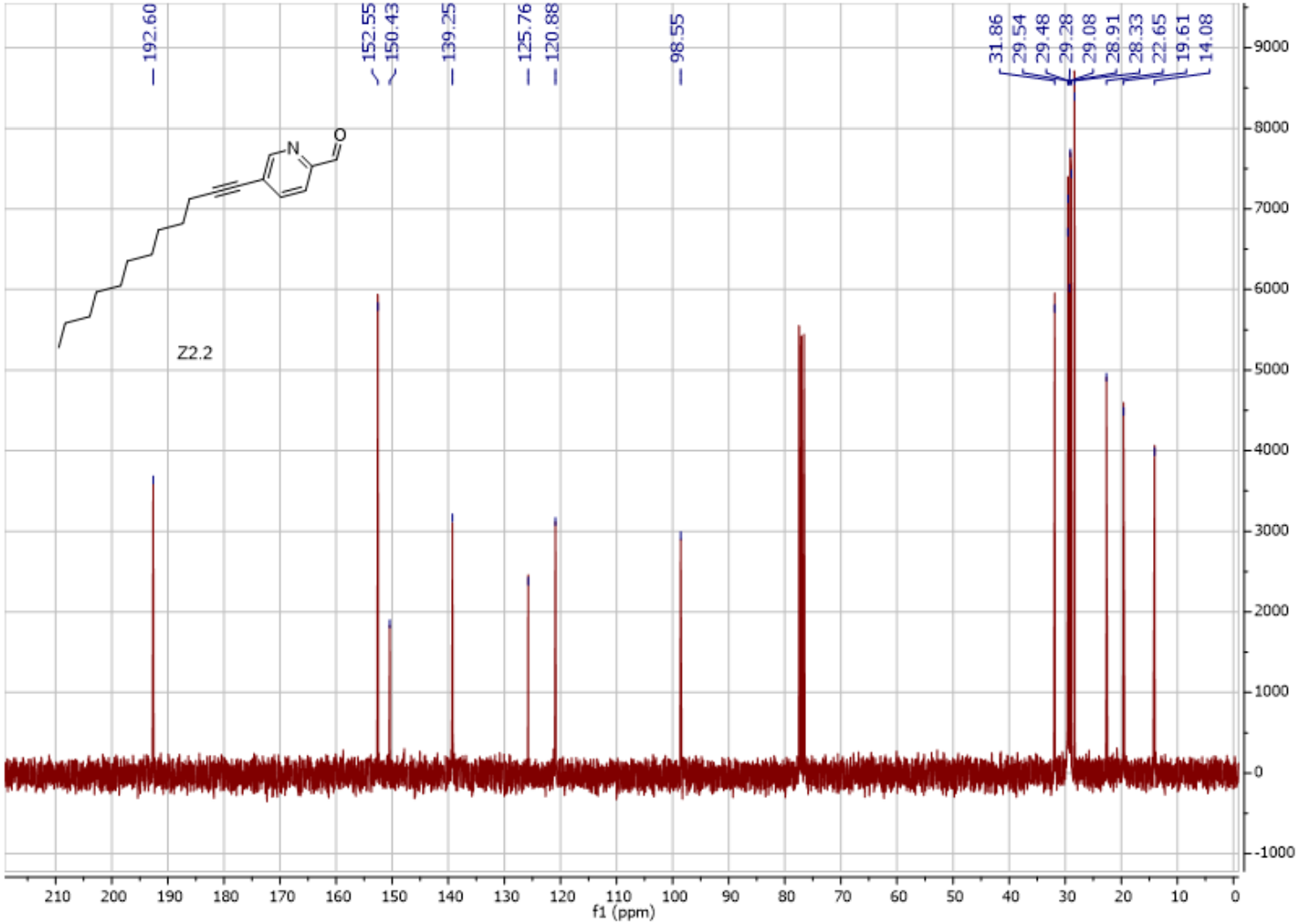

Spectrum 35: ^{13}C NMR (75 MHz, $CDCl_3$) Compound Z2.2

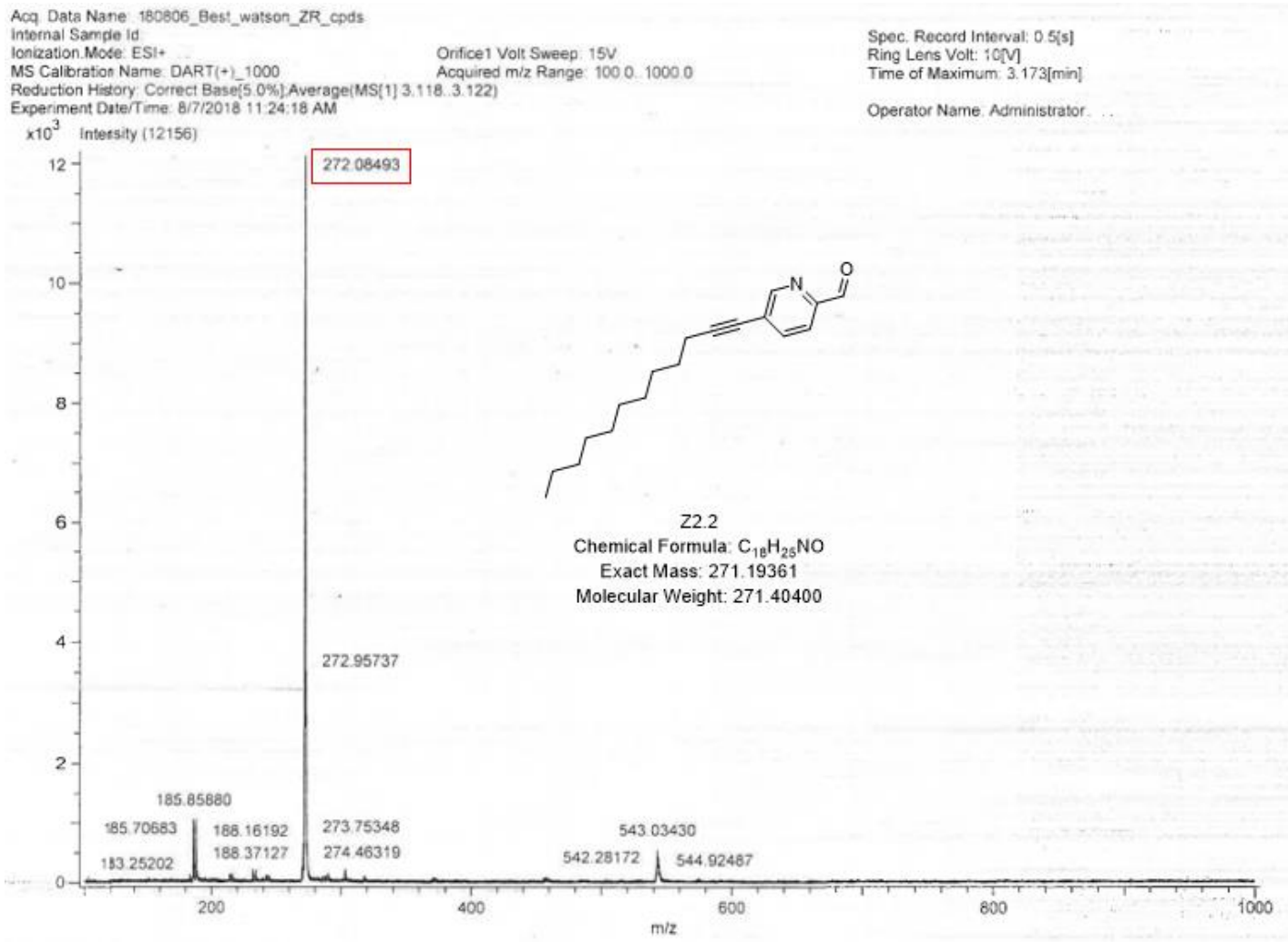

Spectra 36: Mass Spectrum (JEOL DART-AccuTOF Mass Spectometer) Compund Z2.2 [M+1] predicted: 272.20089 [M+1] found: 272.80493

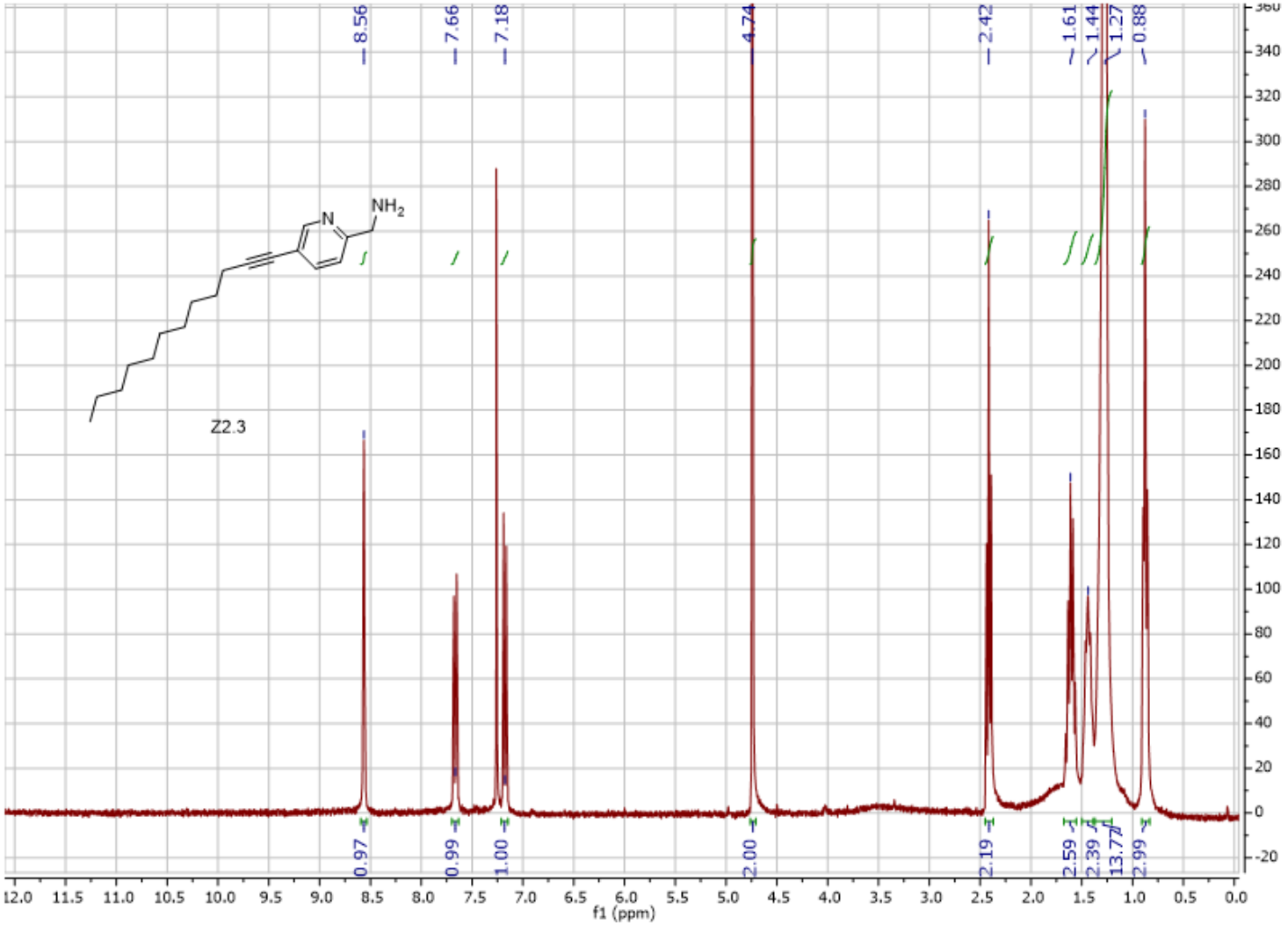

Spectrum 37: ^{1}H NMR (300 MHz, $CDCl_3$) Compound Z2.3

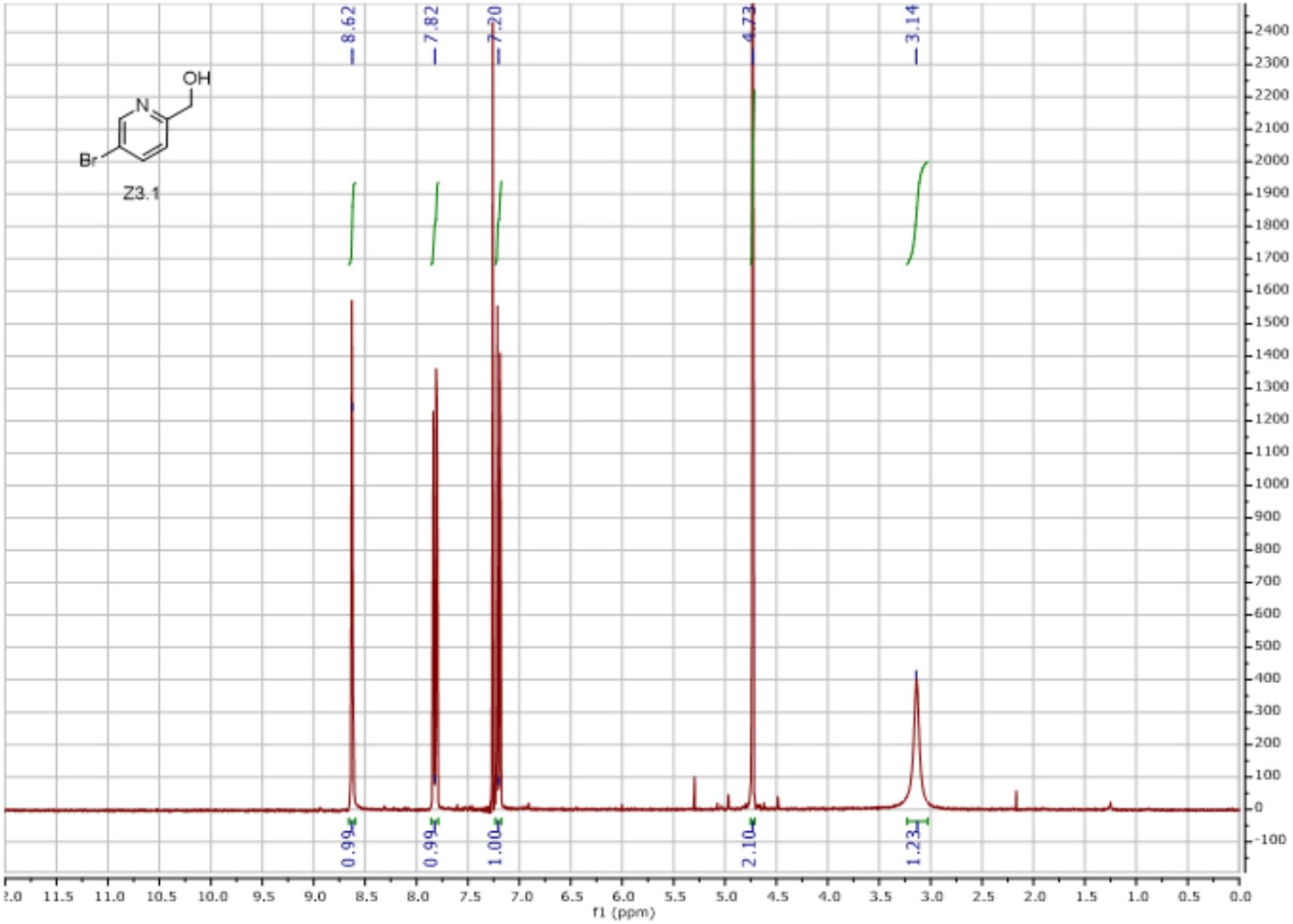

Spectrum 38: ^{1}H NMR (300 MHz, $CDCl_3$) Compound Z3.1

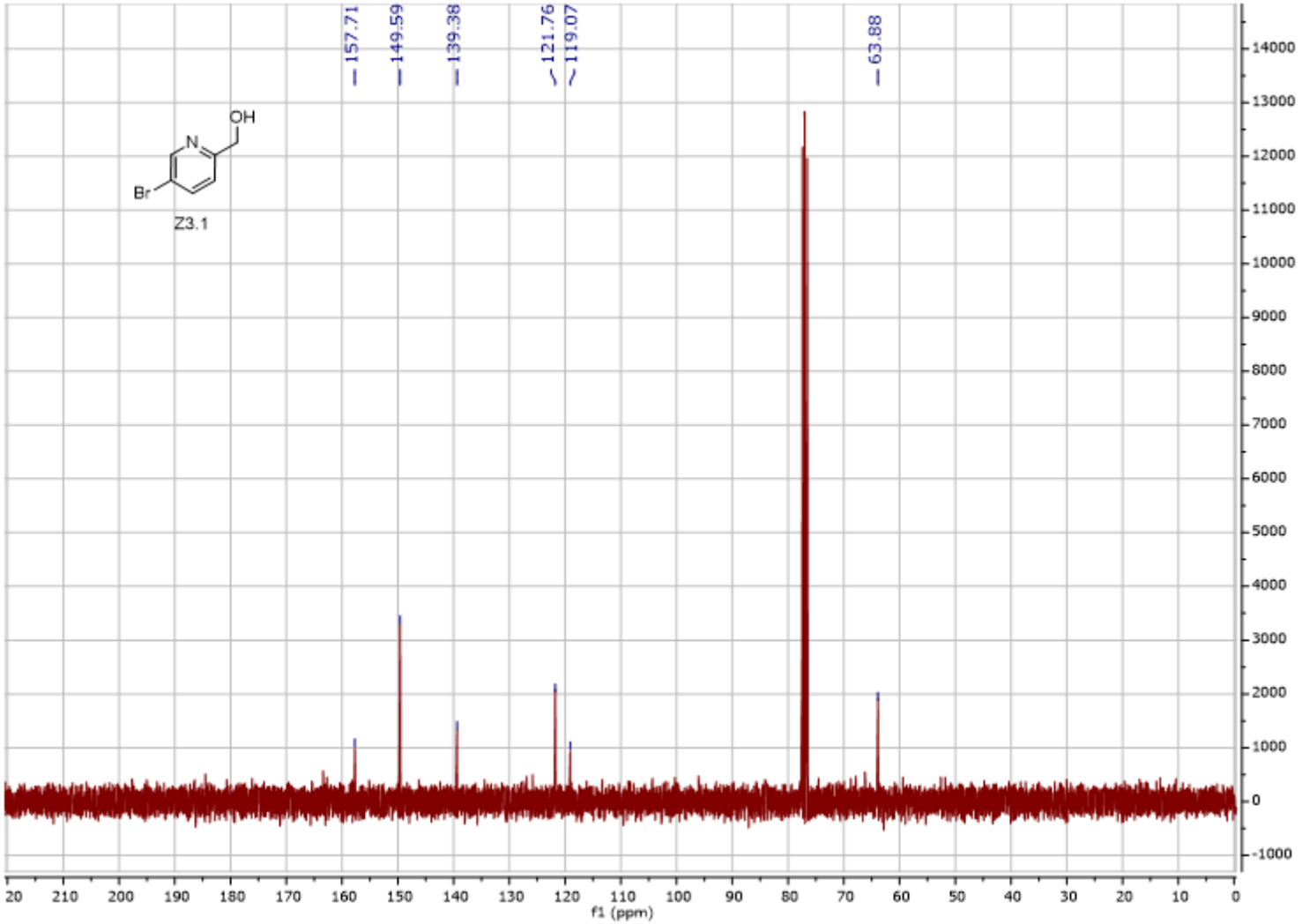

Spectrum 39: ^{13}C NMR (75 MHz, $CDCl_3$) Compound Z3.1

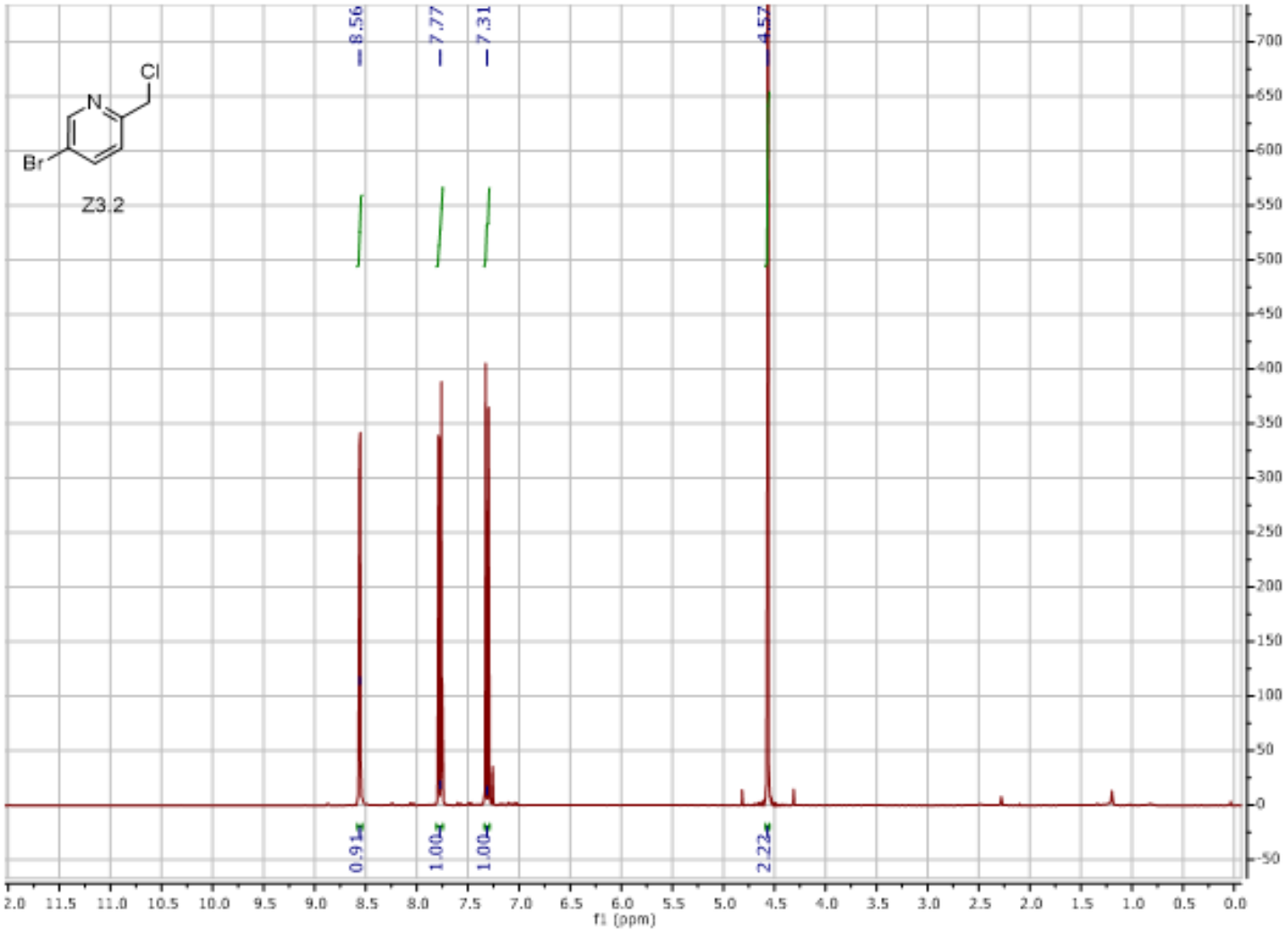

Spectrum 40: ^{1}H NMR (300 MHz, $CDCl_3$) Compound Z3.2

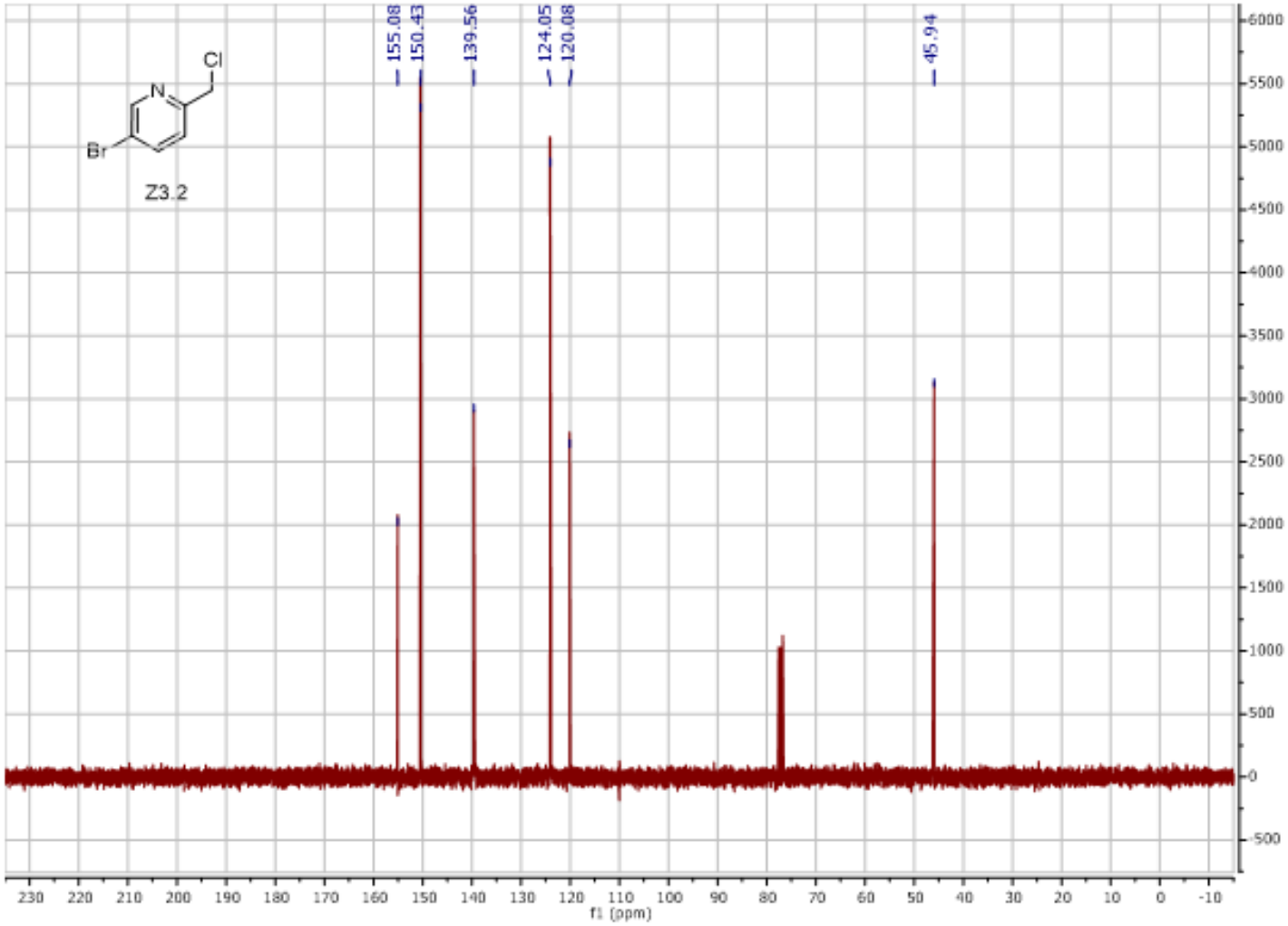

Spectrum 41: ^{13}C NMR (75 MHz, $CDCl_3$) Compound Z3.2

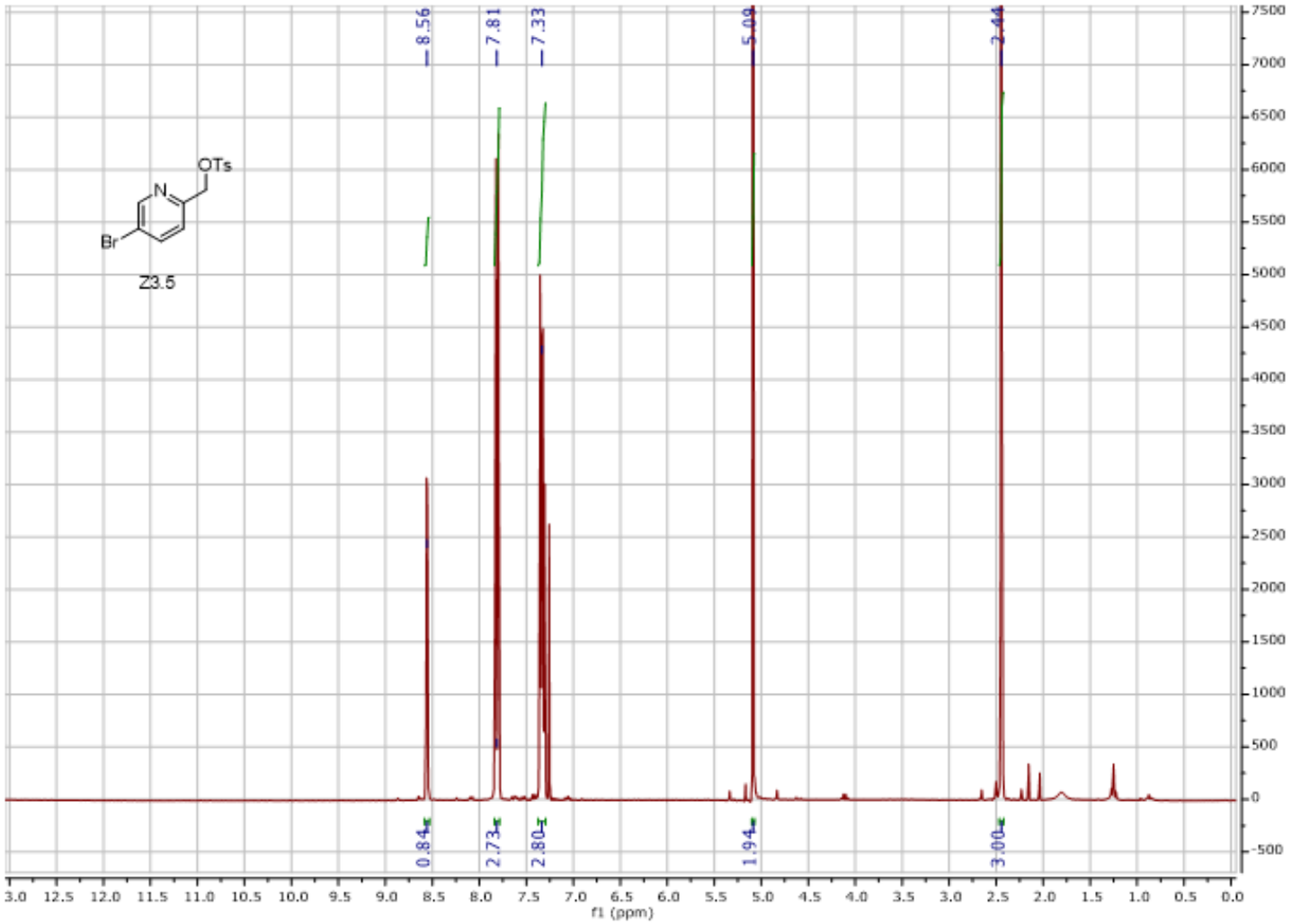

Spectrum 42: ^{1}H NMR (300 MHz, $CDCl_3$) Compound Z3.5

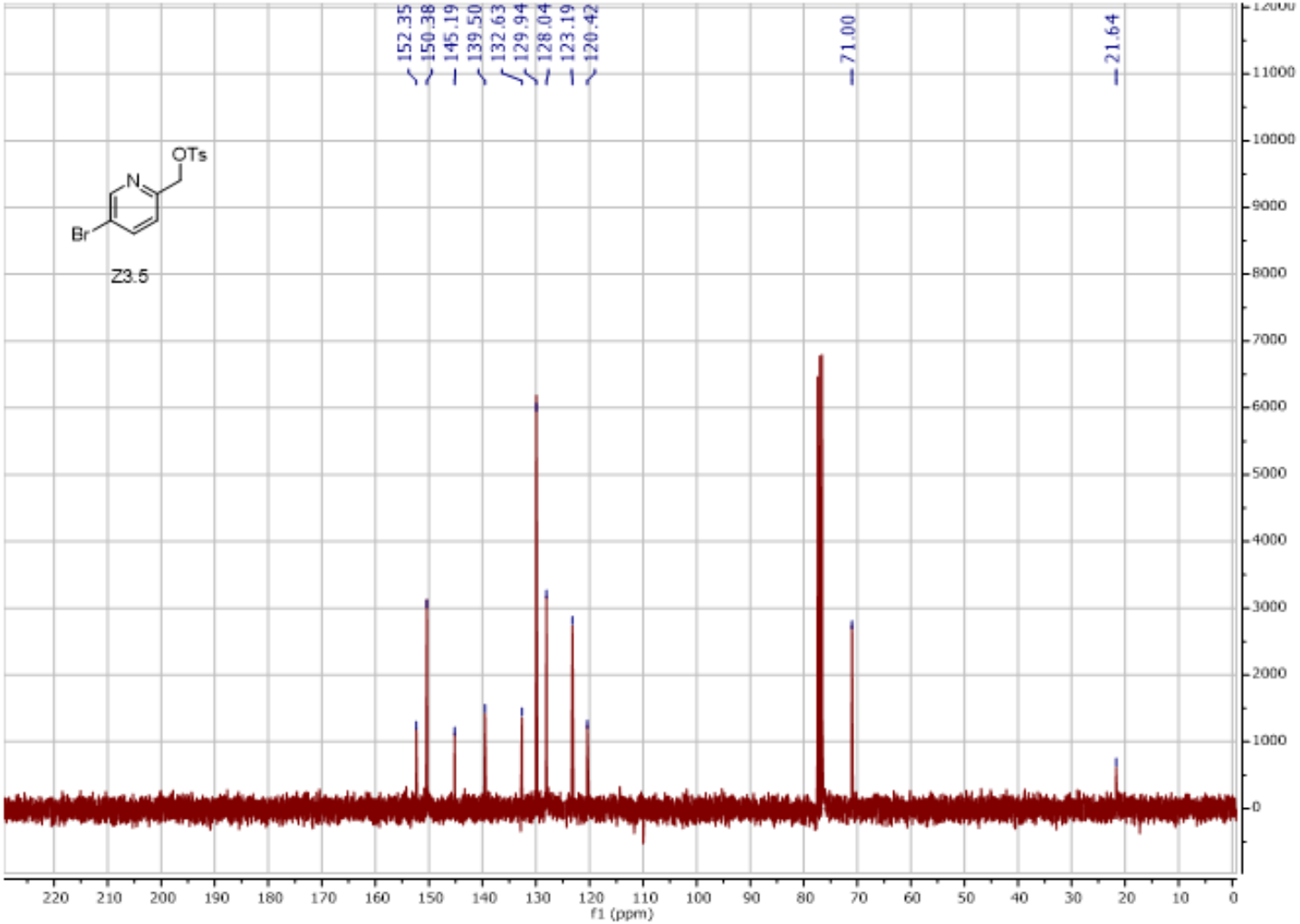

Spectrum 43: ^{13}C NMR (75 MHz, $CDCl_3$) Compound Z3.5

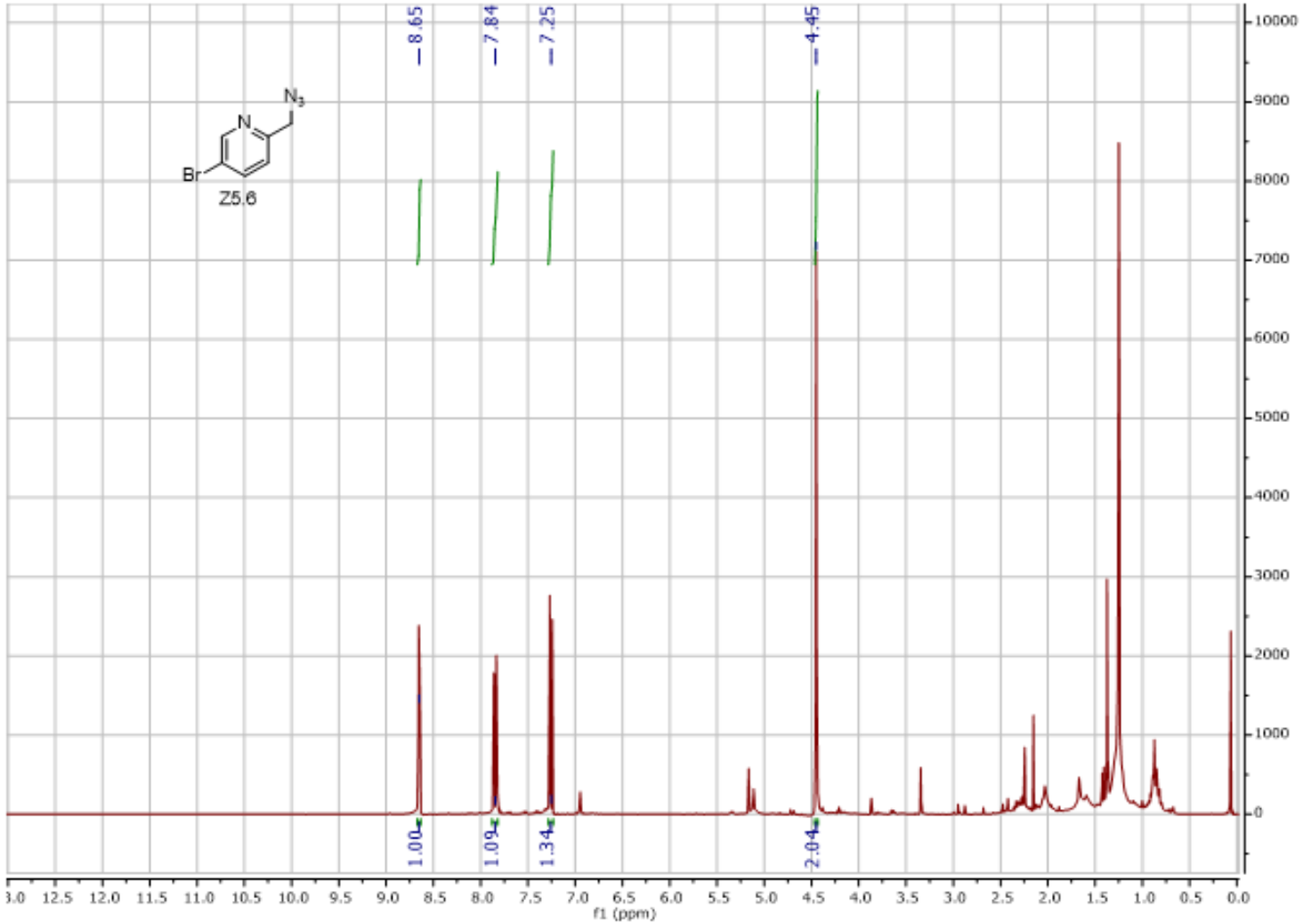

Spectrum 44: ^{1}H NMR (300 MHz, $CDCl_3$) Compound Z3.6

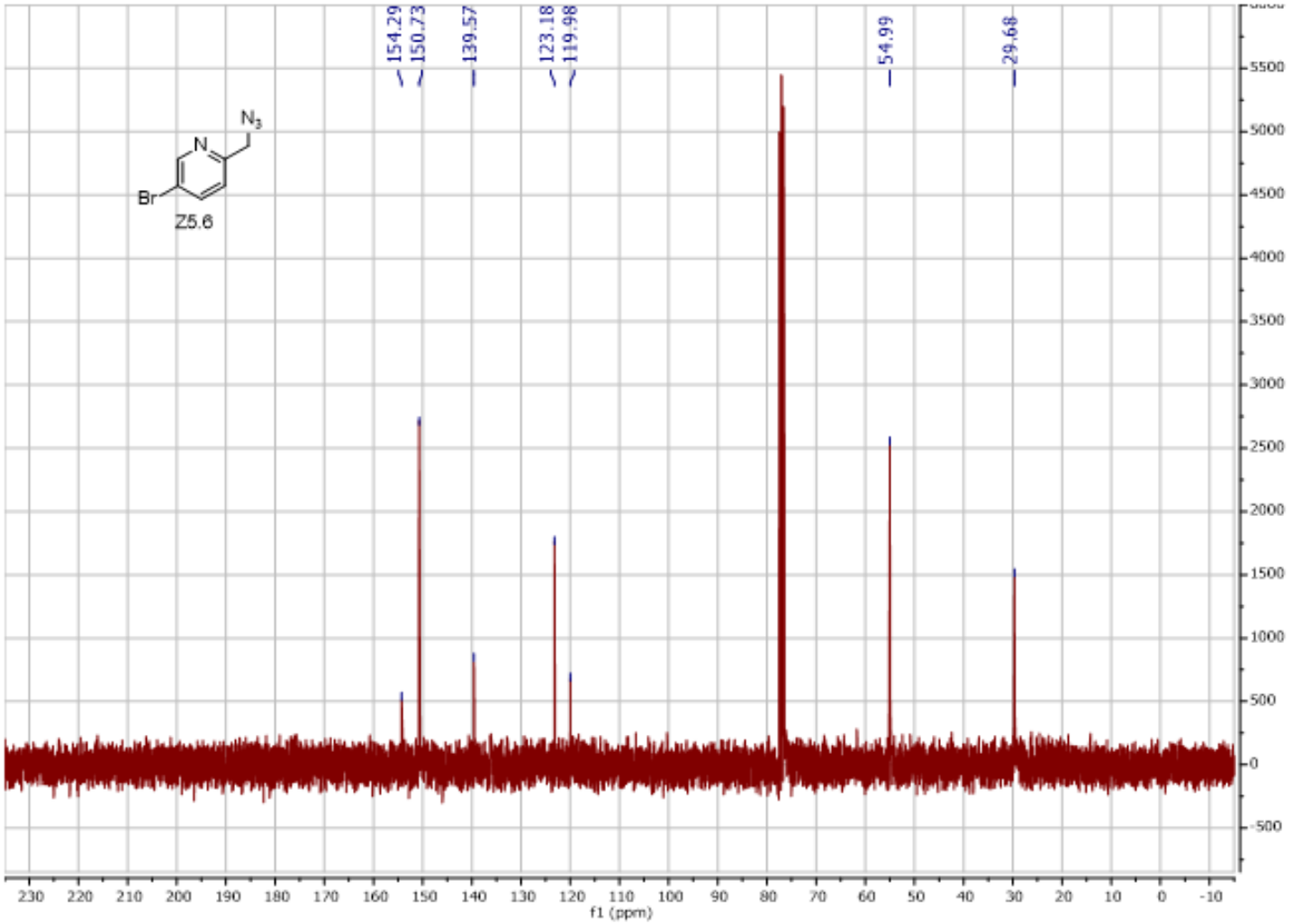

Spectrum 45: ^{13}C NMR (75 MHz, $CDCl_3$) Compound Z3.6

VITA

Alexa Watson was born in Loudon, Tennessee. She attended Tennessee Wesleyan College and received a B.S. in Chemistry with a minor in Biology. While pursuing her undergraduate degree at Tennessee Wesleyan, she spent a summer as a NIH funded undergraduate researcher in the bioorganic synthesis lab of Dr. Michael D. Best at the University of Tennessee. She then went on to attend the University of Tennessee as a graduate student in Dr. Best's lab where she contributed to the synthesis of stimuli responsive lipid switches.